Chem Soc Rev

REVIEW ARTICLE

View Article Online
View Journal

Cite this: DOI: 10.1039/d4cs00071d

Emerging porous materials for cell encapsulation

Francesco Carraro, †[a] Miriam de J. Velásquez-Hernández, ††‡[a] Anita Emmerstorfer-Augustin,[b] Daniel Kracher,[b] Qilu Wu,[c] Robert Kourist,[b] Lien-Yang Chou,[d] Ju Ge,[c] Fa-Kuen Shieh,[e] Christian Doonan[f] and Paolo Falcaro *[a]

Received 29th October 2025

DOI: 10.1039/d4cs00071d

rsc.li/chem-soc-rev

This review summarizes recent progress in cell@MOF, cell@COF, and cell@HOF composites from a synthetic biology and materials science perspective. It outlines key synthetic strategies for the synthesis of porous abiotic exoskeletons, focusing on framework-based materials. Additionally, it discusses the cell surface chemistry and current methods for assessing cell viability. Major applications, including cell therapy, biocatalysis, biosensing, and CO_2 mitigation, are examined alongside approaches for composite preparation and characterization. This review concludes with prospects and challenges for using framework materials to engineer synthetic cells and enhance cellular functions.

Introduction

In nature, the survival of biological species relies on their ability to cope with diverse environmental conditions. To adapt to environmental stress, some microorganisms have developed the ability to construct abiotic coatings *via* the self-assembly of molecular precursors.[1,2] These coatings are purposely designed to confer various functional properties to the enclosed cells, such as mechanical strength, thermal resistance, and physical protection, that ensure cell survival under inhospitable conditions.[1–3] For example, some bacteria produce an organic polymeric network that provides mechanical robustness to withstand external pressures and enhances their desiccation tolerance in water-deficient environments.[4] This survival

[a] *Institute of Physical and Theoretical Chemistry, Graz University of Technology, Stremayrgasse 9, Graz, 8010, Austria. E-mail: paolo.falcaro@tugaz.at*
[b] *Institute of Molecular Biotechnology, Graz University of Technology, Petersgasse 14, Graz, 8010, Austria*
[c] *Key Lab of Industrial Biocatalysis, Ministry of Education, Department of Chemical Engineering, Tsinghua University, Beijing 100084, China*
[d] *School of Physical Science and Technology, ShanghaiTech University, Shanghai, 201210, P.R. China*
[e] *Department of Chemistry, National Central University, Taoyuan, 32001, Taiwan*
[f] *Department of Chemistry and Centre for Advanced Nanomaterials, University of Adelaide, Adelaide, SA, 5005, Australia*
† Equal contribution.
‡ Current affiliation: Center for Membrane Separations, Adsorption, Catalysis, and Spectroscopy (cMACS), B-3001 Leuven, Belgium.

Francesco Carraro

Francesco Carraro received his PhD in Science and Engineering of Materials and Nanostructures from the University of Padova (Italy) in 2018. After postdoctoral work in the Falcaro group at the Graz University of Technology (TU Graz, Austria) on metal–organic framework films and biomolecule encapsulation, he became Assistant Professor at TU Graz in 2022, focusing on the crystal engineering and biotechnological applications of metal–organic and hydrogen-bonded organic framework biocomposites.

Miriam de J. Velásquez-Hernández

Miriam de J. Velásquez-Hernández received her PhD degree from the Universidad Nacional Autónoma de México (UNAM). She subsequently joined Paolo Falcaro's group at the Graz University of Technology (TU Graz, Austria) as a CONACyT postdoctoral fellow, focusing on the synthesis of metal–organic framework based biocomposites for drug delivery applications. She is currently an MSCA postdoctoral fellow in Rob Ameloot's group at KU Leuven.

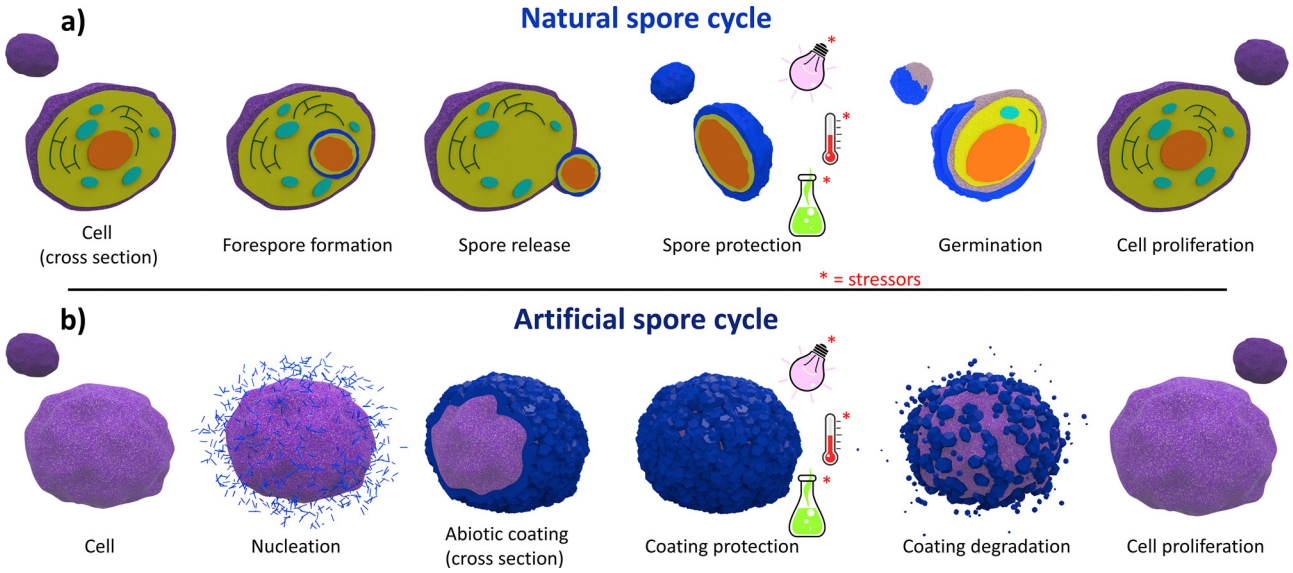

Fig. 1 Schematic of the natural (a) and artificial (b) sporulation. The natural process begins with asymmetric cell division: the mother cell (purple) forms a forespore (orange). The mother cell engulfs the forespore, leading to a mature spore (blue) that is resistant to multiple stressors (UV, chemicals, and heat). The spore can remain dormant until nutrient-rich conditions trigger germination and cell growth. Artificial sporulation similarly employs protective coatings (blue crystals) around individual cells (purple), suppressing proliferation and enhancing resistance. On-demand dissolution of this abiotic coating then restores normal growth and metabolism.

mechanism is called sporulation.[5] Specifically, the cell divides asymmetrically, forming a new compartment: the forespore.[6–8] In the forespore, the cell encapsulates precious biological materials for the strain's survival (*e.g.*, deoxyribonucleic acid (DNA), ribonucleic acid (RNA), and enzymes). Then, the forespore undergoes a maturation process in which a cortex and a multi-layer coating surround the forespore's core, forming a protective shield (Fig. 1a). Subsequently, metabolic inactivation or dormancy is achieved by gradually dehydrating the core by replacing water with dipicolinic acid (DPA) and calcium ions, leading to endospore formation within the mother cell (Fig. 1a). Finally, the mother cell undergoes programmed cell death (apoptosis§), accompanied by release of the endospore into the environment (*i.e.*, spore). The secreted spore can remain dormant until it senses that harsh conditions are alleviated (Fig. 1a). Details of this process can be found in dedicated review papers.[6–8] The natural formation of protective coating materials is not restricted to organic biopolymers. Some cells possess a metabolic machinery to assimilate minerals from the environment and synthesize an inorganic material-based coating.[1,2] This process is called biomineralization and yields rigid and protective exoskeletons for different biological systems.[1,2] Biosilicification is the archetype of individual cell biomineralization, wherein diatoms convert soluble silicic acid into an amorphous silica shell.[1,2] This inorganic coating enhances cell viability when exposed to environmental stresses, such as heat, desiccation, microbial attack, and lytic enzymatic degradation. Simultaneously, the inorganic coating affords optical transparency and enables transport of nutrients necessary for cellular functions. Other typical examples of inorganic cell coatings are calcium carbonate, which can be found in mollusk shells and pearls,[9] and calcium phosphate that is present in bone tissue.[10] Inspired by these natural coatings, multidisciplinary research investigates synthetic methods for the development of abiotic protective exoskeletons on cells that lack natural biomineralization capability. These synthetic cell@shell systems are known as "artificial spores" (Fig. 1b)[11] and can possess three main advantages:

I. Enhanced cell resistance to chemical and physical stressors: unlike naked cells, artificial spores exhibit enhanced tolerance to unfavourable environmental conditions such as enzymatic degradation,[12] changes in the osmotic pressure,[13] high temperatures,[14] and UV radiation (Fig. 1b);[15]

II. On-demand suppression and reactivation of cell division: the formation of rigid artificial shells around living cells hinders cell division, inducing a state of dormancy akin to spores. The cell proliferation and natural metabolic functions can be restored by on-demand shell degradation (Fig. 1b);[11]

III. Tailored exogenous biochemical properties: by designing coatings with specific chemical and biochemical properties, cells can be engineered with abiotic exoskeletons with exogenous chemical functionalities: the new cell@shell systems possess functionalities that are not present in the original naked cells. For example, this material design strategy has enhanced cell adaptability to nutrient-deficient and protease-rich environments.[12,16]

We note that abiotic exoskeletons should satisfy requirements such as (i) perm-selectivity, (ii) durability, (iii) degradability on

§ Apoptosis describes the orchestrated collapse of a cell characterised by membrane blebbing, cell shrinkage, condensation of chromatin, and fragmentation of DNA followed by rapid engulfment of the corpse by neighbouring cells.[215] It is a regulated process essential for maintaining tissue homeostasis, embryonic development, and immune system function. Dysregulation of apoptosis can contribute to various pathological conditions, such as cancer (*e.g.* cell immortalization) and degenerative diseases.

demand, and (iv) functionalizability.[11,17,18] These properties are described as follows:

I. Perm-selectivity: preserving cell viability in a cell@shell system depends on the continuous supply of nutrients to the cytosol. Ideally, artificial cell coatings should act as a molecular sieve allowing the free transport of biologically relevant molecules (*e.g.* see Video S1), such as cell nutrients, oxygen, and metabolites, while preventing the diffusion of cytotoxic macromolecules.[11,17,18]

II. Durability: emulating spore-like features requires the fabrication of artificial coatings sufficiently robust to withstand the mechanical stress caused by changes in the osmotic pressure and dehydration. Additionally, rigid artificial shells retard or suppress cell division, mimicking the spore-like dormancy.[11,17,18]

III. Degradability on demand: achieving programmable recovery of original metabolic cell functions, the artificial shell must be able to degrade upon applying external stimuli. The on-demand removal of the artificial coating grants control over the dormant and active state transition.[19]

IV. Functionalizability: imparting exogenous functional properties artificially enables the fabrication of systems with non-natural functions. This approach can be used to adapt cells to hostile habitats (*e.g.*, nutrient-deficient or cytotoxic environments).[12,16]

Inspired by the potential to design distinctive functional properties, researchers have focused on coating living cells with various inorganic (*e.g.*, SiO_2, $CaCO_3$, and MnO_2), organic (*e.g.*, alginate, polyethylene, chitosan, and cell membranes), and hybrid (*e.g.* metal-phenolic networks and framework materials) materials (Fig. 2a–c).[9,18,20–30] In this review, we focus on framework materials for encasing individual living cells (Fig. 2c).[31] A framework material can be defined as an extended crystalline network comprised of molecular building blocks interconnected *via* directional bonding interactions.[32] The most common framework materials employed to encapsulate living cells are metal–organic frameworks (MOFs). Recently, the encapsulation of living cells within covalent organic frameworks (COFs) and hydrogen-bonded organic frameworks (HOFs) has been reported.[31,33,34] All three framework materials are assembled *via* bottom-up synthetic approaches. MOFs consist of inorganic clusters linked together *via* multitopic organic linkers,[35,36] whereas COFs and HOFs are constructed exclusively from organic building blocks interconnected through covalent and hydrogen-bonding interactions, respectively.[37,38] A common feature of these materials is their bottom-up synthesis, which allows for the chemical and structural properties of the abiotic coatings to be precisely tailored.[32,37] For example, pore sizes can be adjusted to modulate the diffusion of essential cell nutrients while preventing the cytotoxic effects of proteolytic agents.[31]

In this review, we provide a general overview of the emerging research on cell@MOF, cell@COF, and cell@HOF composites from a synthetic biology and materials science perspective. First, we discuss the principles behind the two synthetic strategies used to grow framework materials for abiotic exoskeletons (*i.e.*, one-pot and multi-step processes), the cell surface chemistry, and the best practices for evaluating the viability of the coated cells. Next, we explore the applications of cell@MOF, cell@COF, and cell@HOF composites, including cell adaptability,[11,17] cell therapy,[21,33] biocatalysis,[39] biosensing,[40] and CO_2 mitigation,[41] with a focus on the preparation and characterization of these biocomposites. Then, we discuss the potential of MOF-, COF-, and HOF-based abiotic coatings for the fabrication of synthetic cells. Finally, we provide brief insights into the future opportunities and challenges of using framework materials as exoskeletons to enhance cell functionality, with specific attention to *Escherichia coli* (*E. coli*), or genetically engineered bacteria for targeted therapeutic delivery. Such microorganisms can be encapsulated within MOF materials to enhance their therapeutic performance against cancer. This approach aims to develop a diverse range of bacteria@MOF biocomposites and explore their potential applications in cancer immunotherapy, specifically through bacterial-mediated cancer therapy (BMCT).[42,43]

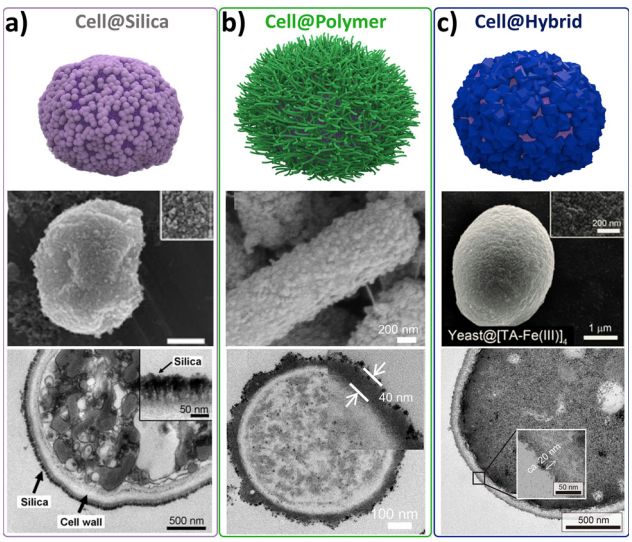

Fig. 2 Schematic representation (top) of the inorganic (a), organic (b), and hybrid materials (c) used as abiotic cell coatings, together with SEM (middle) and TEM (bottom) micrographs of selected examples. (a) SEM micrographs of yeast@SiO_2 at different magnifications. The TEM images of microtome-sliced yeast@SiO_2 indicate silica shells with a thickness above 50 nm (adapted with permission from ref. 22 Copyright 2009, Wiley-VCH). (b) SEM and TEM micrographs of organic polymeric materials for multilayer cell coatings (adapted with permission from ref. 39). (c) Illustration of single cells encapsulated within a metal–polyphenol nanoshell (adapted with permission from ref. 19 Copyright 2014, Wiley-VCH).

Coating approaches for living cells

Two main synthetic approaches have been used for the fabrication of cell@MOF, cell@COF, and cell@HOF composites: (i) the one-pot cell coating (Fig. 3a) and (ii) the multi-step cell cytoprotective encapsulation strategy (Fig. 3b). In this section, we introduce aspects that are at the foundation of these two

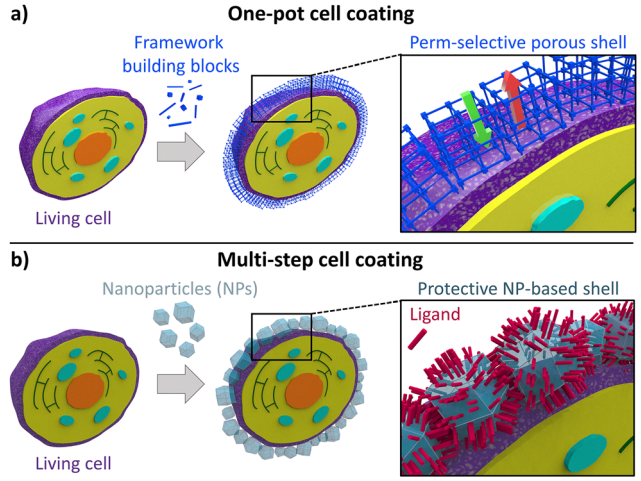

Fig. 3 Schematic representation of (a) the one-pot encapsulation process and (b) the "SupraCell[64] structure" formed by depositing pre-formed abiotic nanoparticles onto the cell membrane.

synthetic approaches and underpin all the examples of artificial spores discussed in this review.

One-pot encapsulation strategy

The one-pot approach requires biological entities regulating the on-site formation of abiotic coatings (Fig. 3a), mimicking natural biomineralization processes. Such a one-pot cell coating method is carried out by mixing a cell suspension with an aqueous solution of the MOF, COF, or HOF precursors. Similar to how biological materials can trigger natural biomineralization, leading to the deposition of inorganic nanoparticles on their surfaces, living organisms can induce the self-assembly of MOF, COF, or HOF materials on their surfaces.[31,33,34,44] At the bio-interface, two main driving forces promote the growth of the porous coatings: (i) the free energy of nucleation and (ii) the electrostatic intermolecular interactions. The first can be explained by a heterogeneous nucleation effect induced by cells: as observed for inorganic nanoparticles,[45,46] these nucleation seeds lower the energy barrier for the nucleation of extended network materials. According to the classical crystal nucleation theory, the free energy associated with the formation of a spherical crystal has a negative bulk contribution and a positive surface contribution, the latter opposing the crystal growth.[47] The presence of cells provides the system with a scaffold for the crystal growth, thus reducing the need to create a new surface and lowering the crystallization energy barrier.[48] Although classical nucleation theory refers to crystalline materials, experimental evidence in biomineralization, especially in biological and biomimetic systems, shows that crystal formation may pass through an amorphous phase that serves as a precursor to the subsequent crystalline structure.[49] The second driving force arises from electrostatic interactions between the cell surface and the MOF/COF/HOF precursors. In this context, the isoelectric point (*i.e.*, the pH at which the cell carries no net electrical charge[50]) and the synthesis environment (*e.g.*, pH, ionic strength) together determine the net cell surface charge during synthesis, which is commonly described by the zeta potential (ζ-potential).[50] A large positive or negative value of the cell ζ-potential (*i.e.*, $>+30$ mV or <-30 mV) will therefore indicate that the cell carries a large positive or negative net charge in the synthetic environment.[51] Similarly, the net charge of the MOF/COF/HOF precursors in the synthetic environment is determined by their chemical nature (*e.g.*, charge of the metal cations and pK_a of an organic ligand). For MOFs, the role of electrostatic interactions between biomacromolecules at the cell surface and framework precursors in porous framework nucleation and growth has been extensively discussed based on *ex situ* observations, whereas for HOFs and COFs the corresponding mechanistic details require further understanding. In fact, research on MOF biomimetic mineralization and biomacromolecule encapsulation has revealed that the presence of surface-exposed charged functional groups reduces the ζ-potential, thus inducing local supersaturation of oppositely charged precursors and ultimately triggering MOF nucleation.[34,52–54] Specific cell membrane components, such as negatively charged glycoproteins, peptidoglycans, and carbohydrates, promote electrostatic interaction between the cell and the MOF metal precursors.[34,52–55] These interactions are recognized as the main variable driving the rapid formation of amorphous MOF layers on biomacromolecules as well as on the outer surfaces of cells and viruses.[34,52–54] This amorphous phase can subsequently transform into crystalline materials.[16,56]

It is important to note that while electrostatic interactions and heterogeneous nucleation are widely suggested to be the primary driving forces for the framework shell formation, direct *in situ* experimental data elucidating the kinetics of framework growth on living cell surfaces are currently lacking. Nevertheless, there are observations supporting the assumption that mechanistic insights derived from protein systems may be extended to cells. In particular, the ability of charged proteins to promote the framework nucleation has been reported as a size-independent phenomenon, consistent with a mechanism governed primarily by interfacial charge density and local coordination chemistry rather than by the dimensions of the biomolecule used as the nucleation seed.[52–54,57] Conceptually, this mechanism is consistent with nucleation strategies developed for synthetic surfaces, on which charged, self-assembled layers are engineered to control the growth of framework-based films; for example, in layer-by-layer (LbL) approaches, self-assembled monolayers provide carboxylate interfaces that enable the formation of a homogeneous MOF film.[58,59] Systems that are conceptually closer to cellular interfaces are protein and fatty acid films: these have been shown to act as effective nucleating systems for different MOF coatings.[60,61] These observations collectively support the notion that charged biomacromolecules, either as individual entities or as densely packed biomolecular interfaces, can induce framework nucleation and growth. However, the direct experimental validation that these molecular-level models accurately describe the formation of abiotic shells on living interfaces remains a significant challenge, primarily due to dimensional constraints. For instance, while time-resolved small angle X-ray scattering (SAXS) is an advanced technique to investigate the

nucleation and early growth of frameworks around proteins, the micrometric size of cells falls outside the observable scattering range of conventional SAXS setups.[54,57] Consequently, the development of adaptable *in situ* characterization techniques capable of bridging the length scale between molecular nucleation and cellular dimensions is urgently needed to move beyond extrapolated models and fully clarify the mechanistic details of cell encapsulation.

When the target cell exhibits a low surface charge density, the spontaneous and rapid formation of a continuous coating is more challenging. This limitation can be overcome by electrostatically adsorbing a charged capping agent onto the cell surface (*e.g.*, PDADMAC: poly(dimethyl diallyl ammonium chloride) (+)/PAA: polyacrylic acid (−)),[62] to synthetically modify the ζ-potential of the cell surface. The abundance of charged groups on the precoated cells, in the presence of the MOF precursors, accelerates the deposition of the abiotic shell around the cell surface.[62]

We note that rapid formation of the cell coating is often a crucial condition in maximizing cell viability during encapsulation processes: upon the rapid shell formation, it is possible to minimize cell exposure to metal cations, toxic linkers, and non-physiological pH conditions. In contrast, unoptimized coating protocols that prolong cell exposure to such non-physiological environments typically result in cell damage and loss of viability.[23,63]

An additional limitation of the one-pot encapsulation strategy is its limited capability to produce shells with controlled thickness and homogeneity across different cell types. For example, the reported cells and zeolitic imidazolate framework-8 (ZIF-8) composites (cell@ZIF-8) show different ZIF shell thicknesses. In general, customized protocols are needed for specific cell batches; this includes optimization depending on cell types, cell density, and the specific media used.

Multi-step encapsulation strategy

Brinker *et al.*[64] have developed a versatile nanoparticle-based cell coating technique, which can be applied to a variety of abiotic materials, including ceramics (*e.g.*, SiO_2 and Fe_3O_4) and MOFs (*e.g.*, MIL-100 and ZIF-8). This approach relies on the electrostatic interactions between proteins on the surface of cells and the nanoparticles (NPs). Typically, NP–cell interactions lead to the accumulation of NPs around the living cell, followed by particle internalization through phagocytosis or micropinocytosis processes (Fig. 3b).[64] Such interfacial interactions between NPs and cells suggest that NPs could be used for cellular encapsulation if the internalization mechanisms of NPs are suppressed. Internalization pathways can be suppressed by promoting inter-particle binding through supramolecular interactions. Therefore, unlike the biomimetic mineralization approach, in the multi-step strategy, the MOF precursors are premixed in the absence of the targeted cell, yielding a colloidal solution of MOF NPs. Then, the cells are added and incubated in a colloidal suspension of pre-synthesized MOF NPs with the addition of tannic acid (an additive that promotes interparticle binding). Non-covalent interactions between the cellular membrane and NPs (*e.g.*, metal–phosphate) promote the accumulation of those particles around the cell wall. Tannic acid enables a strong multivalent metal–phenolic complexation process, causing interparticle binding. This process yields a continuous coating of NPs around individual cells. By engineering the process of NP adsorption onto cells and selecting the appropriate additive for interparticle binding, internalization of MOF nanoparticles can be successfully inhibited, enabling the formation of a protective abiotic coating based on MOF NPs.

We have thus far described the fundamental criteria and general approaches to cell coating. In the following sections, we will further explore how different cell surface properties govern the affinity between cells and abiotic coatings.

Type of cells

All living cells encode their genetic information with DNA and are encased by a semipermeable lipid bilayer – termed the cytosolic membrane in prokaryotes and the plasma membrane in eukaryotes. Prokaryotes and eukaryotes differ in several fundamental aspects. For example, eukaryotic cells have a nucleus in which the DNA is separated from the cytoplasm, whereas prokaryotic cells lack a nuclear envelope. Prokaryotic cells are typically smaller and simpler than eukaryotic cells (*e.g.*, prokaryotic cells do not contain cytoplasmic organelles or a sophisticated cytoskeleton), and their genomes are smaller and less complex.

Cells can further be classified depending on whether a cell can exist in its single-celled form, like microorganisms, or only in tissues of multicellular organisms, like most higher eukaryotes. Microorganisms, including bacteria, archaea, protozoa, algae, or fungi, produce cell walls in addition to their cell membranes. Cell walls serve as outer protective layers for many microorganisms and some multicellular organisms (*e.g.*, plant cells). Beyond its protective role, the cell wall – composed of diverse biopolymers – offers structural cohesion. The specific composition and architecture of the cell wall vary between species and will be discussed in more detail below. Regarding synthetic encapsulation methods, these outermost cell components act as the primary interface for the MOF, HOF, or COF precursor/particle crystallization/accumulation, guiding the formation of the external abiotic layer at the bio-interface.

Bacteria and their cell surface

Bacteria are single-celled prokaryotic microorganisms. Depending on the composition and structure of their membranes and cell walls, bacteria are differentiated between Gram-negative and Gram-positive bacteria.[65]

Gram-negative bacteria are surrounded by two membrane bilayers, the inner (cytoplasmic) and the outer membrane, separated by a space termed the periplasm. The periplasm consists of a thin peptidoglycan layer and provides a distinct reducing environment, which allows more efficient and diverse mechanisms of protein oxidation, folding, and quality control.[66] The outer membrane of Gram-negative bacteria is an asymmetric

bilayer with an inner leaflet consisting of phospholipids and an outer leaflet consisting of lipopolysaccharides (LPSs).[67] Since LPSs are partially phosphorylated, the phosphate group confers a net negative charge.[68] The most prominent example of a Gram-negative bacterium is *Escherichia coli* (*E. coli*). *E. coli* colonizes the human and mammalian intestinal tract, and it is used as a model organism of choice when it comes to DNA cloning and expression of recombinant genes in the field of molecular biology and biotechnology.[69] Core advantages of this bacterium are simple and cheap cultivation conditions, fast growth, and well-established genetic engineering tools. For these reasons, *E. coli* is frequently chosen as the benchmark for novel technologies and was also among the first bacteria used in MOF encapsulation experiments.[70] Another relevant example of Gram-negative bacterium is *Pseudomonas putida* (*P. putida*), a solvent-tolerant bacterium that can be used as a biocatalyst in two-phase fermentation systems for the synthesis of fine chemicals.[71] Both examples show negatively charged surfaces under neutral or slightly acidic conditions. For example, different *E. coli* strains exhibit varying ζ-potentials ranging from -4.9 to -33.9 mV in 150 mM phosphate-buffered saline (PBS) buffer at pH 7.4.[72] For *P. putida*, ζ-potentials were found to be typically close to -30 mV under slightly acidic conditions (*e.g.*, -27.4 mV in 1 mM NaCl);[73] -30 mV in 10 mM KNO_3 at pH 6.2.[71]

In contrast to Gram-negative bacteria, the cell wall of Gram-positive bacteria consists of a thick peptidoglycan layer that surrounds the cytoplasmic membrane, and the peptidoglycan is decorated with teichoic acids, polysaccharides, and proteins.[74] Since teichoic acid is negatively charged, the cell surfaces of Gram-positive bacteria also exhibit a negative charge.[75] Examples of Gram-positive bacteria are *Lactobacillus acidophilus* (*L. acidophilus*), *Staphylococcus aureus* (*S. aureus*), and *Moorella thermoacetica* (*M. thermoacetica*). *L. acidophilus* CRL 640, a Gram-positive bacterium, exhibits a ζ-potential of approximately -45 mV.[76] A direct comparison of the ζ-potential of *E. coli* and *S. aureus* was given, for example, by Oh *et al.*, and it was calculated to be -37.1 mV and -12.7 mV, respectively.[77]

In conclusion, we note that despite the differences in structure and composition of the cell walls of Gram-negative and Gram-positive bacteria, bacteria typically display a negative surface charge under physiological conditions.[78]

Eukaryotes and their cell surface

Eukaryotic cells display a diverse range of surface structures, which serve critical roles in maintaining cell integrity, regulating interactions with the environment, and mediating biochemical processes. This section will explore the distinct characteristics of fungal, mammalian, and plant cell surfaces, illustrating their varied compositions and functions.

Fungal cells have cell walls made up of glucans, chitin, and glycoproteins. In most fungal species, cell walls are layered. The innermost layer typically consists of a core of covalently attached, branched (1,3)-β glucan with 3 to 4% interchain and chitin, and these components assemble into fibrous microfibrils, which provide the cell with the strength required to withstand the substantial internal pressure exerted by the cytoplasm and membrane.[79] The outer layers of the wall tend to be more heterogeneous and tailored to the physiology of particular fungi. In *Saccharomyces cerevisiae* (*S. cerevisiae*), (1,3)-β glucan and (1,6)-β glucan are linked to mannoprotein in the outermost parts of the cell wall, which is thought to control porosity and thus mass transfer across the cell wall.[80] The yeast surface is charged negatively due to the presence of phosphates in mannoproteins.[81] ζ-Potential values of the *S. cerevisiae* cell surface depend on the growth phase and on aerobic or anaerobic cultivation conditions: ζ-potentials dropped at later growth phases (from -10 to -20 mV) and also under anaerobic conditions (from -18 to -26 mV).[82] Single-cell measurements revealed a correlation between the presence of dead cells and reduced ζ-potentials, likely resulting from cell wall damage. Additionally, *S. cerevisiae* was observed to release significant amounts of acids into the culture supernatant, which further contributed to the decrease in ζ-potentials. Similar findings were reported by Rogowska *et al.*[83] While the ζ-potential value decreased from -3 to -18 mV in the 2–6 pH interval, values ranging from -19 to -20 mV were measured for pH > 7.[83]

Plant cells have walls that are arranged in layers and contain cellulose microfibrils, hemicellulose, pectin, lignin, and soluble protein, whereas the exact composition strongly depends on the cell type.[84] In general, these components are organized into three major layers: the innermost secondary cell wall (formed only in specialized, differentiated plant cells), the primary cell wall, and the outermost middle lamella. The secondary cell wall is built from three layers, typically referred to as S1, S2, and S3, and mostly contains cellulose, hemicellulose, and lignin. The primary cell wall is the thickest layer and contains similar components, but more pectin, than the secondary cell wall. The middle lamella is mainly composed of pectic polysaccharides, lignin, and a small amount of proteins and serves as a cementing layer between the primary walls of adjacent cells.[85] For research purposes, so-called protoplasts are often used, which are spherical cells whose cell wall has been removed by mechanical means or digestive enzymes.[86] Removal of the cell wall leaves the protoplast surrounded and protected by the plasma membrane only. Even though protoplasts are usually more sensitive to extracellular stresses than their native counterparts, they exhibit diverse advantages, *e.g.*, simplified handling of single cells, ease of genetic manipulation, and use in screening experiments and single-cell microscopy. ζ-Potentials have also been measured for diverse plant cell protoplasts, *e.g.*, from barley leaf, tobacco leaf, and *Rauwolfia serpentina* cultured cell protoplasts,[87] and their surfaces typically exhibited a negative ζ-potential ranging from -6 to -28 mV.

Mammalian cells, unlike fungi and plant cells, lack cell walls. Instead, mammalian cells are protected by a dense gel-like meshwork abundant in carbohydrates, known as the glycocalyx, which overlays their plasma membrane.[84] The glycocalyx constitutes a physical barrier for nanoparticles like pathogens to enter the cell, and it consists of various proteoglycans, glycosaminoglycans, glycolipids, and plasma proteins, which are important for cellular adhesion and signaling. The absence of cell walls makes mammalian cells more sensitive to

Table 1 Experimental surface net charges (ζ-potentials) of different cells

Types of cells	ζ	Exp. conditions	Ref.
E. coli	−4.9 to −33.9 mV	1 mM NaCl	91
P. putida	−74.8 to −27.4 mV	1 mM NaCl	73
S. aureus	−37.1 mV	1 mM KCl	77
L. acidophilus	−45 mV	1 mM NaCl, pH 7.4	76
S. cerevisiae	−3 to − 26 mV	5 mM $NaNO_3$ at pH range 2–11	83
Tobacco leaf protoplasts	−25 mV	0.01 M KCl, 0.6 M sucrose, 6.7 mM sodium phosphate buffer (pH 5.8)	87
Barley leaf protoplasts	−18 mV	0.6 M sorbitol, sodium phosphate buffer (pH 5.6)	92
HeLa	−19.4 ± 0.8 mV	PBS (1.7 mM KH_2PO_4, 5.2 mM Na_2HPO_4, 150 mM NaCl)	89
Erythrocytes	−31.8 ± 1.1 mV	PBS (1.7 mM KH_2PO_4, 5.2 mM Na_2HPO_4, 150 mM NaCl)	89
Diverse fixed human cell lines	−50 to −30 mV	Fixed cells resuspended in ultrapure water	90

changes in turgor pressure and shear forces.[88] The surface charge of mammalian cells is typically negative at physiological pH. At pH 7.4, the ζ-potential for different types of cells showed variations over a wide range and was equal to −19.4 ± 0.8 mV for HeLa cells and −31.8 ± 1.1 mV for erythrocytes.[89] The difference could presumably be attributed to the differences in the biochemical composition of the cell plasma. Exposure to 45 °C for 30 min induced apoptosis‡ and necrosis¶ in 65% of the cells and decreased the ζ-potential from −19 mV to −25 mV. The authors argue that this can be attributed to the presence of larger amounts of the phospholipid phosphatidylserine on the cell surface, which is considered to be an early marker of apoptosis. In another study, ζ-potentials of different fixed cells were measured. Cell fixation is achieved by treating cells with fixatives (*e.g.*, paraformaldehyde), which quickly kill the cell, prevent autolysis, and preserve the cell structure as faithfully as possible compared to the living state.[90] Fixed cells can then be applied to different staining and microscopy analyses. The cell surface charges of CytoRich Red-fixed cells were found to be lower (−30 mV to −50 mV) than those reported for living cells (summarized in Table 1).[90]

Having disclosed different classes of cells and examined their surface composition and charge, we will next discuss various methods to study their viability. This toolkit of knowledge is crucial for assessing abiotic coatings for cells and guiding the future development of this research field.

Cell viability methods

The viability of cells reflects their ability to sustain metabolic activity and structural integrity over a certain time frame. Typically, cell viability is defined as the number of actively proliferating or dividing cells in a sample or population;[93] it is therefore an important parameter in many biological and biomedical settings. In the context of cell encapsulation, viability assays are commonly used to determine cell survival after encapsulation, or to assess the resistance of encapsulated cells to toxic chemicals (*e.g.*, antibiotics) or physical stressors such as elevated temperature, extremes of pH, or radiation.[17,18,22]

Cell viability assays can be classified into direct measurements that quantify the number of dividing cells (*e.g.*, plating assays) or indirect assays, which measure various parameters as a proxy of cell viability (*e.g.*, conversion of dyes or quantification of metabolic key intermediates). Due to the complexity of cells and their underlying metabolism, it may not always be straightforward to distinctly quantify cell viability, and the outcome likely depends on the assay that is used. The ''culturability‖'' of cells remains the preferred definition of cell viability.[94] Numerous techniques are available to assess cell viability (summarized in Table 2), including (i) cell counting of colony-forming units, (ii) membrane permeability assays, (iii) metabolic activity tests, (iv) luminometric adenosine triphosphate (ATP) measurements, (v) mitochondrial function assays, and (vi) inclusion dye evaluations.[43]

Cell counting methods

Counting of viable cells is a classical technique in microbiology and relies on the ability of cells to grow and divide on a nutrient-rich medium. When a cell suspension is spread onto a solid surface, only proliferating cells undergo binary fission and eventually form colonies of visible size referred to as colony-forming units (CFUs). CFUs therefore provide a direct readout of actively dividing cells in a sample. However, it should be noted that a variety of Gram-positive and Gram-negative bacteria, including *E. coli* (EHEC strains), can enter a dormant state in which cells remain alive and show metabolic activity, but do not show significant growth. Such a state was observed in response to starvation, at extremes of temperature and non-physiological oxygen concentrations. Wei *et al.*[95] and Yuan *et al.*[21] determined the viability of bacterial strains (*L. acidophilus* and *Bifidobacterium longum subspecies infantis* (*B. infantis*)[95] and *Bifidobacterium breve* (*B. breve*))[21] encapsulated in ZIF-8 biomineralized compartments by viable cell counting after removal of the MOF shell using ethylenediaminetetraacetic acid (EDTA). The strains showed diverse viabilities: while CFUs of *L. acidophilus* and *B. breve* were only slightly reduced compared to unencapsulated cells, the viability of

¶ Necrosis is a passive, accidental cell death triggered by environmental perturbations, leading to the unregulated release of inflammatory cellular components.[216]

‖ Culturability is defined as the ability of a single cell to yield a population discernible by the observer, usually a visible colony on the surface of a nutrient agar plate. Such culture-based techniques have been in use for many decades, have generated a coherent body of information, and have a proven track record in protecting public health at relatively low cost.[147,217]

Table 2 Comparison of cell viability assays

Assay	Principle	Advantages	Disadvantages	Types of cells	Framework	Ref.
Agar plating	Detects viable cells based on colony formation on solid media	– Simple, rapid, and low-cost – Applicable to a broad range of microorganisms – Provides direct quantification of viable cells in a sample	– Limited to organisms that form isolated colonies – Time-consuming – Not suitable for multicellular cell types – Many cells may be viable but non-culturable	Bacteria (*L. acidophilus; B. infantis*)	ZIF-8	95
				Bacteria (*B. breve*)	ZIF-8	21
				Bacteria (*E. coli*)	ZIF-8	96
Membrane permeability assays	Assesses the permeability of a substance or substrate across the cell membrane	– Rapid and highly sensitive – High specificity of dyes for nucleic acids – Compatible with flow cytometry and fluorescence microscopy	– Matrix components may affect enzyme activity – Apoptotic cells can retain membrane integrity – Membrane integrity can be influenced by growth conditions – Limited penetration of SYTO9 into Gram-negative bacteria	Bacteria (*P. putida*)	MIL-100(Fe)	108
				Bacteria (*B. breve*)	ZIF-8	21
				Yeast (*S. cerevisiae*)	Cu-MOP	109
Luminometric ATP assays	Measures intracellular ATP levels	– Rapid with sensitive and robust signal output – High specificity – Enables real-time analysis – Suitable for high-throughput screening	– ATP levels can vary between different cell types or microorganisms – ATP concentrations are dependent on growth conditions	Mammalian cells (HeLa, A549, MCF-7, HLF, MCF-10A, RAW264.7, and B16 cells)	ZIF-8	123
				Mammalian cells (human embryonic kidney, lung bronchial epithelial, and lung carcinoma epithelial cells)	MOF-801	124
				Mammalian cells (HeLa)	ZIF-8, MIL-100(Fe), UiO-66-NH_2, MET-3-Fe	64
Metabolic assays	Measures the activity of cellular metabolic pathways	– Simple, rapid, and cost-effective – Applicable to a wide range of cell types	– Results can be influenced by the physiological state of cells (*e.g.*, dormancy) – Susceptible to interference from reducing agents and ROS scavengers – Cu(II)-containing complexes may affect absorption readings	Mammalian cells (neural stem cells)	HOF	33
				Mammalian cells (sperm cells)	ZIF-8	114
				Mammalian cells (CHO-K1)	Mn-based MOF	115
				Mammalian cells (breast cancer cells MDA-MB-231)	ZIF-8	116
				Bacteria (*E. coli*)	ZIF-8	70
				Yeast (*S. cerevisiae*)	ZIF-8	12
				Bacteria (*Micrococcus luteus*)	ZIF-8	12
				Bacteria (*E. coli*)	ZIF-90	97
Flow cytometry assays	Detects changes or alterations in the cell membrane	– High-throughput compatible – Does not require staining – Sensitive ratiometric probes available	– Requires expensive equipment – Some stains are sensitive to EDTA – Light-sensitive reagents	No examples yet		

Table 2 (*continued*)

Assay	Principle	Advantages	Disadvantages	Types of cells	Framework	Ref.
		– Compatible with a wide range of fluorescent dyes	– Time-consuming procedure			
Mitochondrial assays	Measures mitochondrial membrane integrity or membrane potential	– Provides insights into the cellular energy status	– Requires live cells (fixation is not possible)	No examples yet		
Dye exclusion assays	Assesses cellular membrane integrity	– Simple and rapid – Compatible with a variety of dyes	– Prone to over- or underestimation of cell numbers – Requires preparation of cell suspensions – Results can be affected by the physiological state of the cells	No examples yet		

B. infantis decreased by 2–4 orders of magnitude. For *B. breve*, CFU values after the dissolution of the MOF shell were comparable to a control using free cells.

Luzuriaga *et al.*[96] investigated the viability of *E. coli* cells encapsulated in a polycrystalline ZIF-8 shell. To determine viability, the ZIF-8 shell was removed by treatment with 500 mM sodium acetate buffer, pH 5, and the cells were spread on agar plates to test their ability to form visible colonies. However, no growth was observed, indicating that the cells were deactivated during the encapsulation and/or immobilization with the ZIF-8 shell.

Optical density (OD) measurements provide an alternative, inexpensive, and rapid method for qualitatively and quantitatively measuring positive variation in the cell number (cell growth) in a liquid medium. This method is based on the principle that cells scatter visible light; thus, a UV-vis spectrophotometer is typically used with a monochromatic wavelength at 600 nm. The extent of the scattered light, and thus the measured variation in the transmittance, is proportional to the density of cells (the number of cells per unit of volume) in a sample. This method was used by Gan *et al.*[16] to assess the growth of *S. cerevisiae* cells released from ZIF-8- and ZIF-C-based shells with a thickness of 60 ± 20 nm. The released cells were inoculated into a liquid, nutrient-rich growth medium, and their proliferation was tracked by measuring the optical density at 600 nm. Although this technique does not provide a direct measure of cell viability in the ZIF composite, it revealed that coated cells exposed to external stressors had a shorter lag phase before the onset of exponential growth compared with uncoated cells.

Li *et al.*[97] showed that *E. coli* cells encapsulated in ZIF-90 can be released and maintain viability. After removal of the ZIF shell and transfer to a nutrient-rich LB medium, bacterial growth was restored, although a delay in the onset of exponential growth was observed.

Ji *et al.*[98] used cell counting to determine the growth of the photosynthetic anaerobic bacterium *Moorella thermoacetica* enclosed in MOF-shells with a thickness of 1–2 nm. The cells maintained full viability, with growth curves for both encapsulated and free cells being identical. The authors used super-resolution 3D-structured illumination microscopy (3D SIM) to directly visualize cell division of MOF-enclosed cells. The growth of encapsulated bacteria in an oxygen-containing atmosphere was found to be faster than that of free cells.

Flow cytometry is a technique that allows for the simultaneous multi-parametric analysis of the physical and chemical characteristics of single cells suspended in a liquid medium. Cells are first singularized before being subjected to a laser beam. As these cells pass through a laser beam, they scatter light and, if labeled with fluorescent markers, emit a fluorescence signal.[99] Scattered and emitted light is detected and analyzed for various properties, such as size, granularity, and the presence of specific molecules, providing detailed insights into individual cellular characteristics. These parameters offer insights into the cell distribution and viability within the analyzed cell population.

In addition to scattering-based measurements, labeling of cells with a variety of fluorescent dyes that can be excited by the

laser greatly extends the utility of flow cytometry. For example, the ratiometric membrane probe F2N12S** produces a green fluorescence ($\lambda_{excitation}$ = 405 nm; $\lambda_{emission}$ = 530 nm) when bound to the membrane of healthy cells. When cells undergo apoptosis, a change in the membrane potential (*i.e.*, the difference in the electric potential between the inside and outside of the cell) results in a red shift of the emission wavelength to 585 nm. The ratio of the two emission maxima allows for a quantitative and qualitative estimation of the cell viability. Flow cytometry can be combined with various dyes and staining techniques, as elaborated in detail by Kessel *et al.*[100] In the following section, we discuss frequently employed methods in the context of cell encapsulation and coating.

Membrane permeability assays

Membrane permeability assays are based on alterations in membrane integrity that occur in dying or dead cells. Cell viability can be assessed by measuring the ability of certain molecules to penetrate the cell membrane.[101] This method involves fluorescent or colorimetric dyes that interact with intracellular components inside the cells. Typically, these assays are carried out as live/dead staining by combining exclusion dyes, which penetrate cells with compromised membranes, with inclusion dyes that can pass through intact membranes. However, membrane permeability does not necessarily reflect cellular metabolic activity, as membrane integrity can also be affected by growth conditions, such as growth phase or environmental stress, potentially leading to under- or overestimation of cell viability in some cases.[102] In mammalian cells, membrane permeability assays are often complemented by additional methods to distinguish between necrosis and apoptosis, as these processes play distinct roles in cellular responses. Apoptosis is a highly conserved, controlled, and programmed cell death.[103] In contrast, necrosis is an uncontrolled process that results from external damage, such as toxins or environmental stress, and is associated with pathological responses.[104] Importantly, the plasma membrane integrity is lost in necrotic cells, but is generally preserved during early stages of apoptosis; consequently, apoptotic cells may not be detected by many exclusion dyes.[105] This distinction is crucial in the choice of staining methods.[105]

Propidium iodide (PI) is a widely used membrane permeability probe that functions as an exclusion dye to stain dead cells. PI cannot enter living cells with intact plasma membranes, but readily penetrates dead or dying cells with compromised membrane integrity. Once inside the cells, the positively charged PI stoichiometrically intercalates with double-stranded nucleic acids. Upon excitation $\lambda_{excitation}$ = 488 nm, the PI-bound DNA complex exhibits fluorescence at $\lambda_{emission}$ = 550 nm, enabling the quantification of inactive cells *via* fluorescence microscopy or flow cytometry. However, depending on the growth state, this method may yield a high fraction (up to 40%) of false positives, particularly during the early exponential growth phase of the cells. This increased uptake of PI by viable cells was linked to a temporary instability of the cell membrane due to cell wall reconstruction during cell division and growth, which may allow the dye to penetrate viable cells.[106]

Exclusion dyes are commonly used in conjunction with inclusive counterstains that have non-overlapping fluorescence spectra and can penetrate intact membranes of living cells. A frequently employed stain is SYTO9, which can enter both living and dead cells and exhibits enhanced fluorescence when bound to DNA ($\lambda_{excitation}$ = 485 nm; $\lambda_{emission}$ = 498 nm) or RNA ($\lambda_{excitation}$ = 486 nm; $\lambda_{emission}$ = 501 nm).[102,107] SYTO9 is frequently used in combination with PI for live/dead staining since both dyes have distinct fluorescence profiles. Furthermore, PI has a higher affinity for DNA than SYTO9; thus, in situations where both dyes are present inside a cell, SYTO9 will be displaced.[102] One known constraint of SYTO9 dyes is their limited ability to penetrate the cell walls of Gram-negative bacteria, which depends on their composition or active export from the cell.[102]

Permyakova *et al.*[108] used fluorescence staining with SYTO9 and PI to discriminate living and dead *P. putida* cells encapsulated in MIL-100(Fe). This staining method allowed the qualitative evaluation of the living/dead cell ratio when coated with a MIL-100(Fe) exoskeleton. Under optimized conditions, the large majority of the encapsulated cells displayed intact cell membranes.

Using cell counting, Yuan *et al.*[21] showed that the ZIF-8 coating moderately reduced the viability of *B. breve* cells. However, live/dead staining with PI and SYTO9 indicated pronounced damage to the cell walls after removal of the ZIF-8 shell. This damage was also evident from growth curves recorded by optical density: following inoculation with these cells of growth medium, the onset of exponential growth was significantly delayed when compared to an untreated control sample of *B. breve* cells. This study highlights the importance of employing a combination of different viability methods to obtain a more comprehensive understanding of the effect of encapsulation methods on cell viability.

An alternative counterstain that detects living cells or early apoptotic cells is Acridine Orange, which enters intact membranes and causes green fluorescence upon binding to DNA ($\lambda_{excitation}$ = 502 nm, $\lambda_{emission}$ = 525 nm). A drawback of this dye is the necessity of washing steps to remove the unbound dye, since the fluorescence intensity is not notably enhanced upon binding to DNA. Qin *et al.*[109] used a combined ethidium bromide/acridine orange stain to assess the effect of heat, reactive oxygen species, UV-radiation, and proteases on *S. cerevisiae* cells encapsulated in a copper metal–organic polyhedron (MOP) hydrogel. In this study, the authors showed by fluorescence microscopy that encapsulation decreased the percentage of dead cells after exposing the cell@MOP composite to the aforementioned physical, chemical, and biological stressors.

Metabolic assays

Metabolic assays are widely used to assess cell viability. Using these methods, viable cells with intact metabolism produce a

** F2N12S: *N*-[[4′-*N*,*N*-diethylamino-3-hydroxy-6-flavonyl]-methyl]-*N*-methyl-*N*-(3-sulfopropyl)-1-dodecanaminium is a fluorophore which is highly sensitive to the lipid order of lipid bilayers.[218]

measurable fluorimetric or colorimetric signal upon the addition of specific substrates, which can be correlated to the number of living cells. Conversely, dead or dying cells with compromised metabolism exhibit decreased or no conversion rates at all. Such assays can be conducted in conventional spectrophotometers or plate readers that are routinely available in biochemical or biological laboratories and thus can also be used in a high-throughput format.[110]

An excellent indicator for cell viability is the presence of reducing nicotinamide cofactors (NADH or NADPH), which are metabolic key components. Several selective tetrazolium dyes are available to indirectly assess the concentration of these cofactors through the activity of intracellular, NAD(P)H-dependent redox enzymes. MTT (3-(4,5-dimethylthiazol-2-yl)-2,5-diphenyltetrazolium bromide) is a widely used positively charged substrate that can easily penetrate through cell walls.[110] It is converted through an unknown NAD(P)H-dependent metabolic process to insoluble formazans, which can be quantified spectrophotometrically at 570 nm after a solubilization step, providing a quantifiable measure of cell viability. Derivatives of MTT, such as MTS (3-(4,5-dimethylthiazol-2-yl)-5-(3-carboxymethoxyphenyl)-2-(4-sulfophenyl)-2*H*-tetrazolium), XTT (2,3-bis-(2-methoxy-4-nitro-5-sulfophenyl)-2*H*-tetrazolium-5-carboxanilide) or WTS (2-(2-methoxy-4-nitrophenyl)-3-(4-nitrophenyl)-5-(2,4-disulfophenyl)-2*H*-tetrazolium), have been developed with negative sulfone groups and release soluble formazan derivatives.[111] However, the dyes cannot cross the cell membrane due to their net negative charge. To overcome this, electron carriers such as PMS (5-methyl-phenazinium methyl sulfate) or PES (phenazine ethyl sulfate) are added to the assay. These carriers facilitate formazan reduction by shuttling electrons between the cytoplasm and the dye, producing a soluble formazan product that can be measured *via* spectroscopy.[112]

We note that under certain growth conditions, cells may undergo a state of dormancy in which they show greatly reduced metabolic activity but maintain viability. Therefore, assays require diligent control of the reaction conditions, including the concentration of the dye and the incubation time. The outcome of the assay can be influenced by the physiological state or the microbial strain being used. Tetrazolium-based assays are prone to a variety of interferences, as reviewed by Grabowiecka and coworkers.[113] For example, unspecific reduction of MTT in the growth medium and the presence of radical scavengers can interfere with the assay and affect the result. Also, the presence of copper(II)-containing complexes can influence the original absorption of formazan.[113] We note that shifts induced by the presence of cations may be of particular relevance in experiments with cell encapsulation into MOFs and other coordination compounds (*e.g.*, MOPs). Yu *et al.* used the commercially available CCK-8 (cell counting kit-8) viability assay to assess cell viability of HOF-encapsulated neural stem cells.[33] This colorimetric assay is based on the reduction of the tetrazolium salt WST-8 (2-(2-methoxy-4-nitrophenyl)-3-(4-nitrophenyl)-5-(2,4-disulfophenyl)-2*H*-tetrazolium, monosodium salt), which is converted to a water-soluble formazan derivative. In this case, encapsulation showed little effect on the biological activity of cells. The same assay was also used to determine the viability of "ZIFSpermbots", consisting of spermatozoa encapsulated in a ZIF-8 framework.[114]

Ohtani *et al.*[115] used the cell counting kit-8 to assess the viability of Chinese hamster ovary K1 cells (CHO-K1) in response to cyanide-bridged 2D coordination polymers (CPs) consisting of metal ions and networking metal complex lipids. The cells maintained more than 90% viability when challenged with 40 μM $NiCl_2$ but lost 50% viability in the presence of the metal complex lipid (*i.e.* 10 μM $(dabco\text{-}(CH_2)_{15}\text{-}CH_3)_2[MnN(CN)_4]$).

The tetrazolium derivative MTS (3-(4,5-dimethylthiazol-2-yl)-5-(3-carboxymethoxyphenyl)-2-(4-sulfophenyl)-2*H*-tetrazolium) has been used to determine the viability of ZIF-8-encapsulated breast cancer cell line (MDA-MB-231 cell), showing that the viability of coated cells was ~75% after incubation for 6 h.[116]

Calcein acetoxymethyl ester (calcein-AM) is another frequently used non-fluorescent metabolic marker that can passively cross the membranes of intact cells. Inside the cell, it is enzymatically hydrolyzed by unspecific esterases into the acidic, cell impermeable calcein ($\lambda_{excitation}$ = 494 nm; $\lambda_{emission}$ = 517 nm), resulting in a strong, green fluorescence.[117] Calcein-AM is frequently used as an indicator of metabolic activity and finds widespread application as an inclusion dye to visualize viable cells in live/dead fluorescence staining. Frequently, it is used in combination with PI. For example, Yu *et al.*[33] used a differential staining with the dyes PI and calcein-AM to visualize the viability of HOF-encapsulated neural cells. Similarly, a dual calcein-AM/PI live/dead staining was used to assess the viability of MOF-encapsulated cancer cells.[116] Chen *et al.* used a combination of the WST-8 dye and calcein-AM staining to show that "ZIFSpermbots", consisting of spermatozoa encapsulated in a ZIF-8 framework, remained largely viable inside the framework, while the cell growth was arrested.[114]

Yan *et al.*[70] determined the viability of *E. coli* cells encapsulated in ZIF-8 with the colorless probe fluorescein acetate (FDA). Upon metabolization, the chemical is cleaved by hydrolytic enzymes, thus releasing the highly fluorescent fluorescein. Enzymes facilitating this cleavage are unspecific esterases, lipases, or proteases.[118] In this study, the authors did not observe viability differences in encapsulated *E. coli* cells. Similarly, Chen *et al.*[119] used the FDA method in combination with CFU counting and growth curves to assess the viability of *E. coli* and *S. cerevisiae* following encapsulation by different ZIF-8 shells. Also, Falcaro and co-workers[12,120] used FDA to monitor the time-dependent viability of *S. cerevisiae* cells encapsulated in a β-galactosidase/ZIF-8 shell. In some cases, fluorescent proteins produced by the cells themselves have been utilized to assess cell activity in ZIF-90-coated cells. Li *et al.*[97] encapsulated *E. coli* cells that recombinantly produced the fluorescent reporter protein mCherry. However, protein expression had to be induced prior to MOF encapsulation, as the inducer (isopropyl β-D-1-thiogalactopyranoside, IPTG) could not permeate the molecular-sieving ZIF-90 shell. As a consequence, both viable and non-viable cells may exhibit fluorescence, and the fraction of encapsulated viable cells could not be determined.

A different viability assay is based on the quantification of intracellular ATP, the primary carrier of chemical energy in living cells. ATP is continuously synthesized and consumed as a result of various anabolic and catabolic processes, and its concentration is an indicator of intact cellular metabolism and physiology. At the onset of cell death, ATP levels typically decrease because cells lose their ability to replenish ATP. ATP levels can be quantified using commercial kits containing the enzyme firefly luciferase.[121] In these assays, cells are first lysed to release intracellular ATP, and the resulting lysate is mixed with a luciferase solution. Luciferase catalyzes the ATP- and O_2-dependent conversion of luciferin to oxyluciferin, producing a luminescent signal that correlates with the ATP concentration in the sample and thus overall cell viability. To ensure accurate ATP quantification, cells are lysed using detergents in the presence of ATPase inhibitors to prevent enzymatic ATP depletion. Several commercially available kits employ engineered, robust luciferase systems yielding luminescent signals stable for several hours. ATP assays are typically fast, with a workup procedure of a few minutes, and can be implemented in a high-throughput format, including 1536-well plate configurations.[110] Additionally, the ATP assay can detect as few as 20 cells, while the MTT assay requires the presence of a minimum of ~25 000 cells.[97] It is important to note that ATP concentrations can vary between different cell types and microbial strains and may also be influenced by the physiological state of the cell. Because ATP assays rely on enzymatic activity, careful consideration of media composition is required to avoid inhibition of luciferase. Overall, ATP assays offer a reliable and sensitive method for assessing cell viability.

A recently introduced variation of the ATP assay allows real-time assessment of viability. Here, a membrane-permeable pro-substrate of luciferin is added to the sample. Upon uptake, the pro-substrate is enzymatically converted to luciferin, which diffuses into the culture supernatant and is converted by luciferase to yield a luminescence signal.[122]

Previously, several commercially available ATP-quantification kits (CellTiter-Lumi Plus Luminescent Cell Viability Assay Kit and the CellTiter-Glo cell viability kit) have been used to monitor the viability of MOF-encapsulated mammalian cells[125] and to test the tolerance of various cell lines including the human cervical carcinoma cell line (HeLa), human lung adenocarcinoma cell line (A549), human breast cancer cell line (MCF-7), and mouse melanoma cell line (B16) in ZIF-8, which has been proposed for cryoprotective applications.[124] For example, ATP-based viability measurements indicated ~90% viability for mammalian cell lines such as HeLa, A549, human promyelocytic leukemia (HL-60), and mouse macrophage Raw 264.7 cells encapsulated in ZIF-8 and were also used to determine the pH- and UV-tolerance of the cells.[64]

Another class of assays used to investigate cell viability are mitochondrial assays. Mitochondria are eukaryotic organelles central to cellular energy metabolism. Through oxidative phosphorylation, mitochondria consume oxygen while producing ATP as the main metabolic energy carrier. The functional state of mitochondria can therefore serve as an indicator of cellular viability and can be assessed using dyes that specifically target mitochondria.[122] Commercially available mitochondrial membrane potential kits use cationic, lipophilic dyes (*e.g.*, JC-10), which accumulate in the mitochondria and form aggregates. In this state, JC-10 produces red fluorescence ($\lambda_{excitation}$ = 570–590 nm).[126] During apoptotic events, the dye diffuses into the cytoplasm, where it becomes monomeric, resulting in a shift in emission to 520–540 nm and the appearance of green fluorescence.[126] Alternatively, calcein-AM in combination with $CoCl_2$ has been used to assess the integrity of mitochondrial membranes. Calcein-AM is readily cleaved by intracellular esterases, producing fluorescence that is readily quenched by $CoCl_2$ in the cytoplasm. In intact cells, the fluorescence is retained within mitochondria, allowing selective evaluation of mitochondrial membrane integrity. Upon membrane damage, the dye diffuses into the cytoplasm, resulting in a loss of mitochondria-localized fluorescence.[126] Thus far, only a few studies applied mitochondrial assays to assess the viability of MOF-encapsulated cells. For example, Wang *et al.* demonstrated that the mitochondrial dye JC-1 can be used to quantify the mitochondrial membrane potential of mitochondria (Mito) encapsulated in ZIF-8 (Mito@ZIF-8).[127] While the membrane potential of the free mitochondria rapidly decreased after isolation, the Mito@ZIF-8 samples maintained a relatively stable membrane potential and sustained ATP production for 48 hours. These results show the potential of the JC-1 assay for viability assessment in encapsulated cells, offering a sensitive and quantitative approach that could expand the current tools for assessing eukaryotic cell viability. In particular, mitochondrial dyes like JC-1 can detect the early onset of cell death, often before the cell membrane is compromised. This assay is less influenced by factors such as the shape, size, or density of mitochondria, which can alter the fluorescence intensity in single-component assays.[128] However, researchers should carefully assess the potential barriers to implementation: these might primarily stem from the specific porous properties of the framework shells, which could restrict the diffusion of assay reagents. Additionally, the chemical instability of many frameworks (*e.g.*, ZIF-8) when exposed to acidic or phosphate-rich environments could be incompatible with typical standard metabolic assay protocols. Furthermore, the potential light scattering or background autofluorescence introduced by the porous shell could interfere with the precise ratiometric readings required for probes like JC-1.

Other exclusion dyes

Trypan blue staining is a commonly used technique to assess the live-to-dead cell ratio.[129] Addition of the trypan blue dye to a cell suspension results in the accumulation of the dye inside dead or dying cells with compromised cell membranes. Conversely, the dye cannot penetrate the cell membrane of intact cells, which remain unstained. The stained and unstained cells can be counted under a microscope using a cell counting chamber. Trypan blue staining is a simple and inexpensive technique that is commonly used in cell biology and immunology.[129] Other commonly used stains that target cytoplasmic structures include eosin, Congo red, and erythrosine B. Erythrosine B staining is

based on the ability of the dye to diffuse into the cytoplasm of cells with compromised membranes, where it binds to basic proteins. Viable cells remain unstained, whereas dead or dying cells appear pink. Congo red is a sulfonated azo dye that binds to amyloid proteins present in the cytoplasm.[130] Eosin, a derivative of fluorescein, is an acidic dye that binds to basic cellular components, primarily cytoplasmic proteins.[130] Upon binding, it retains a pink color. To date, none of these dyes has been applied to assess the viability of MOF-encapsulated cells.

The following section builds upon the basic principles of artificial spores, cell types, and viability assessment methods and summarizes current progress in materials and coating strategies, providing detailed insights into reported protocols.

Materials and coating methods

Initial studies on cell encapsulation focused on using sol–gel methods to prepare rigid cell exoskeletons of porous SiO_2 or TiO_2.[4,17,22,123] These archetypal oxide-based shells protect cells from mechanical stressors while allowing mass transfer between the environment and the encased cells. Although these oxides fulfilled key requirements such as permselectivity and durability, their chemical stability made controlled degradation challenging, especially without affecting cell viability. Interesting developments in engineering other inorganic nanoparticles, such as manganese dioxide, could be translated into protective shells, as MnO_2 NPs can be degraded *via* glutathione (GSH) exposure. However, further progress in this field is required to examine the pros and cons of MnO_2 for cell coating.[131] Thus, the intrinsic chemical robustness of inorganic NPs could significantly limit their use in specific biotechnological applications aiming at the controlled release of cells, such as cell therapy.

To address these challenges, current research focuses on the development of artificial coatings that meet all four criteria necessary for artificial spore formation (*vide supra*). A variety of natural and synthetic materials are under intense research for the fabrication of degradable exoskeletons under conditions that maintain cell compatibility. Examples include polysaccharide-based coatings such as starch, chitosan, and alginate, which can be enzymatically degraded,[132] making them strong candidates for cell therapy. In addition, recent studies have merged the properties of organic and inorganic materials in hybrid coatings. Caruso *et al.*[133] demonstrated the self-assembly of metal–organic coatings, utilizing Fe^{3+} and tannic acid, on *S. cerevisiae* cells. These metal–organic coatings are mechanically stable yet degradable on demand, thus meeting the criteria for artificial spore formation. The selection of appropriate building blocks allows control over chemical properties such as shell functionalization, self-assembly conditions, and degradability.

Building on these developments, three notable classes of microporous materials have emerged as promising options for encapsulating living cells and fragile biomolecules: MOFs, COFs, and HOFs.[31,33] MOFs consist of inorganic clusters linked by multitopic organic linkers,[35,36] while COFs and HOFs are assembled from organic compounds connected through covalent and hydrogen-bonding interactions, respectively.[93] By carefully selecting the molecular building blocks, the stability, porosity, crystalline phase, and chemical and structural properties of these materials can be fine-tuned.

The microporous nature of the coatings provides permselective barriers that allow for the transport of small molecules such as glucose and oxygen, while preventing contact between the cell membrane and cytotoxic macromolecules like enzymes (*e.g.*, trypsin and lyticase).[16] These coatings can also be degraded on demand using chemical stimuli, such as chelating agents or pH changes for MOFs,[31,56,134] or physical stimuli, such as light for HOF composites.[33]

Though post-synthetic modification methods have not yet been widely tested in this context, they have the potential to further expand the chemical versatility of these coatings.[114] Given the properties of MOFs, COFs, and HOFs, they represent promising materials for the development of artificial spore-like systems. Two main approaches have been used for fabricating cell@MOF and cell@HOF composites: (i) the one-pot coating strategy and (ii) the multi-step cytoprotective encapsulation strategy.[16]

Cells@shell: one-pot encapsulation

One-pot encapsulation of microorganisms: pioneering examples. The most extensively studied MOF for cell encapsulation *via* the one-pot strategy is the zeolitic imidazolate framework-8 (ZIF-8). This material is comprised of Zn^{2+} cations tetrahedrally coordinated by 2-methylimidazolate (mIM^-) linkers.[19] ZIF-8 can be synthesized under mild reaction conditions, such as aqueous media and room temperature. The topology of ZIF-8 can be tuned by modifying synthesis conditions such as precursor concentration, metal-to-ligand ratio, and the presence and type of macromolecules. For instance, the sodalite topology (**sod** ZIF-8) is an extended network with a pore aperture of 3.4 Å and pore diameter of 11.6 Å.[19] Other topologies with the same molecular formula, $Zn(mIM)_2$, can be accessed, including diamondoid (**dia** ZIF-8), katsenite (**kat** ZIF-8), and ZIF-L.[135] In addition, the self-assembly of Zn^{2+} and mIM^- in the presence of carbohydrates, proteins, and cells can lead to the formation of other crystalline materials with distinct chemical compositions.[136] For example, it was observed that other anions (CO_3^{2-} and OH^-), present in the solution, could replace some molecules of mIM^- to yield the formation of $Zn_2(mIM)_2CO_3$ (ZIF-C)[56] and $Zn_3(mIM)_4OH$ (ZIF-EC1), while other observed phases (*e.g.*, U12) are yet to be solved.[137] The crystalline arrangement (topology or phase) and the chemical composition influence the porosity, chemical stability, and hydrophobicity of a given MOF.[56,137,138] As a result, it was shown that different ZIF-based cell coatings will afford unique properties, as shown by Gan *et al.*[16] Nevertheless, all Zn-imidazolate-based systems can be degraded upon exposure to acidic conditions (pH $<$ 6), chelating agents such as EDTA, and certain buffer solutions.[139]

In 2016, Falcaro and co-workers reported the one-pot encapsulation of *S. cerevisiae* and *Micrococcus luteus* (*M. luteus*) within a ZIF-8 exoskeleton (Fig. 4a).[120] The cell coating was formed by

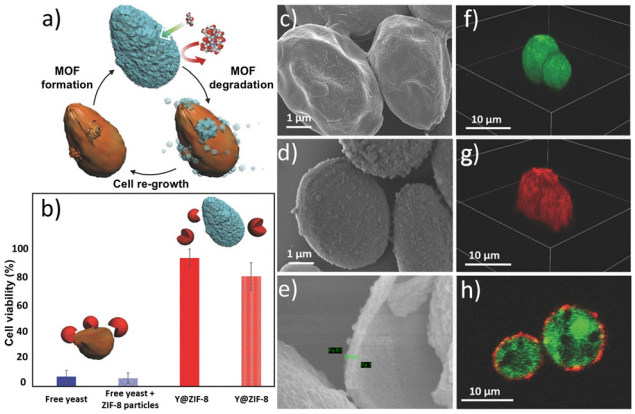

Fig. 4 Biomimetic mineralization of yeast cells within a ZIF-8 coating. The schematic of the encapsulation and release processes is shown in (a). The cell viability (b) of yeast (blue) and yeast plus free ZIF-8 particles (patterned blue) after exposure to lyticase for 3 h and of yeast released from yeast@ZIF-8 previously exposed to lyticase for 3 h (red) and 24 h (patterned red) demonstrates the protection offered by the MOF shell. The homogeneity of the ZIF-8 coating was demonstrated by SEM (see images of native yeast (c) and ZIF-8 coated yeast (d) and of the calcined yeast@ZIF-8 sample (e)) and by labelling the living yeast cells with FDA (green), and the ZIF-8 coatings with Alexa Fluor 647 fluorescent dye (red) (see the 3D cellular reconstruction of CLSM images (f) and (g) and a cross-section CLSM image (h) of yeast@ZIF-8). Adapted with permission from ref. 120 Copyright 2016, Wiley-VCH.

mixing an aqueous zinc acetate solution with a premixed aqueous dispersion of cells and 2-methylimidazole (HmIM). After 10 min, the coated cells were recovered by centrifugation and washed with deionized water (DI water). X-ray diffraction (XRD) analysis confirmed the formation of ZIF-8 with sodalite topology (**sod** ZIF-8), and scanning electron microscopy (SEM) images showed individual cells encased in a continuous ZIF-8 exoskeleton with an average shell thickness of 100 ± 10 nm (Fig. 4c–e). Confocal scanning laser microscopy (CLSM) was also employed to assess the homogeneity of the ZIF-8 coating (Fig. 4f–h). The permselectivity of the cells@ZIF-8 composites was tested by incubating the coated and uncoated cells in a medium containing glucose (used as a nutrient) and lyticase, a cytotoxic biomacromolecule (molecular weight = 54.6 kDa). According to the viability test assay, the coated cells displayed a decrease of 19% in cell viability after 24 hours of exposure to lyticase. On the other hand, the control sample shows that non-coated cells experience a reduction of 95% in viability after only three hours of exposure (Fig. 4b). The bioprotection capabilities of the **sod** ZIF-8 coating were further validated by exposing the cells@ZIF-8 composites to an antifungal agent called filipin (molecular weight = 655 Da).[140] The cell viability assay indicates that 90% of the cells surviving the coating process remain metabolically active, even after 24 h of exposure to filipin. In contrast, the control sample (naked yeast cells) showed nearly 100% mortality.

Finally, the optical density measurements at λ = 600 nm (OD_{600}) obtained from the coated and uncoated cells incubated in a rich-nutrient medium demonstrated that the MOF shell formation inhibits cell division; this configuration mimics a spore-induced state. Upon exposure of cells@ZIF-8 to an EDTA solution, the decomposition of the MOF shell allows the resumption of cell division in those cells that remain viable after the coating/de-coating process.

In a following study, the authors used *S. cerevisiae* as model cells to fabricate a bioactive MOF exoskeleton; such an exoskeleton was designed to impart cell adaptability in nutrient-deficient environments.[12] The yeast cells were first coated with β-galactosidase (β-gal),[141] an exogenous enzyme adsorbed onto the cell wall due to electrostatic interaction between the positively charged enzyme and the negatively charged cell wall. The protein-decorated cell system was then resuspended in an aqueous solution of HmIM, followed by the rapid addition of aqueous zinc acetate to induce the spontaneous formation of the ZIF-8 exoskeleton. CLSM was used to demonstrate the co-localization of the β-gal (labeled with purple Alexa Fluor 568) and the MOF coating (infiltrated with red Alexa Fluor 647). The SEM images of yeast@β-gal@ZIF-8 composites confirm the formation of a continuous ZIF coating with an average thickness of 100 nm ± 10 nm. The yeast@β-gal@ZIF-8 composite was incubated in an aqueous solution of lactose, a sugar that cannot be metabolized by *S. cerevisiae* cells. The immobilization of β-gal in the ZIF shell allowed the hydrolysis of lactose to glucose and galactose, two sugars that can be used by the cell as nutrients. Thus, the immobilization of a non-native enzyme (β-gal) between the cell wall and the MOF coating conferred adaptability to nutrient-depleted environments. In the same study, naked yeast (control) and the coated cells (yeast@β-gal@ZIF-8) were incubated in a nutrient-deficient medium containing biomacromolecules that are detrimental to both yeast (*e.g.*, lyticase) and β-gal (*e.g.*, proteases). The cell viability tests indicate that after seven days, ~70% of the coated cells that were initially viable after the coating process remained alive, while the viability of naked yeast rapidly decreased to 10% within the first days of incubation. Overall, this study showed that the ZIF-8 coating acts as a semipermeable barrier (*i.e.*, molecular sieve) allowing the diffusion of non-nutrients and their conversion into nutrients *via* the immobilized β-gal and preventing contact between cytotoxic lyticase and cells. Lastly, on-demand release of the protective coating was demonstrated by exposing the enzyme-functionalized ZIF-coated cells to EDTA.

The potential of abiotic ZIF shells was further expanded by Gan *et al.*,[16] who reported the synthesis of bioactive multilayered ZIF coatings on yeast cells (Y). Specifically, the authors immobilized a protease inhibitor, alpha-1-antitrypsin (AAT), between the two MOF layers constituting the abiotic exoskeleton to impart cell adaptability against protease-rich environments (Fig. 5a). The synthesis of a multilayered ZIF-8 coating was achieved by inducing a **sod** ZIF-8 layer *via* the biomimetic mineralization strategy to afford the Y@ZIF-8 biocomposite. Then, Y@ZIF-8 was exposed to AAT, which was adsorbed onto the outer surface of the ZIF-8 exoskeleton to yield Y@ZIF-8@AAT. Finally, Y@ZIF-8@AAT was exposed to a fresh solution of ZIF precursors, in which the pre-adsorbed AAT triggered the on-site formation of a second ZIF layer. This work showed that the bio-replication approach previously applied to synthetic

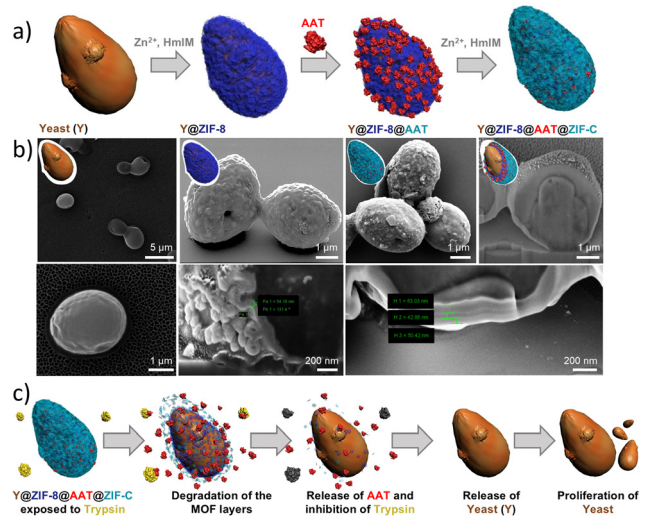

Fig. 5 Multi-layered ZIF-coated cells. Schematic of the encapsulation process (a). SEM images and cross-section analysis of Y@ZIF-8, Y@ZIF-8@BSA@ZIF-8, and Y@ZIF-8@BSA@ZIF-C composites (b). Schematic of yeast cell proliferation upon release of yeast cells in the presence of trypsin (c). Adapted with permission from ref. 16 Royal Society of Chemistry.

substrates (*e.g.*, silicon, glass, polystyrene, and polypropylene)[61,120] to facilitate the MOF growth can be successfully implemented in biological systems. We note that the crystalline phase and composition of the second yeast ZIF coating could be tuned by varying the Zn^{2+}:HmIM ratio, *i.e.* the outer MOF layer could be either **sod** ZIF-8 or ZIF-C (Fig. 5b). This allows for the preparation of two different systems: (i) Y@ZIF-8@AAT@ZIF-8 and (ii) Y@ZIF-8@AAT@ZIF-C. It should be noticed that **sod** ZIF-8 and ZIF-C display differences in their chemical compositions ($Zn(mIM)_2$ for **sod** ZIF-8 and $Zn_2(mIM)_2CO_3$ for ZIF-C), crystalline structures, and porosity. The different MOF outer layers can imbue the MOF biocomposites with unique properties. For example, in terms of porosity, **sod** ZIF-8 is microporous, and ZIF-C is nonporous.[56] The release profile for ZIF-C is faster for encapsulated biomolecules at pH = 6.5,[56] and ZIF-C has lower cytotoxicity in specific cancer cells (*e.g.* human prostate cancer cells (PC-3)).[142] To investigate the biopreservation performance of both materials (*i.e.*, **sod** ZIF-8 and ZIF-C), the authors incubated both composites, Y@ZIF-8@AAT@ZIF-8 and Y@ZIF-8@AAT@ZIF-C, in a protease-rich medium. The latter was prepared by dissolving trypsin in a phosphate-buffered solution (pH = 6.5); the presence of phosphate anions in the incubation media triggered the slow degradation of the ZIF shell,[139] followed by the controlled release of the AAT in solution (Fig. 5c). The release profiles recorded for AAT show that Y@ZIF-8@AAT@ZIF-C releases 50% of the biomacromolecule within the first 2 h. In contrast, the Y@ZIF-8@AAT@ZIF-8 composite requires about 18 h to release 50% of AAT. These results indicate that the crystalline phase of the outer shell directly affects the MOF degradation and, thereby, the release kinetics of AAT. Finally, a trypsin activity assay was used to assess protease inhibitor efficiency. This test revealed that the trypsin becomes completely inhibited once the AAT is fully released from the abiotic coating. Subsequently, the released cells were incubated in a yeast growth medium (yeast extract-peptone-dextrose, YPD) to evaluate the cell proliferation by OD_{600} measurements. This experiment demonstrated that the released yeast cells exhibit exponential proliferation when placed in nutrient-rich media. A similar concept, combining yeast and enzyme by utilizing MOFs to enhance enzyme activity, was reported by Zhan and co-workers in 2023.[143] These studies indicate that yeast@ZIF-8 composites can serve as a platform for biocompatible immobilization materials and effective biocatalysts. Wang and co-workers reported a vaccine adjuvant application from the yeast-derived MOF composite named yeast@Mn-MOF-74@ZIF-8.[144] Yeast and MOFs can serve as antigen display carriers, but they cause different immune responses. Yeast can activate the adjuvant properties of cellular immunity, while MOFs can induce strong humoral immune responses. The yeast@Mn-MOF-74@ZIF-8 composite can not only be used as a delivery system for subunit vaccine antigens but also as an immunostimulant in subunit vaccine and inactivated virus vaccine preparations. In this study, the yeast@Mn-MOF-74@ZIF-8 composite demonstrated promising application potential.

The progress of ZIF-based abiotic shells showcases that protective exoskeleton functions of biomineralized MOFs can be engineered with biomacromolecules; by selecting the MOF coating property (*e.g.*, phase and thickness) and the biomolecule property (*e.g.*, enzymes and enzyme inhibitors), the coating enables functional adaptability, converting hostile environments (*e.g.*, nutrient-deficient and lyase-rich media) into biocompatible ones. Subsequent programmable release of cells from their ZIF coating can enable the restoration of the proliferation functions of the cells surviving the coating/decoating procedure.

One-pot encapsulation of microorganisms: cell viability. While the aforementioned proof-of-concept studies focused on the potential of ZIF coatings, it is worth noting that the assembly of artificial exoskeletons should have minimal influence on cell viability. With this aim, Chen *et al.*[119] employed *S. cerevisiae* and *E. coli* as model cells to evaluate the influence of the ZIF-8 precursors on cell viability. The authors compared the cytotoxicity between three different zinc precursors ($ZnSO_4 \cdot 7H_2O$, $Zn(OAc)_2 \cdot 2H_2O$, and $Zn(NO_3)_2 \cdot 6H_2O$) by exposing cells separately to various concentrations of the individual ZIF precursors dissolved in a 0.9% NaCl solution. The yeast cells showed no significant toxicity when exposed to zinc salts or HmIM alone at concentrations ranging from 4 to 20 mM. However, upon simultaneous exposure to zinc salts and HmIM, the viability of yeast cells varied significantly depending on the zinc precursor used during the encapsulation process. These findings suggest that cytotoxic effects are enhanced during the MOF shell formation, rather than by the individual precursors. Notably, the cytotoxic effect depends on the zinc salt used as a precursor, which was attributed to differences in the byproducts generated during MOF formation. The highest toxicity was observed for $ZnSO_4$: cell viability dropped to 50% for the lowest concentration (4 mM). In contrast, for $Zn(OAc)_2$ and $Zn(NO_3)_2$, a cell viability of 70% and 90% was reported under

the same conditions. Furthermore, according to this study, the ζ-potential of *S. cerevisiae* rises from ζ = −7 to ζ = 10, ζ = 5, and ζ = 3 when the cell is coated with three different zinc sources: $ZnSO_4$, $Zn(OAc)_2$, and $Zn(NO_3)_2$, respectively. The authors further used the $Zn(OAc)_2$ and $Zn(NO_3)_2$ precursors to investigate their cytotoxic effect during the coating process of *E. coli.* In contrast to yeast cells, MOF shell formation did not compromise the viability of *E. coli*. The authors hypothesized that lipopolysaccharides (LPS), located on the outer cell membrane of *E. coli*, could strongly interact with the zinc ions. Similar to other biomacromolecules used as bioreplication agents (fatty acids, negatively charged proteins, and carbohydrates),[52,145,146] LPS may induce rapid ZIF nucleation, thereby forming a protective shell that limits subsequent interactions between free metal ions and the cell.

One-pot encapsulation of microorganisms: expanding the portfolio of porous frameworks. The use of ZIFs for encapsulation has been extended to ZIF-90, a single crystalline material composed of Zn^{2+} cations coordinated with imidazolete-2-carboxaldehyde (ICA^-) anions.[97] ZIF-90 forms a continuous, defect-free shell, which enhances the perm-selective properties of the MOF by minimizing the formation of grain boundaries, a common issue observed in polycrystalline ZIF-8 shells. This property enables effective encapsulation with mass diffusion that is exclusively controlled by the ZIF microporosity, thus preventing the influence of intercrystalline defects. Specifically, an *E. coli* strain was genetically engineered to contain a plasmid with the gene for the expression of red fluorescent protein mCherry under the control of the T7 promoter. Upon addition of IPTG, transcription of the mCherry gene was induced, leading to the production of the red fluorescent protein. Subsequently, polyvinylpyrrolidone-assisted aqueous encapsulation of the genetically activated *E. coli* was performed. The expressed red fluorescent protein is larger than the micropores of ZIF-90; thus, the Tsung group demonstrated that proteins expressed in living organisms can be confined within cells by a defect-free ZIF-90 shell. After mCherry protein expression, the engineered bacteria exhibited strong red fluorescence (610 nm) when excited by 580 nm green light, making the ZIF-90-encapsulated cells easily detectable using fluorescence microscopy. To evaluate the protective effect of the ZIF-90 shell, the *E. coli*@ZIF-90 composites were exposed to toxic bactericides such as benzaldehyde, cinnamaldehyde, and kanamycin, while free *E. coli* exposed to the same toxic environment were used as controls. After treatment with benzaldehyde and cinnamaldehyde, free cells lost fluorescence, whereas ZIF-90 encapsulated cells retained fluorescence signals. These results demonstrate that cells encased within ZIF-90 remain viable after exposure to cytotoxic environments and can proliferate following removal of the ZIF-90 exoskeleton by exposure to EDTA. This finding suggests that the ZIF-90-based exoskeleton is a feasible system for protecting and prolonging the lifespan of bacterial cells. Importantly, this work demonstrates that ZIF coatings can be used to retain expressed proteins within a living organism, providing a new tool for bioengineering applications. In addition to the one-pot, water-based synthesis method mentioned above, the Shieh group has proposed the mechanochemical approach (*i.e.*, inducing chemical reactions through mechanical force, such as grinding or ball milling, with minimal solvent use) for the encapsulation of cells in MOFs. By applying mechanical forces to a mixture of *E. coli* and ZIF-90 precursors through ball milling, the authors encapsulated *E. coli* within ZIF-90.[147] This method is not only environmentally friendly and ultrafast, requiring only a few seconds, but also demonstrates that the ball milling process is compatible with bacterial viability, highlighting the suitability of this rapid mechanical approach for encapsulating fragile biomaterials. These findings suggest that ZIF-90-based exoskeletons provide a viable strategy for protecting and prolonging the lifespan of bacterial cells.

More recently, Luo *et al.*[148] reported the cascade biosynthesis of D-phenyllactic acid (D-PLA) from L-phenylalanine using two *E. coli* strains (pET28a-lrldh and pET28a-ladd2) immobilized in an amorphous ZIF-90 (aZIF-90) exoskeleton. The encapsulation was achieved *via* a one-pot method by mixing $Zn(NO_3)_2$ with imidazole-2-carboxaldehyde (HICA) in the presence of the *E. coli* strains in a 1:1 mixture. The resulting amorphous *E. coli*@aZIF-90 biocomposites were characterized *via* SEM, infrared spectroscopy, thermogravimetric analysis (TGA), XRD, X-ray photoelectron spectroscopy (XPS), and CLSM, confirming successful cell encapsulation and a mesoporous structure conducive to substrate diffusion. Catalytic performance assays revealed that aZIF-90 encapsulation enhanced the cells' thermal and pH stability, tolerance to metal ions and organic solvents, and retained >75% of activity over four reuse cycles. In a fed-batch system, the immobilized biocatalyst reached a peak yield of 9.00 g L^{-1} D-PLA with an 89.4% conversion rate after 12 hours. Compared to free cells, *E. coli*@aZIF-90 exhibited a 1.15-fold increase in space–time yield and superior resistance to harsh environmental conditions. These results underscore the potential of aZIF-90 as a robust platform for whole-cell catalysis in industrial bioproduction of D-PLA.

One-pot encapsulation of living cells within abiotic MOF coatings is not restricted to Zn-based MOFs. Recent studies suggest that Fe-based MOFs are suitable candidates for one-pot encapsulation of living microorganisms. Lee *et al.*[63] reported the encapsulation of the model cell *S. cerevisiae* within a MOF coating made of Fe^{3+} ions and benzene-1,3,5-tricarboxylate (BTC) linkers. This abiotic coating was formed by mixing an aqueous solution of $FeCl_3$ with a premixed aqueous dispersion of cells and BTC. After 1 min of stirring, the resulting yeast@Fe-BTC composites were recovered by centrifugation and washed with DI water. This MOF coating process was repeated three times to obtain a robust MOF coating. The ζ-potential for uncoated *S. cerevisiae* cells is ζ = −37.8, while for the resulting yeast@Fe-BTC composite, it is ζ = −13. Cell viability was assessed by the live/dead assay, which monitors cell membrane integrity and internal esterase activity. This test indicates that 95% of yeast cells remained metabolically active after the encapsulation process, confirming the cytocompatibility of the MOF coating process. Then, to impart cell adaptability against cytotoxic agents like octyl-β-D-glucopyranoside, the MOF shell was functionalized with a set of exogenous enzymes,

including β-glucosidase (β-glu), glucose oxidase (GOx), and horseradish peroxidase (HRP), yielding a yeast@β-glu&GOx&HRP@Fe-BTC composite with a bioactive MOF shell. This bioactive shell was designed to enable an enzymatic cascade reaction that starts with β-glu, which cleaves the *O*-glycosidic bond at C1 of octyl-β-D-glucopyranoside to yield 1-octanol and D-glucose. Then, GOx transforms D-glucose and O_2 to D-gluconic acid and H_2O_2. Finally, HRP uses H_2O_2 as a co-substrate for the catalytic oxidation of 2,2′-azino-bis(3-ethylbenzothiazoline-6-sulfonic acid) (ABTS) into its radical cation ($ABTS^{+\bullet}$). The radical cation, which has a distinct blue color, was used to monitor the feasibility of the enzymatic cascade reaction when exposing the encased cells to an octyl-β-D-glucopyranoside-rich medium.

Then, to evaluate the bioprotection capabilities of the bioactive coating to the encased cells, the authors compared the viability of the yeast@β-glu&GOx&HRP@Fe-BTC and the free yeast cells after being exposed to lethal concentrations of octyl-β-D-glucopyranoside (20×10^{-3}, 50×10^{-3}, and 100×10^{-3} M) for 48 h. Cell viability measured upon exposing yeast@β-glu&GOx&HRP@Fe-BTC at each lethal concentration was 47.7%, 47.3%, and 42.7%, respectively. In contrast, for the free cells exposed to the same cytotoxic conditions, the viability values obtained were 17.4%, 16.2%, and 14.6%, respectively. These observations support the integration of multiple exogenous enzymes into the MOF coating without compromising their catalytic activity. This study further expands the versatility of MOF coatings for designing bioactive shells capable of mitigating the adverse effects of specific cytotoxic agents.

More recently, Sicard and co-workers reported the one-pot encapsulation of *P. putida* CFBP 5039 within a Fe-based MOF known as MIL-100(Fe) (MIL = Matériaux Institut Lavoisier).[108] MIL-100(Fe) is a mesoporous crystalline material comprised of Fe-oxo trimers interconnected by BTC linkers.[149] The synthesis of MIL-100 around living cells required carefully optimized conditions to form a crystalline MOF coating without compromising cell viability. To determine the concentration threshold at which each molecular precursor begins to drive cell stress, the authors exposed the *P. putida* cells to various concentrations of MOF precursors. Then, the bacteria's integrity was assessed by a live/dead assay using propidium iodide (PI), a fluorescent dye that only permeates damaged cell membranes, and SYTO9, a fluorescent probe that permeates healthy membranes. The study indicates that when using diluted concentrations of BTC (8.5 mM) and iron(III) nitrate (13 mM), the cell membrane remains intact, suggesting that these are the optimal concentrations to prepare a MIL-100 MOF coating. The one-pot synthesis was performed by mixing aqueous solutions of MOF precursors in the presence of the cells; this mixture was kept at 30 °C for 21 h. The XRD pattern of the resultant biocomposite indicates the successful formation of crystalline MIL-100(Fe). Furthermore, the TEM micrographs (Fig. 6a–c) and elemental mappings (Fig. 6d) indicate the formation of a continuous MOF coating with a thickness of 30–60 nm. Interestingly, TEM images reveal that the MOF particles are not directly attached to the cell wall; instead, a gap of ~60–80 nm is observed between the MOF coating and the cell. The authors

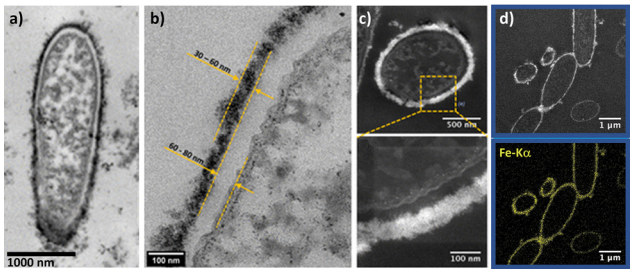

Fig. 6 One-pot encapsulation of *P. putida* within MIL-100. TEM images (a) and (b) and STEM-HAADF images (c) of *P. putida*@MIL-100(Fe). The STEM-HAADF image and STEM-XEDS elemental maps of the biohybrid material (d) demonstrate the localization of the MOF shell on the bacterial surface. Adapted with permission from ref. 108 Copyright 2022, American Chemical Society.

suggested that this separation might be caused by an exopolysaccharide (EPS) network surrounding the bacterium. The EPS secretion is typically observed in many Gram-negative bacterial strains during their stationary phase. The author claimed that the functional groups of the EPS network (–OH, –COOH, $–NH_2$) might enhance local interactions between the cell and Fe ions, leading to the heterogeneous nucleation of MOF crystals at the cell's surroundings, mimicking the natural mineralization process.

In 2024, the one-pot encapsulation of living cells within abiotic coatings was expanded from MOFs to COFs. J. Liang and co-workers coated *S. cerevisiae* cells with a COF based on *p*-phenylenediamine and benzene-1,3,5-tricarboxaldehyde (COF-LZU1).[150] After suspending the cells in a solution containing the two COF precursors, COF formation was induced by subsequent addition of acetic acid and sodium hydroxide, for a reaction time of 15 min. Microscopy studies showed that the COF shell was a uniform thin film of approximately 40 nm firmly adhering to the cell wall and particle aggregates. The authors attributed the film homogeneity to the formation of covalent bonds between the COF material and the amine or thiol groups of (glyco) proteins in the yeast cell wall during the one-pot reaction. Notably, upon encapsulation within COFs, 72.5% of cellular activity was retained (resazurin assay results), suggesting that the rapid formation of the COF coating minimizes the harmful effects on yeast cells induced by exposure to acetic acid and sodium hydroxide. The COF coating provided a high degree of protection against different stressors (high temperatures, pH fluctuations, oxidative stress, high metal ion contents, bisphenol A, and UV radiation). Furthermore, by incorporating exogenous enzymes (*i.e.*, catalase) into the COF coating, stable yeast fermentation and ethanol production were achieved. Building on this approach, in 2025, *P. thermoglucosidasius* Gt-08, a Gram-positive bacterium genetically optimized for high riboflavin production, was encapsulated into COF-42.[151] Upon encapsulation, the authors showed that the production of riboflavin was preserved, demonstrating that the COF shell effectively safeguards cells. The one-pot encapsulation is based on the exposure of the bacteria to an acetic acid and water solution of one of the COF-42 precursors (1,3,5-triformylbenzene). Subsequent addition of the second COF

precursor (2,5-diethoxyterephthalohydrazide) induced immediate COF formation and precipitation. Microscopy and structural investigations confirmed the growth of a COF thin film (35–80 nm) around the cells. ζ-Potential measurements demonstrated the interaction between the cell surface and the acid-activated 1,3,5-triformylbenzene: bare cells showed a ζ-potential of −12.4 mV, whereas the exposure to the COF ligand increased the ζ-potential to +15.5 mV. Based on these data, the authors hypothesized that the enrichment of the cell surface with 1,3,5-triformylbenzene promoted the COF nucleation directly at the cell surface, leading to the homogeneous coating observed *via* electron microscopy. Overall, these findings indicate that COF precursor–cell surface interactions follow principles analogous to MOFs on cell surfaces, where electrostatic interactions between the cell and precursors play a crucial role, highlighting mechanistic similarities in the growth of different extended framework materials on living cells.

One-pot encapsulation of complex cells. Mammalian cells, which lack a cell wall, are much more sensitive to environmental changes than microbial cells. Therefore, single-cell encapsulation has gained attention as an engineering strategy, for example, to endow mammalian cells with greater durability and strength or to develop whole-cell cancer vaccines. In a biomimetic approach, biocompatible biohybrids can be considered as artificial exoskeletons. Due to its excellent biocompatibility, ZIF-8 is the most often applied biocomposite for higher eukaryotes. For example, a MOF exoskeleton coating of mammalian cells was developed *via* a one-pot biomimetic mineralization process in PBS as the solvent system. The ZIF-8-coated mammalian cells were produced by incubating the glass-adhered MDA-MB-231 cell line in a 1 × PBS solution containing $Zn(OAc)_2{\cdot}2H_2O$ and HmIM with gentle shaking.[152] The resulting exoskeleton was shown to protect individual cells successfully against proteolytic enzymes (*i.e.*, proteinase K), whereas smaller-sized nutrients could still cross the exoskeleton. As expected, ZIF-8-coated cells exhibited arrested replication behavior, yet maintained excellent viability for up to 72 h. Moreover, the function of transmembrane GLUT transporters was unaffected by the formation of the MOF exoskeleton on the cell surfaces.[116] Following the same approach, the group also described the preparation of MOF-coated Janus cells.[116] Janus carrier cells were produced by asymmetrically immobilizing MOF nanoparticles (*i.e.* ZIF-8) containing cytotoxic enzymes on one hemisphere of the cell surface. These Janus cells served as cell-mediated drug delivery systems, preserving the intrinsic binding capacity of the cells to their microenvironment and demonstrating the ability to carry a variety of enzymes.

Yang *et al.* encapsulated cancer cells using ZIF-8[125] to apply these cells as whole-cell cancer vaccines. Here, a biocompatible and selective cell encapsulation strategy based on a precursor-functionalized nucleolin aptamer and *in situ* MOF mineralization on the aptamer-identified cancer cell surface was developed. After MOF coating, the encapsulated cancer cells (HeLa, A549, MCF-7, and B16 cells) underwent immunogenic cell death, which was associated with variations in cell stiffness. As aspired, immunogenic dead cancer cells efficiently exposed calreticulin, a hallmark of efficient whole-cell cancer vaccines, on their cell surface, and were able to release antigens and induce *in vivo* antitumor T-cell immune responses.

An alternative strategy was shown for neural stem cells, which were encapsulated with biocompatible HOFs.[33] These composites formed at the cytomembrane of neural stem cells *via* electrostatic interaction, as well as hydrogen-bonding interactions between protein residues on the cytomembrane and the HOF building blocks. Additionally, porous carbon nanosphere nanozymes (PCNs) were doped into the HOF shells to endow the cellular exoskeletons with hierarchical hydrogen bonds, NIR-II triggered degradation, and antioxidant activity. Neither the biological activity nor the cell viability of neural stem cells was influenced by the encapsulation process. Neural stem cells are of great interest for the treatment of neurodegenerative diseases, but successful transplantations are often impeded due to loss of 'stemness', cytomembrane damage, and apoptosis resulting from the oxidative stress in the adverse pathological microenvironment. To prove that HOF-encapsulated cells can be transplanted, they were injected into the brains of neurodegenerative disease mouse models. These mice indeed exhibited ameliorated neurogenesis.

Even though the number of these pioneering examples is still limited, they suggest that this could be a promising approach for creating high-performing carriers for biotherapeutics and vaccines in the near future.

Cells@shell: multi-step encapsulation

Multi-step encapsulation of microorganisms. One of the main advantages of the multi-step encapsulation strategy is the possibility of encapsulating cells into MOFs that cannot be synthesized under biocompatible conditions. In this way, it is possible to employ MOFs with enhanced hydrolytic stability (*e.g.* Zr-based MOFs). For example, Yang, Yaghi, and co-workers reported the use of pre-synthesized monolayers of a Zr-based MOF ($Zr_6O_4(OH)_4(BTB)_2(OH)_6(H_2O)_6$) to wrap *M. thermoacetica* cells.[98] The deposition of the MOF layers over the microorganism was induced by the formation of coordination bonds between the zirconium clusters and the phosphate moieties of the cell surface. The scanning transmission electron microscopy (STEM) analysis indicated the formation of a homogenous MOF coating with a thickness of 1–2 nm. Interestingly, wrapping the cells with pre-synthesized MOF monolayers did not induce a dormant state in the coated cells; the bacteria preserve their reproductive capacity when cultured under anaerobic conditions. To demonstrate the cytoprotective effect of the MOF coating on *M. thermoacetica* under oxidative stress, the authors exposed the coated and uncoated cells to an O_2 environment (21%) for 2 days. The viability assay obtained upon the O_2 exposure indicated that the coated cells exhibit a viability of 76 ± 8%, whereas the population of bare cells decayed to 50 ± 7%. Subsequently, the coated and non-coated cells were exposed to different concentrations of H_2O_2 to evaluate the ROS-scavenging properties of the Zr-based coating. This study further confirmed that the MOF coating prevents the oxidative stress caused by reactive oxygen species (ROS). The authors suggested that the protection against

oxidative stress might be caused by the presence of active metal sites on the zirconium clusters, which mediate the decomposition of H_2O_2 and prevent its accumulation in the cell culture medium.

Multi-step encapsulation of bacterial spores. Spores can be formed in some bacteria, like *Bacillus subtilis*, to survive in challenging environments.[153] When exposed to favorable growth conditions, spores can germinate and begin to grow. Therefore, using abiotic exoskeletons to coat spores instead of cells for artificial sporulation may bring additional benefits.[153,154] Firstly, spores have stronger environmental resistance compared to cells and can adapt to harsher encapsulation conditions of certain exoskeletons. Secondly, the controllable germination of spores can not only extend the storage period, but also provide the opportunity for use in environments outside the laboratory. Thirdly, transportation is simplified, avoiding the low-temperature environment typically required for cells. Given that spores can be combined with various materials and genetically modified, spore-based biomaterials have great potential for applications, yet they are rarely used in MOF systems.[154–157] For example, Zhong, Chou, and co-workers demonstrated the encapsulation of *Bacillus subtilis* spores in hollow ZIF-8.[154] The ZIF-8 hollow shell was synthesized by the soft template method, using microscopic water-in-oil droplets. The synthesis conditions are relatively harsh for bacteria, so this proves the adaptability of the spores. The hollow ZIF-8 layer provides enhanced environmental resistance for spores, shielding them from harsh conditions that bare spores cannot bear, such as hypochlorous acid, ultraviolet radiation, and even vacuum conditions. The release and germination of spores can be regulated based on nutrient concentration. Furthermore, the spores were genetically engineered using environmentally sensitive genetic circuits, resulting in bacteria capable of detecting specific molecules such as IPTG or citric acid.

Multi-step encapsulation of complex cells. For higher eukaryotes, the use of nanoparticles (NPs) has fewer difficulties than *in situ* cell encapsulation, presumably due to the lower concentrations of toxic compounds required for this method. The Brinker lab has shown that HeLa cells can be encapsulated by applying the SupraCell approach.[64] SupraCell formation requires the preparation of synthetic nanoparticles (*e.g.*, from ZIF-8, MIL-100, or UiO-66-NH_2), which attach to the cell surface *via* tannic acid acting both as a chemical binder between NPs and the cell membrane and as an interparticle crosslinker, forming a continuous porous exoskeleton. The use of different NP building blocks enables the formation of different pore sizes, which results in selective permeability. SupraCells were shown to maintain normal cellular functions (*e.g.*, viability and metabolism), while remaining in a spore-like state. The artificial exoskeleton confers resistance to mechanical and osmotic stresses, ROS, pH changes, and UV exposure. In a similar approach, functional MOF NPs, including ZIF-8, MIL-100 (Fe), UiO-66-NH_2, magnetic iron oxide (Fe_3O_4) NPs@ZIF-8, and hybrid mesoporous silica NP@MOF (MSNs, dye-labeled MSNs, sensing probe-loaded MSNs@ZIF-8), have been prepared and used to coat red blood cells.[1,133] Exoskeletons were generated within seconds through MOF NP interlocking based on metal–phenolic coordination and RBC membrane/NP complexation *via* hydrogen-bonding interactions at the cellular interface. Encapsulated red blood cells showed enhanced tolerance against diverse external stressors, including detergents, toxins, antibody-mediated agglutination, osmotic stress, and freezing. Interestingly, MOF encapsulation was shown to positively affect cryopreservation, a process that includes quick freezing and thawing of cells. Cryopreservation is a method in which cells are rapidly frozen, stored at very low temperatures (~ -80 °C), maintaining their viability until defrosted months or years later. The method is used to preserve all different types of cells, including important medical samples required for blood transfusion, bone marrow transplantation, artificial insemination, and *in vitro* fertilization. The most problematic step of cryopreservation is the thawing step, which often compromises cell viability. Several studies have shown that nanoparticle-facilitated MOF-encapsulation can be an alternative, even more efficient solution to protect mammalian cells during freezing and thawing events and help cells fully recover. Red blood cells could be preserved by applying zirconium (Zr)-based metal–organic framework (MOF) nanoparticles (NPs).[64] Altogether, five Zr-based MOF NPs, namely, UiO-66, UiO-66-NH_2, UiO-66-OH, UiO-67, and MOF-808, were selected and synthesized according to the reported solvothermal methods. The Zr-MOF NPs exhibited well-defined surface chemistries and were found to inhibit ice recrystallization while also accelerating ice crystal melting. Cryopreservation tests revealed cell recoveries of up to 40% after freezing and thawing.

Jeon *et al.* applied zirconium (Zr)-based MOF-801 NPs as a cryoprotectant for human embryonic kidney (293T), non-tumorigenic lung bronchial epithelial (BEAS-2B), and lung carcinoma epithelial (A549) cell lines.[124] MOF NPs with diameters of 10, 35, 100, and 250 nm were prepared. In this approach, the amino acids valine and threonine were introduced into the MOF NP-surface through the acrylate-based functionalization to mimic ice-binding proteins and provide surfaces with hydrophilic and hydrophobic dualities. The MOF-801 NPs were biocompatible regardless of concentration or NP surface-functionalization, whereas the smaller-sized surface-functionalized NPs showed a good cell recovery rate after freezing/thawing by inhibiting ice recrystallization.

So-called ZIFSpermbots were created by encapsulating sperm cells using pre-synthetized ZIF-8 NPs.[114] Coating of sperm membranes was facilitated through complexation with tannic acid, resulting in selectively permeable, porous ZIF-8 wrappings. This cell surface engineering had a negligible impact on sperm motility under optimized conditions, whereas it efficiently blocked the binding of antisperm antibodies. These so-called ''ZIFSpermbots'' may be used as active drug delivery systems by making use of the drug-loading capacity of ZIF-8 NPs.

MOF cell–surface coatings can also be applied to create microdomains on the cell membrane of mammalian cells like Chinese hamster ovary K1 (CHO-K1).[115] For this approach, a metal complex lipid (dabco-$(CH_2)_{15}$-$CH_3)_2$[MnN-$(CN)_4$] was inserted into mammalian cell membranes through simple incubation

and cross-linked by adding Ni cations, forming stable MOF microdomains and leading to phase separation. The induced phase separation systems remain stable even in the absence of the actin cytoskeleton. Moreover, these cells showed enhanced cellular calcium response to ATP due to the activation of P2 purinoceptors.

Emerging applications of framework-encapsulated cells

Immunotherapy

The preservation of cell viability during cell@shell formation opens the possibility of using these composites in novel applications. For instance, degradable abiotic shells to encase living bacteria may significantly improve bacterial-mediated antitumor therapy (BMAT).[27,43,158–160] Although the use of live bacteria for cancer treatment has been known since the 19th century, the risks of uncontrolled bacterial infection have hindered the clinical application of BMAT.[161] Nevertheless, with the advent of new antibiotics and genetic engineering techniques, researchers have developed safe strategies for using attenuated bacteria in cancer therapy.[158] When compared to traditional chemotherapy, BMAT provides several advantages: (1) tumor targeting: the hypoxic tumor microenvironment promotes bacterial colonization,[162] (2) intratumoral penetration: the bacterial flagella enhance the bacteria's ability to penetrate within the tumor mass,[163] (3) tumor colonization: the immunosuppression of the tumor microenvironment promotes the preferential accumulation of bacteria in the cancer tissue;[43,158] and (4) development of bacteria-based delivery systems, where by genetic engineering and bacterial surface modification, it is possible to create delivery systems that use living cells as carriers.[43,158] Therefore, these systems are ideal for delivering antitumoral therapeutics with high spatial and temporal precision.[14,158,161]

One effective way to enhance the efficacy of bacteria-based therapy is encapsulation of living microorganisms within an abiotic shell. This strategy enables co-delivery of therapeutic agents to cancer cells, prolongs bacterial circulation lifespan, and improves regulation of bacterial proliferation at the treatment site.[43,158] A recent study by Yan and co-workers showcased the synergistic potential between the abiotic MOF coating and bacterial-based cancer therapy.[70] In this work, the authors reported the one-pot encapsulation of *E. coli* ($\zeta = -23$) within a bioactive ZIF-8 coating to yield *E. coli*@ZIF-8 composites (ζ = 7.5).[70] The ZIF-8 coating preserved the viability of the encased cells while preventing uncontrolled bacterial replication in healthy tissue. To further improve the therapeutic efficacy of the *E. coli*@ZIF-8 composites, the researchers used the MOF shell for the co-immobilization of two therapeutic agents, doxorubicin (DOX) and chlorin e6 (Ce6), resulting in an *E. coli*@DOX&Ce6@ZIF-8 composite ($\zeta = -14$). DOX is an anthracycline antibiotic commonly used in chemotherapy,[164] and Ce6 is an FDA-approved photosensitizer utilized in cancer photodynamic therapy (PDT).[165] Ce6 is known for its high reactive oxygen species (ROS) generation efficiency upon exposure to mild near-infrared (NIR) irradiation. The NIR radiation, which ranges from 800 to 2500 nm, is less phototoxic than UV or high-energy visible light. In addition, in mammalian tissues, NIR light penetrates more deeply than visible light, making it more suitable for treating deeper-seated wounds, infections, and cancers.[166]

The chemo-photodynamic therapeutic efficacy of the *E. coli*@DOX&Ce6@ZIF-8 composite was evaluated through both *in vitro* and *in vivo* experiments. The *in vitro* tests were performed by evaluating the cell viability of mouse breast tumor (4T1) cells after different treatments with and without laser exposure (L). These treatments included: (1) free *E. coli*, (2) *E. coli*@ZIF-8, (3) *E. coli*@DOX&Ce6@ZIF-8, (4) *E. coli*@Ce6@ZIF-8 + L, and (5) *E. coli*@DOX&Ce6@ZIF-8 + L. The results showed that 4T1 cells retained over 80% viability after being exposed to *E. coli*@ZIF-8. This observation confirms the biocompatibility of the *E. coli*@ZIF-8 composite. However, the cell viability dropped to ~60% after exposure to the *E. coli*@DOX&Ce6@ZIF-8 composite. The moderate toxicity of the *E. coli*@DOX&Ce6@ZIF-8 composite was attributed to the release of the chemotherapeutic drug DOX. Nevertheless, the therapeutic efficacy of the *E. coli*@DOX&Ce6@ZIF-8 composite could be intensified with NIR laser exposure. Thus, the dual chemo-photodynamic therapy provided by the *E. coli*@DOX&Ce6@ZIF-8 + L treatment resulted in a cell viability of ~25%. These observations indicate that the strong synergy between Ce6 and DOX leads to higher therapeutic efficacy in *in vitro* tests. To explore the efficacy of the dual chemo-photodynamic therapy, the authors investigated the biodistribution of *E. coli*@DOX&Ce6@ZIF-8 in mice. *E. coli*@DOX&Ce6@ZIF-8 was injected into tumor-bearing mice, and the biodistribution analysis after 24 h revealed that the accumulation efficacy of *E. coli*@DOX&Ce6@ZIF-8 was ~6.1%. This value was obtained from the ratio of *E. coli* colonies in tumor sites to the injected number of *E. coli*@DOX&Ce6@ZIF-8. Then, by tracking the tumor size and weight, the authors demonstrated that *E. coli*@DOX&Ce6@ZIF-8 inhibits tumor growth after a one-time NIR laser treatment (10 min, λ = 600 nm). This study highlights the versatility of using bacteria@MOF coatings as a cell-based delivery platform for biotherapeutic applications.

The MOF bioprotection can also be extended to cellular organelles. This was recently demonstrated by Zhou and co-workers, who reported a novel strategy to biomineralize isolated mitochondria within ZIF-8,[167] to preserve their bioactivity and enhance their transplantation efficiency into cancer cells for therapeutic purposes. The mitochondria were isolated from non-tumorigenic mammary epithelial cells (MCF-10A). The encapsulation was achieved through a one-pot synthesis method by mixing the freshly isolated mitochondria with Zn^{2+} and HmIM in a 0.9% NaCl solution. To improve intracellular delivery, the resulting MIT@ZIF-8 nanostructures were further surface-functionalized by incorporating polyethyleneimine (PEI) and the cell-penetrating peptide TAT during the synthesis process. TEM images confirmed the formation of a distinct ZIF-8 layer around the mitochondria, and cut-section analysis revealed the inclusion structures. Fluorescence lifetime measurements of a mitochondrial-binding dye (MVG)

further confirmed the full encapsulation of mitochondria by the ZIF-8 shell. This study indicates that the encapsulated mitochondria effectively maintained their bioactivity, assessed by mitochondrial membrane potential and ATP synthesis capability, for at least 4 weeks at room temperature. In contrast, non-encapsulated controls, even when stored on ice, lost a significant portion of their membrane potential within 6 hours. The MIT@ZIF-8 nanostructures were shown to release the encapsulated mitochondria in response to an acidic environment, with approximately 70% release at pH 5.0 after 6 hours, compared to minimal release at pH 7.4. The surface modification of MIT@ZIF-8 with PEI and TAT resulted in improved aqueous dispersion, which enhanced cellular uptake. The modified MIT@ZIF-8 was successfully delivered into breast cancer cell lines (BT-549 and MDA-MB-231) with uptake efficiencies of 11.8% and 17.2%, respectively, after 4 days of incubation. CLSM imaging showed the presence of these exogenous mitochondria within the recipient cancer cells, and instances of fusion between the transplanted and endogenous mitochondria were observed. Functional analysis *via* Seahorse assays revealed an increased oxygen consumption rate (OCR) and an extracellular acidification rate (ECAR) in cancer cells that received MIT@ZIF-8, indicating improved mitochondrial function. Therapeutically, the transplantation of these non-tumorigenic mitochondria into cancer cells resulted in significant inhibition of cancer cell proliferation, reduced the cancer stem cell population in MDA-MB-231 cells from 95.5% to 76.5%, and suppressed the epithelial–mesenchymal transition (EMT) process in these cells. The authors concluded that this MOF-based biomineralization technique represents an advancement for mitochondrial research and transplantation, offering a robust method to preserve mitochondrial activity and enhance mitochondrial delivery for potential cancer therapy.

Probiotic bacteria and enzyme delivery

A different research direction to explore the potential of cell@ZIF-8 composites targets the encapsulation of probiotics. Probiotics are microorganisms that confer health benefits when administered in adequate amounts to humans or animals, as they maintain, restore, and balance intestinal microflora.[168,169] The latter is especially crucial for the clinical control of intestinal tract infections.[170,171] However, the beneficial effects of the probiotic bacteria can only be achieved if the microorganism reaches the intestinal target in a viable state.[168,169] Nevertheless, from a practical point of view, this represents an important challenge, since orally administered probiotics are subjected to strong acidic conditions during their journey through the gastrointestinal tract.[169] Such acidic[172] conditions can severely hamper the probiotic viability, limiting their efficacy in restoring gut flora. On the other hand, the clinical treatment of intestinal infections typically requires the co-administration of antibiotics and probiotics. Therefore, to ensure the effectiveness of the treatment, it is crucial to develop strategies that provide probiotics with protection against antibiotics, such that antibiotics only kill infectious pathogens without altering the viability and functionality of probiotics.[173]

Microencapsulation technology has emerged as a promising solution to tackle these issues and boost probiotic viability when deployed alongside antibiotics for treating intestinal infections. Traditional microencapsulation techniques involve immobilizing probiotics within organic matrices.[174,175] One crucial aspect of microencapsulation is ensuring that the encapsulating material can release the probiotic cells at the site of action. Advances in nanotechnology have led to the development of novel abiotic coatings that enable targeted delivery of probiotics upon exposure to an external stimulus while protecting them against the harsh conditions of the gastrointestinal tract. In this regard, Busscher and co-workers explored the encapsulation of probiotic bacteria such as *B. breve*,[21] and *L. acidophilus*[76] within various abiotic coatings, including (i) protamine-assisted SiO_2 nanoparticle yolk–shell coating, (ii) alginate hydrogel, and (iii) **sod** ZIF-8. Then the authors compared the bioprotection properties of *B. breve* against simulated gastric fluid (SGF††) and a model antibiotic (*i.e.*, tetracycline).[21] The SiO_2 yolk–shell encapsulation was obtained through the pre-adsorption of a protamine film onto a bacterial cell, followed by exposure to a colloidal suspension of SiO_2 NPs. The SiO_2 NPs get assembled onto the protamine film, leading to the formation of a silica shell. The protamine film was subsequently internalized into the bacterium to create a void between the bacterial cell surface and the nanoparticle shell. The alginate hydrogel shell was prepared by adding dropwise a PBS suspension of either *B. Breve* or *L. acidophilus* and alginate into a $CaCl_2$ solution. The electrostatic interaction between Ca^{2+} ions and the alginate chains triggers the formation of a three-dimensional hydrogel around the microorganisms. Finally, the ZIF-8 coating was deposited by mixing an aqueous solution of zinc acetate with a premixed aqueous dispersion of probiotics and HmIM. The authors demonstrated that the ζ-potential of non-coated *B. Breve* cells remained negative across the pH range from 2 ($\zeta = -0.1$ mV) to 9 ($\zeta = -0.2$ mV). However, protamine-assisted SiO_2 encapsulation increased the ζ-potential over the entire pH range. For example, at pH = 2, the reported ζ-potential was $\zeta = 8$ mV, whereas at pH = 9, the ζ-potential -18 mV. Interestingly, when using ZIF-8 as a cell exoskeleton, the *B. breve* ζ-potential only changed in the pH range from 7 to 9 (see Table 1). The ζ-potentials *B. Breve* cells encased within the alginate-hydrogel were not reported. The elemental surface composition of the cell@shell systems was analysed by XPS. The marked differences in the elemental composition of free probiotics and the cell@shell composites indicated the successful encapsulation of *B. Breve* and *L. acidophilus* within the SiO_2, alginate, and ZIF-8 abiotic coatings. Then, the authors evaluated, for each abiotic coating, how the encapsulation process affected the viability of the encapsulated cells (*B. breve* and *L. acidophilus*). The number of viable cells before and after the encapsulation was determined by the colony-forming unit technique (CFU). The cell viability assay showed that, on agar plates, the growth of *B. breve* cells coated with SiO_2 and alginate hydrogel shells had a cell death comparable to the non-coated cells (control). However, on

†† SGF: simulated gastric fluid, a lab-prepared solution mimicking the acidic conditions in the human stomach.

agar plates, the cells coated within ZIF-8 showed slightly decreased bacterial viability, indicating an enhanced cytotoxic effect of the MOF coating. To assess potential cell wall damage produced by the different abiotic coatings, the authors used the SYTO9/propidium iodide staining test (BacLight Bacterial Viability Kit). In this experiment, microorganisms with cell wall damage present red fluorescence, while those without cell wall damage exhibit green fluorescence. This study concluded that neither the protamine-assisted SiO_2 coating nor the alginate hydrogel damaged the cell wall. However, the formation of a ZIF-8 coating induced cell wall damage. The authors hypothesized that this might be attributed to the strong interaction between the bacterial surface proteins and the zinc cations. Subsequently, the authors determined the protection offered by the three different abiotic coatings against SGF and the antibiotic tetracycline. Thus, to mimic the conditions encountered by the probiotics on their way to an intestinal infection site, the same number of uncoated cells and the three different cell@shell composites were suspended in SGF medium at pH = 2. Then, the exposed microorganisms were collected by centrifugation and analyzed by the CFU test. *L. acidophilus* encapsulated within ZIF-8 and alginate-based shells exhibited around 75% viability upon being exposed to SGF. By contrast, the cell viability dropped to 50% for the cells encased within the SiO_2 yolk–shell. The results obtained from *B. breve* composites indicated that only the alginate-based coating provided effective protection to the cells against SGF. Similarly, the coated and non-coated cells were cultured in a modified medium supplemented with a model antibiotic (*i.e.*, tetracycline), and then the *L. acidophilus* and *B. breve* cells were plated on agar for CFU counting. The results obtained from *L. acidophilus*@shell composites indicated that none of the abiotic coatings protected against negatively charged tetracycline. Nevertheless, cell viability assay of *B. breve* composites exposed to the model antibiotic indicates that only the alginate-based coating provides full protection against tetracycline. Finally, the authors performed *in vitro* experiments to determine the therapeutic effect of the coated probiotics against pathogenic *E. coli* adhered to intestinal epithelial layers. This experiment indicated that *B. breve*@alginate operated synergistically with tetracycline in protecting intestinal epithelial layers against tetracycline-resistant *E. coli*.

In combination with probiotic bacteria, researchers are investigating the delivery of enzymes (*e.g.* lipase) as a therapeutic strategy designed to enhance digestive efficiency, boost the survival and efficacy of the probiotics, and improve metabolic health. In 2024, Qi and co-workers reported the engineering of *E. coli* with a ZIF-8 exoskeleton for long-term oral delivery of lipase.[176] The ZIF-8 coating was formed by first mixing an aqueous dispersion of *E. coli* with lipase, followed by sequential addition of HmIM and $Zn(NO_3)_2$ under stirring for 10 min; the resulting *E. coli*@ZIF-8 composites were then recovered by centrifugation and washed with deionized water. Transmission electron microscopy (TEM) confirmed the formation of a continuous ZIF-8 shell surrounding individual *E. coli* cells without altering their rod-shaped morphology. Confocal laser scanning fluorescence microscopy, combining DAPI/SYTOX Green live–dead staining with Cy5-lipase imaging, showed homogeneous distribution of lipase within the ZIF-8 exoskeleton and demonstrated that ~10.3% of bacteria remained viable after coating. IR spectroscopy revealed a P–O stretching band shift from 1080 cm^{-1} to 1146 cm^{-1}, consistent with coordination between Zn^{2+} and phosphates on the bacterial surface, while PXRD patterns matched the **sod** ZIF-8 topology. In simulated gastric fluid (SGF, pH ~ 2.0) and simulated intestinal fluid (SIF), the encapsulated lipase retained 8.5% and 23.4% of its activity, respectively, whereas free lipase activity dropped to <5% in SGF and was severely impaired in SIF, indicating that the ZIF-8 shell conferred protection against harsh gastrointestinal conditions. Upon oral gavage of Cy5-labeled *E. coli*@ZIF-8 in BALB/c mice, *in vivo* fluorescence imaging demonstrated pronounced retention in the gastrointestinal tract, as lipase@ZIF-8 persisted for ~4 h, and *E. coli*&lipase@ZIF-8 was detectable up to 48 h post-administration. Finally, histological analysis of major organs (heart, liver, spleen, lung, and kidney) as well as stomach, small intestine, and large intestine after 48 h of exposure showed intact tissue architecture and no signs of inflammation or damage, confirming the biocompatibility of the ZIF-8-engineered *E. coli* platform.

Bioremediation

E. coli@ZIF-8 composites can also be included in bio-remediation applications. For instance, in 2023, Ghasemi *et al.*[177] synthesized rod-shaped *E. coli*@ZIF-8 *via* biomimetic mineralization, mixing an aqueous suspension of *E. coli* with HmIM and $Zn(OAc)_2{\cdot}2H_2O$ followed by centrifugation and drying, which yielded ~3 μm rods mirroring the bacterial template. SEM and PXRD analyses confirmed the homogeneous coating with the **sod** ZIF-8 topology. These *E. coli*@ZIF-8 particles were then incorporated (40 wt%) into polyacrylonitrile (PAN) nanofibers *via* electrospinning (10 wt% PAN in DMF, 20 kV, 15 cm), producing *E. coli*@ZIF-8@PAN composites. The resultant material was then employed for thin-film microextraction (TFME) of benzoylurea insecticides (hexaflumuron and teflubenzuron). The performance of the synthesized *E. coli*@ZIF-8@PAN composite mat was compared with bare PAN and ZIF-8@PAN fiber mats by using HPLC-UV to evaluate their extraction efficiency. The results indicated that *E. coli*@ZIF-8@PAN fibers showed better extraction than the other fiber mats. This result was attributed to the increased surface area and the variety of functional groups obtained from the inclusion of the biocomposite into PAN fibers.

More recently, Liu *et al.*[178] reported the biomimetic mineralization of *B. subtilis* ZL09–26 using ZIF-8 and the green modifier citric acid (CA), forming a protective shell (ZIF-8-CA) to enhance phenanthrene (PHE) biodegradation. The mineralization was achieved by co-incubating *B. subtilis* with HmIM and zinc acetate, followed by surface modification with CA. SEM and EDS analyses confirmed the formation of uniform ZIF-8 and ZIF-8-CA coatings, with the latter exhibiting a more compact and negatively charged shell.

The encapsulated bacteria demonstrated a significantly improved PHE removal efficiency of 94.1% within 6 days, which was 1.9 times that of non-encapsulated cells. Proteomic and

enzymatic analyses revealed that the MOF coating reduced oxidative stress and upregulated key metabolic pathways, including central carbon metabolism and oxidative phosphorylation. Additionally, encapsulated cells retained over 83.31% degradation efficiency after five cycles and showed superior viability and storage stability. These results underscore the utility of ZIF-8 coatings in enhancing microbial resilience and bioremediation efficacy under environmental stress.

Whole-cell vaccines

Recently, studies have demonstrated the applicability of micoorganisms@MOF even though the encased cells were inactivated during the coating process. For instance, Luzuriaga *et al.*[96] reported the encapsulation of *E. coli* (CFT073) within ZIF-8 to treat urinary tract infections. Developing immunity against bacterial infection can be achieved through the administration of inactivated bacteria or a lysed fraction of dead cells. The whole-cell formulations contain strain-specific proteins that trigger antibody production against pathogenic bacteria. However, whole-cell vaccines often fail to provide long-term immune protection, because they elicit weak immune responses, resulting from the short half-life of whole-cell formulations in the body and surface antigen degradation caused by harsh fixation methods.[179] Thus, to enhance the bioprotection of the cell-surface antigens, the authors prepared *E. coli*@ZIF-8 composites, obtained by mixing a zinc acetate aqueous solution with a premixed aqueous dispersion of cells and HmIM. Both solutions were prepared in saline media (NaCl, 100 mM) to keep bacteria near isotonic conditions. After 20 min of stirring, the resulting composite *E. coli*@ZIF-8 was recovered by centrifugation. Then, the authors employed the CFU assay to evaluate the viability of the encapsulated cells. This experiment revealed that the ZIF-8 shell formation process itself inactivated bacteria; this effect was explained by overexposure to Zn^{2+}, causing cell death. Nevertheless, the challenge in whole-cell formulation is inactivating the bacteria with minimal damage to the surface epitopes, including membrane proteins and oligosaccharides. Therefore, to demonstrate that the encapsulation process inactivates the bacteria while preserving the native protein conformation, the authors performed an agglutination assay to monitor the binding affinity of bacterial glycoproteins towards carbohydrates. This test demonstrated that the growth of the MOF coating does not significantly influence the surface epitopes. Preservation of natively folded bacterial proteins might result in a stronger immune response against *E. coli* than traditional inactivation methods. To test this hypothesis, the authors measured antibody titers in mice injected with a saline solution containing different formulations of inactivated *E. coli*: (i) uncoated and thermally inactivated *E. coli*, (ii) formalin-fixed *E. coli*, and (iii) *E. coli*@ZIF-8 composite. Mice immunized with the *E. coli*@ZIF-8 composite produced the highest antibody levels, whereas the uncoated and thermally inactivated *E. coli* formulation induced the lowest antibody production. The authors explained the difference by suggesting that the high temperatures required to inactivate cells cause denaturation of proteinaceous and sugar-based epitopes. By contrast, in the case of the *E. coli*@ZIF-8 formulation, the ZIF encapsulation helped to prevent protein denaturation. In addition, it provided a depot effect by prolonging the presence of *E. coli*@ZIF-8 in the tissue compared to the uncoated bacteria.

Energy storage

Another attractive application of cells@ZIF-8 composites is for energy storage. Gassensmith and co-workers reported the application of the *E. coli*@ZIF-8 composite as a soft template for fabricating hierarchical porous carbons employed in energy storage.[180] The fabrication of *E. coli*@ZIF-8 was performed by using biomimetic mineralization conditions. However, the authors stated that, unlike *S. cerevisiae*, the encapsulation of *E. coli* required a higher ligand-to-metal ratio to form a homogenous cell coating. The TEM micrographs of the *E. coli*@ZIF-8 composite revealed the formation of a MOF shell comprised of closely packed nanocrystals. Interestingly, the nitrogen sorption isotherm of the *E. coli*@ZIF-8 composite, collected at 77 K, shows a hysteresis loop at a P/P_0 of 0.45–1.0. The latter is typically associated with the capillary condensation of the adsorbate in mesopores. Then, pore size distribution analysis confirmed the presence of mesopores of $\sim$60 nm.

Mesopore formation was attributed to crystalline defects arising during the rapid MOF nucleation process. Then, the *E. coli*@ZIF-8 composite underwent a carbonization process to remove the bacterial matter. The TEM images showed that calcinated samples, calc-*E. coli*@ZIF-8, retained the rod-like morphology from the starting biocomposite. However, unlike the *E. coli*@ZIF-8, the calc-*E. coli*@ZIF-8 exhibited reduced contrast in the inner region of rod-like structures. This observation confirmed successful removal of the biological entity, leading to a material with high graphitic carbon content. The gas sorption isotherm and the pore size distribution analysis indicated that calc-*E. coli*@ZIF-8 material retains the mesoporosity, confirming the formation of hierarchical porous carbon (HPC). Finally, the authors compared the electrochemical properties of the calc-*E. coli*@ZIF-8 sample against the calc-ZIF-8. The cyclic voltammetry analysis indicated that calc-*E. coli*@ZIF-8 presented superior electrochemical capacity compared to calc-ZIF-8. Overall, this study demonstrated the potential of cells as templating agents for the preparation of hierarchical porous carbons for energy storage.

Recently, Teng and colleagues used the *E. coli*@ZIF-8 system for the fabrication of a biological nanoreactor.[181] They achieved this by expressing alcohol dehydrogenase (ADH) and glucose dehydrogenase (GDH) within *E. coli* and then coating the cells with ZIF-8. The ADH&GDH multi-enzyme cascade catalytic system demonstrated high efficiency in asymmetrically reducing ketones to produce chiral alcohols with high enantioselectivities ($<$99%). The researchers also investigated the recyclability of the *E. coli*@ZIF-8 system. They found that although catalytic reactivity decreased gradually, possibly due to hydrolysis of the ZIF-8 shell under acidic conditions, the system still retained 80% after four cycles. Similarly, Wang and co-workers reported the encapsulation of two bacterial strains (*E. coli*/pET28a-world and *E. coli*/pET28a-ladd2) within an amorphous ZIF-90 shell for the catalytic synthesis of D-phenylacetic

acid from L-phenylalanine through a two-step cascade reaction.[148] Using *E. coli*@ZIF-90 as a bioreactor for D-PLA production resulted in a yield of 9.00 g L^{-1} with a conversion rate of 89.4%. After 7 cycles, the immobilized material retained 43.8% of its relative activity. After 9 days of storage at 4 °C, the activity of immobilized cells remained above 75%. In contrast, free cells became almost inactive under the same conditions. This demonstrates the successful catalytic conversion of L-phenylalanine to D-PLA without the need for coenzymes or intermediate substances. Furthermore, compared with free cells, the immobilized cells exhibited good stability toward high temperatures, acidity, alkalinity, organic reagents, and metal ions. This work showed that the immobilized cell method has great potential as an industrial production tool for cost-effective D-PLA production.

Biosensing

The fabrication of cell@MOF composites obtained from inactivated microorganisms has been recently studied for biosensing applications. As an example, Xiang and co-workers reported the use of microorganism@UiO-66-NH_2 as a diagnostic probe for the detection of colorectal cancer.[182] Specifically, three different microorganisms were used for the cell@shell preparation, including (i) *S. cerevisiae*, (ii) *E. coli* (DH5a), and (iii) *Synechocystis* sp. PCC 6803 (PCC 6803). These microorganisms were inactivated using formaldehyde treatment before the MOF coating. Then, the dormant cells were suspended in a solution of the MOF precursors ($Zr(OnPr)_4$ and H_2BDC-NH_2) for 18 h. The coated cells were collected by centrifugation and dried in an oven at 60 °C for 12 h. The SEM images collected from the three different cell@MOF composites showed the presence of a uniform abiotic coating. The structural characterization of this artificial coating confirmed the formation of porous UiO-66-NH_2. The high surface area of this MOF resulted in advantages for immobilizing biologically relevant molecules, as the Zr^{4+} ions located on the outer surface of the MOF shell acted as multiple binding sites for protein immobilization. Following this approach, the authors adsorbed streptavidin (SA) onto the outer surface of the MOF shell. Then, the biotinylated-capture probes were immobilized through the strong SA–biotin non-covalent interaction. Using cytometry-based analysis technology, the functionalized cell@MOF composites were used to detect three different miRNA biomarkers (miRNA-21, miRNA-17, and miRNA-182) for colorectal cancer. This study indicated that due to the large amount of protein immobilization on cell@MOF composites, miRNA detection sensitivity could be enhanced to the picomolar range. The reported limit of detection (LOD) values for miRNA-21, miRNA-182, and miRNA-17 biomarkers are 0.75, 0.30, and 0.25 pM, respectively.

Biocatalysis

Chen and co-workers developed protocols to co-immobilize enzymes (*i.e.*, inulinase and lipase) and cells (*e.g.*, *S. cerevisiae*) or bacteria (*e.g.*, *E. coli*) into a series of parent COFs (*i.e.*, NKCOF-98, COF-42-B, and NKCOF-141) to produce cascade biocatalysts with high efficiency, stability, and recyclability (Fig. 7a and b).[44] The COFs investigated in this manuscript

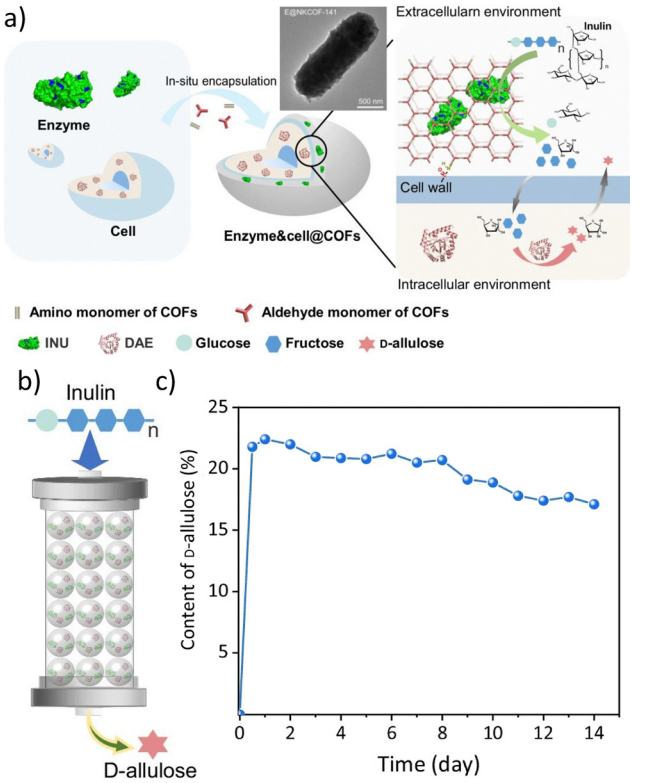

Fig. 7 Pioneering example of the co-encapsulation of cells and enzymes within COFs. Schematic diagram of the *in situ* assembly approach of enzyme&cell@COFs and SEM micrograph of a representative example (a). Schematic diagram of the continuous-flow reaction for the production of D-allulose from inulin and *E. coli*/D-allulose 3-epimerase co-encapsulated in NKCOF-141 (b). Time-dependent content D-allulose for the continuous-flow reaction at room temperature (30 °C) and 0.1 mL min^{-1} (c). Adapted with permission from ref. 44 (licensed under CC BY 4.0, https://creativecommons.org/licenses/by/4.0/).

are based on 1,3,5-triformylbenzene and derivatives of terephthalohydrazide that differ in the presence of hydrophilic (NKCOF-98), hydrophobic (COF-42-B), or amphiphilic (NKCOF-141) functionalization. The authors showed that coating with NKCOF-98 did not result in effective surface coverage, coating with COF-42-B was non-uniform, and only NKCOF-141 produced homogeneously coated cells. The authors hypothesized that, since cell walls usually exhibit amphiphilic features, the amphiphilic nature of the NKCOF-141 ligand facilitated the homogenous growth of the COF on the cell surface. The authors focused their attention on NKCOF-141 for further biocatalytic tests. In particular, by integrating inulinase in *E. coli* cells expressing D-allulose 3-epimerase coated with NKCOF-141, the authors developed a flow reaction apparatus for the continuous production of D-allulose. The performance of these innovative biocatalysts (*e.g.*, inulinase/*E. coli*@NKCOF-141: productivity of D-allulose of 161.3 g L^{-1} day^{-1}, with >76% initial catalytic efficiency retained after 2 weeks of continuous reaction) showed that the co-immobilization of enzymes and cells into COFs could lead to innovative and customizable platforms for biocatalysis, favoring the development of enzyme–cell cascade production of high value products.

The cells@MOF composites have been recently investigated to boost the performance of strictly anaerobic bacteria for photocatalysis, in particular for artificial photosynthesis applications. One example is *M. thermoacetica*: this bacterium employs solar energy and CO_2 as the only carbon source to produce acetate, which is attractive for carbon remediation applications. However, *M. thermoacetica* exhibits high susceptibility to O_2 and reactive oxygen species (ROS), reducing its performance as a photocatalytic agent.[41,183] To tackle this drawback, Yang, Yaghi, and co-workers reported the use of a pre-synthesized Zr-based MOF ($Zr_6O_4(OH)_4(BTB)_2(OH)_6(H_2O)_6$) to coat *M. thermoacetica* cells and exploit the ROS-scavenging properties of the Zr-based coating.[98] The authors tested the performance of *M. thermoacetica* and *M. thermoacetica*@MOF in the photocatalytic conversion of CO_2. This study revealed that the bare cells could only fix CO_2 within the first day of reaction since the accumulation of ROS and O_2 by-products caused cellular damage. By contrast, the *M. thermoacetica*@MOF system remained photo-catalytically active for 2.5 days. Such results showcase the suitability of cell@MOF composites to enhance the bioproduction of value-added chemicals.

MOF-based coatings for cell-like systems

In addition to investigating the encapsulation of living cells, inspired by nature, researchers are engaged in developing synthetic cell-like structures or systems to achieve analogous biological functions *in vitro*. The capacity of cells to perform chemical reactions with high efficiency and selectivity is attributed to the spatial organization of cell-restricted reaction media and cellular components, which enables the attainment of high local concentrations and spatially directed transport of cellular components.[184] Consequently, the fabrication of micro/nanoreactors (MNRs) that emulate the internal configuration of cells is a highly active area of biomimetic study (Fig. 8). Such reactors can be regarded as highly functional material units that can function as biosensors,[185] therapeutics,[186] and especially in biocatalysis[187] either independently or in conjunction with other material matrices. One of the most crucial elements of the reactor is the shell, which can also be defined as the exoskeleton. The outer coating plays a dual role in the reactor, providing robust protection against external factors while regulating the transport of substances and molecules. This phenomenon enables these reactors to perform specific biological functions.

At the outset, liposomes based on phospholipid bilayer membranes were the most prevalent type of coating used for cell-like reactors.[188] This is because liposomes most closely resemble the phospholipid bilayer structure of cell membranes in nature, affording them the potential to exhibit states and functions analogous to those observed in living cells. In addition to liposomes, MNRs based on polymersomes,[189,190] colloidosomes,[190] and proteinosomes[191] have also been developed. Nevertheless, these classes of MNRs continue to exhibit

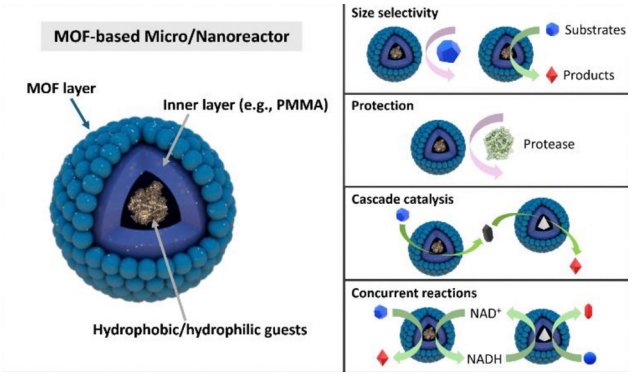

Fig. 8 Schematic illustration of MOF-based MNRs. MOF-based MNRs offer several advantages, including size-selection capability for substrates, protection of internal guests from external environmental factors, and the capacity to construct cascade or concurrent catalytic reactions using MNRs with different catalysts as guests.

shortcomings, including suboptimal membrane permeability, limitations imposed by osmotic pressure, diminished mechanical stability, and inadequate modulation of small molecules. The advent of organic and hybrid framework materials presents an additional avenue for engineering cell-like MNRs, distinguished by selective molecular diffusion and enhanced protection. As previously stated, MOF materials are notable for their porousness, tunable synthesis, adaptable modification, and extensive diversity, which collectively position them as competitive tools in a multitude of fields. As with the encapsulation of living cells, MOF shells of MNRs can provide effective enhancement of stability, ensure space for molecular reactions, and increase the functional versatility of the reactor (Fig. 8).[192] Furthermore, the tunable organic and metal components of the MOF provide a rich chemical microenvironment conducive to reactor functionality.[193]

Pickering emulsion-based coating strategy

A fundamental attribute of living cells is compartmentalization, which safeguards the integrity of biological processes from external influences. It follows that the majority of cell-like MNRs also exhibit a well-defined compartmentalized structure. To achieve this structural feature, these MNRs are typically encapsulated using a Pickering emulsion-based strategy, which can be described as the self-assembly of MOFs as shells around emulsion droplets.[194] Enzymes with dimensions larger than the MOF micropore can be encapsulated, and the dynamic environment facilitates the transport of biomolecules within the compartment.[187] In addition, the Pickering emulsion strategy permits the encapsulation of guest molecules with diverse properties in oil-in-water (O/W) systems or water-in-oil (W/O) systems.[195] For instance, in W/O systems, the construction of hollow composite microspheres called MOF capsules (MOF-Cs) is achieved through the self-assembly of hydrophobic MOF nanoparticles at the water–oil interface.[194] The structural stability of the capsules is enhanced through the precipitation of polymers. Xu *et al.* demonstrated that such MOF-Cs possess a MOF layer regulating molecular migration, a hollow structure

facilitating a confined reaction space, and an encapsulation capability providing catalytically active sites.[187] Additionally, these characteristics enable MOF-Cs to encapsulate incompatible substances and facilitate mass diffusion for tandem reactions.[187] Therefore, MOF-Cs can be considered analogous to cells in that they can occupy different regions to compartmentalize enzymes or molecules that might otherwise interfere with each other, yet still allow the free diffusion of external molecules necessary for reactions.

Despite the exceptional functionality of some hydrophobic molecules, such as organic dyes and organic catalysts, the challenge of dispersing them in aqueous solutions due to their hydrophobic nature can impede their practical applications. Accordingly, researchers introduced hydrophobic molecules (also known as guests) into the oil phase, subsequently forming stable O/W emulsions through the self-assembly of UiO-66-NH_2 NPs at the water–oil interface. The hydrophobic guests were encapsulated within the MOF-Cs, followed by PMMA deposition.[196] The successful encapsulation of a hydrophobic dye, Nile red, in MOF-Cs resulted in an improvement in energy transfer and promoted size-selective catalysis.[196] Therefore, O/W systems are relevant for the utilization of hydrophobic molecules.

Recently, researchers have aimed at expanding single-chambered MOF-Cs into multi-compartmental MOF microreactors, structures much closer to living cells that can catalyze cascade reactions. Tian *et al.* prepared hierarchically multi-compartmental MOF microreactors through a general Pickering double emulsion-based interfacial synthesis method (Fig. 9a).[197] The stabilized Pickering double emulsion (oil-in-water-in-oil double emulsion, O/W/O) can be employed as a growth-oriented template for the formation of a crystalline MOF structure in a large liquid–liquid interfacial region, thereby creating dense MOF layers. The double emulsion system is influenced by many forces, including van der Waals forces between droplet surfaces, intrinsic migratory interactions of droplets generated by interfacial tension, and interactions between metal nodes and organic linkers.[198,199] These forces collectively influence the formation of the MOF shell. Accordingly, the interior microstructure of multi-compartmental MOF microreactors can be modified by adjusting the volume fraction of O/W droplets.[197] The results demonstrate that the Pickering double emulsion-based synthesis method exhibits robust scalability,[197] which will further accelerate rapid development and application of MOF-based MNRs. The structure of MOF-encapsulated MNRs is approaching a configuration that closely resembles the overall structure of living cells. MOFs serve as both a potential outer shell for the reactor and a pivotal element for internal partitioning, offering a broader range of possibilities for MOF-based cell-like reactors and artificial cells.

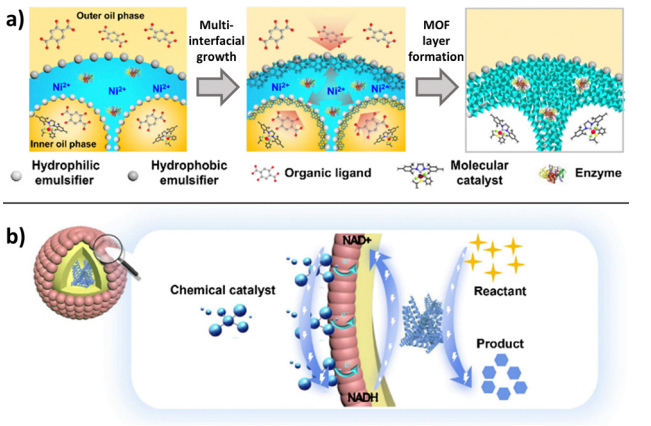

Fig. 9 Schematic illustration of (a) the construction of multi-compartmental MOF microreactors *via* Pickering double emulsions and multi-interfacial growth (adapted with permission from ref. 197, licensed under CC BY 4.0, https://creativecommons.org/licenses/by/4.0/) and (b) and of the electrostatic interaction between MOF-MNRs and chemical catalysts.

Development in cascade catalysis

Cascade catalysis is a pervasive phenomenon in natural systems, whereby multiple enzymes are confined within subcellular compartments. An efficient and highly selective series of catalytic reactions within cells are crucial for maintaining normal metabolic processes and overall organismal functioning. In addition to the requisite reactants and catalysts, the spatial environment in which these biocatalytic reactions occur is particularly important. To be more precise, a confined space can effectively isolate and compartmentalize incompatible substances, while the cascade reactions that take place therein can enhance effective communication between catalysts by facilitating the diffusion of intermediates.[200] In light of this natural phenomenon, MOF-Cs have been employed to serve as cell-like structures, encapsulating enzymes within the capsule. The outer MOF shell assumes a cell membrane-like function, providing protection and size-selectivity, thus ensuring that the specific substrate enters the capsule to undergo the reaction. The capacity for protection and size selection is attributable to the hierarchical pore structure of MOF-Cs, which is achieved through the self-assembly of MOF nanoparticles (MOF NPs).[187] In particular, the intrinsic microporous structure of MOF NPs regulates molecular transport, while the hollow structure inside the capsule allows for the loading of different enzymes. For example, Xu *et al.* synthesized MOF-Cs in W/O emulsions comprising UiO-66-NH_2 NPs as components, encapsulating GOx within them (GOX@MOF-Cs). Their findings demonstrated that GOx@MOF-Cs exhibited efficient glucose oxidation without being affected by proteases in the external environment.[187] Consequently, MOF-Cs exhibit the ability to transport, encapsulate, and compartmentalize.

Biocascade reactions in one-pot. It would be interesting to investigate whether MOF-Cs encapsulating different species could achieve similar subcellular or intercellular molecular transport, thus enabling cascade reactions. Therefore, in addition to GOx, Xu *et al.* encapsulated a protease in another batch of MOF-Cs. The two enzymes are not compatible with one another, but the protection afforded by the MOF shell allows them to coexist in the same system. Experimental results demonstrate that they are capable of glucose production and oxidation in a tandem reaction.[187] In other words, MOF-Cs enable intermediate

transfer, allowing glucose produced by protease catalysis to reach GOx. This effectively transforms the opposing enzyme into an ally, establishing a connection between the two.

Chem-biocascade reactions in one-pot. MOF MNRs are not only capable of performing biological cascade reactions; they are abiotic reactors, thereby broadening the range of catalytic reactions that can be catalyzed by cell-mimetic reactors, *e.g.*, enabling chem-biocascade reactions. Chemical catalysts are subject to much more rigorous reaction conditions than enzymes, which are vulnerable to damage and can only function under relatively mild conditions. It is evident that biocatalysts and chemical catalysts typically operate in disparate environments, rendering it challenging to integrate both types of catalysts into a unified reaction system for cascade reactions.[201] In light of the distinctive attributes of MOF-Cs, researchers successfully established a connection between catalysts from disparate domains. Zhang *et al.* synthesized MOF-Cs in Pickering W/O emulsions with internally encapsulated alcohol dehydrogenase (AlcDH) and a Pt chemocatalyst dispersed in the external environment of the capsule. The linkage between the Pt chemocatalyst and AlcDH was established through the mediation of the redox reaction between NAD^+ and NADH, and the results showed that the Pt-catalyzed depletion of formate enabled AlcDH to convert pyruvic acid to lactic acid in one-pot (Fig. 9b).[202] The compartmentalization effect of MOF-Cs effectively separates chemical and biological catalysts from one another and from the surrounding environment. Concurrently, the MOF shell exhibited robust transport properties, as evidenced by the movement of NADH and NAD^+ within it, facilitating the interconnection between the two catalytic reactions.

Cascade reactions in a single MOF microreactor. The previously mentioned biological and chemical-biological cascade reactions rely on synthesizing two MOF-Cs encapsulating different species, placed in one-pot for the reaction to occur. However, the researchers extended this approach by encapsulating the different catalytic components into a multi-compartmentalized MOF-Cs microreactor. As mentioned in the section on coating strategies, hierarchically multi-compartmental MOF-Cs structures can be synthesized using the O/W/O Pickering double emulsions-directed interfacial encapsulation method.[197] The multi-compartmental structure of the MOF microreactor is analogous to the subcellular structure observed in cells. Each inner O/W capsule serves as a distinct compartment for the molecules, while the corridor-like sections outside the compartments facilitate the dispersion of molecules that are incompatible with the inner droplet. Additionally, the intermediates of the reaction are transported in and out of the compartments through the pores of MOFs, enabling the completion of the cascade reaction. To illustrate, the researchers validated that multi-compartmental MOF microreactors exhibit excellent encapsulation efficiency and size selectivity. They proceeded to encapsulate two different chemo-biocascade catalysts, the well-known Grubbs' catalyst/CALB lipase and GOx/Fe-porphyrin, in the internal oil-phase compartments and aqueous-phase compartments of the microreactor.[197] The success of the two cascade reactions verified that multi-compartmental MOF-Cs have good applicability in cascade reactions. In the future, such cascade reactions are likely to find application in microreactors for complex cascade biocatalytic processes.

Future opportunities and challenges

Research on living cells encapsulated in MOF, COF, and HOF exoskeletons has made considerable progress, but several key challenges and questions remain unaddressed. As the field of emerging porous materials is more advanced for MOFs, we will predominantly refer to this class. Below, we highlight several promising directions, ranging from advanced therapeutics to synthetic biology, while also highlighting roadblocks that must be overcome to enable wide-scale translation.

Biomedical applications

Next-generation immunotherapy and synergistic combination strategies

Immunotherapy. Cancer immunotherapy has emerged as a powerful clinical treatment, utilizing specialized cells (*e.g.*, T-lymphocytes, NK cells, and dendritic cells) and bacterial-mediated cancer therapy (BMCT) to target malignancies. While BMCT harnesses the inherent tumor-targeting ability of specific bacterial strains, clinical translation has been historically hindered by risks of systemic toxicity, uncontrolled bacterial proliferation, and insufficient drug loading. In this context, cell encapsulation within porous frameworks (MOFs, COFs, and HOFs) offers a transformative solution. Framework shells, particularly zinc imidazolate frameworks (ZIFs), act as cloaking devices that physically restrict pathogen-associated molecular patterns (PAMPs, *e.g.* lipopolysaccharides) during transport. This shielding delays immune recognition and reduces off-target inflammation until the vehicle reaches the tumor microenvironment.

Opportunities in synergistic delivery. The most significant opportunity in this domain lies in the transition from simple cell carriers to multifunctional combination therapies. Beyond protecting the cargo, porous frameworks can serve as dual-delivery systems, co-encapsulating small-molecule chemotherapeutics or immunomodulators alongside the cellular payload.[203] These systems are designed to degrade in response to tumor microenvironment specific stimuli (*e.g.*, acidic pH and high ATP concentrations),[38,56,139] ensuring the simultaneous, localized release of both the therapeutic agent and the biological cargo. Furthermore, integrating genetically engineered bacteria capable of secreting anticancer proteins within these confined frameworks represents a high-potential avenue for increasing drug-loading capacity and advancing toward more potent combination therapies.

Next-generation tissue engineering

Engineered cell interactions. In tissue engineering, controlling spatial organization and communication among cells is crucial.[204–206] Porous framework exoskeletons can be designed to promote or inhibit specific cell–cell interactions by selectively

allowing growth factors, cytokines, or other signaling molecules to diffuse through the framework material. Such coatings might also help cells endure mechanical stresses or nutrient fluctuations common in early tissue scaffolding stages.

Integration with biopolymer scaffolds. A major advance would be the integration of encapsulated cells into larger 3D scaffolds, where biocompatibility and structural stability must be maintained for long periods (*e.g.*, weeks and months). Future work on hybrid materials, combining organic polymers (*e.g.*, collagen and alginate) with MOF/COF/HOF, could yield composite scaffolds that simultaneously offer mechanical support and molecular sieving. Success in this goal may offer new ways to engineer tissues with higher viability and functionality, yet it will require new characterization methods (*e.g.*, *in situ* imaging of shell integrity) and standardized viability assays in complex, multi-component systems.

Translational barriers and safety considerations. Despite their promise, ensuring the safety of cell@framework systems in *in vivo* applications, ranging from tissue engineering to cancer immunotherapy, remains a complex challenge. A primary concern is the biocompatibility of MOF degradation products. While metal ions and organic linkers (*e.g.*, zinc ions and imidazole derivatives) released during framework decomposition are often considered non-toxic in low doses, their local accumulation could induce cytotoxicity in non-target tissues or exacerbate inflammation. For example, in coating processes, it was observed that the viability of cells can drop by using certain MOF coating protocols.[31,119] Additionally, the administration of live bacteria, even when attenuated or encapsulated, poses a persistent risk of systemic infection or cytokine storm if the framework degrades prematurely or if the bacterial load overwhelms the clearance capacity of the reticuloendothelial system.

Concerns are also related to the antibiotic resistance of bacteria-based therapeutics. ZIF-encapsulated bacteria often exhibit improved tolerance to antibiotics[97] and UV irradiation.[109] As a result, the use of antibiotic-resistant plasmids—which raise safety and regulatory issues—may be unnecessary, and UV sterilization could be employed to enhance manufacturing safety without compromising bacterial viability. In immunotherapy applications, this would simplify clinical translation by lowering the risks of antibiotic resistance and facilitating Good Manufacturing Practice (GMP) protocols.

Future directions. To bridge the gap between laboratory success and clinical application, future research must balance shell stability with precise degradability. Material design should prioritize ligands with inherently low immunogenicity and metal centers with established metabolic clearance pathways. Ultimately, the field must move beyond simple cytotoxicity assays toward rigorous *in vivo* assessment of long-term immune activation, biodistribution, and toxicology to validate these next-generation cell@MOF/COF/HOF therapeutics.

Industrial biotechnology

Engineered porous framework coatings for selective separation. In biomanufacturing, downstream processing, specifically protein purification, often requires multiple, expensive steps.[207–209] While current cell encapsulation strategies primarily focus on cytoprotection, there is a significant underutilized opportunity to engineer the framework shell as a selective, semi-permeable membrane for integrated production and purification. By adjusting the pore size and functionality of the encapsulating porous layer, researchers can engineer selective binding sites for target proteins, coenzymes, or other biomolecules. The majority of current research utilizes microporous shells (*e.g.*, ZIF-8, pore aperture $\sim$3.4 Å), which effectively transport small nutrient molecules but restrict the diffusion of macromolecular protein products. By transitioning toward mesoporous frameworks (pore apertures $>$2 nm), engineered framework shells can function as molecular sieves with a defined molecular weight cut-off. This allows therapeutic proteins to be secreted from the encapsulated cell while physically blocking the influx of destructive exogenous proteases, thereby preserving product integrity at the source. Furthermore, by functionalizing pore walls with charged groups (*e.g.*, amines or carboxylates), researchers can implement electrostatic gating. This enables the *in situ* fractionation of target molecules based on their isoelectric point, potentially streamlining the purification workflow and advancing the feasibility of continuous bioprocessing.

Engineered coatings for the use of enzymes within cells. Whole-cell biocatalysis, where enzymes are expressed and function within living cells rather than as free enzymes, offers advantages including enhanced enzyme stability and efficient cofactor regeneration, as exemplified in the synthesis of fine chemicals.[210] However, even in this cellular context, enzymatic performance is often compromised by rapid degradation, suboptimal reaction environments, and uncontrolled substrate diffusion.[211–213] Engineered porous framework coatings offer a promising approach to address these challenges. By encapsulating enzymes within a tailored porous framework shell, researchers can protect the enzyme from intracellular proteases while creating a microenvironment that enhances catalytic performance.[210] Adjusting the pore size and surface functionality of the porous layer allows for selective substrate entry and product exit, ensuring that only molecules of the desired size or chemistry interact with the encapsulated enzyme.

Artificial cell coatings for whole-cell biosynthesis. Coating living cells with artificial membranes enables enhanced control over biocatalytic processes, offering benefits such as improved cell and enzyme stability, selective permeability, and protection from external stressors, as demonstrated in various whole-cell biotransformations.[1,44] However, challenges remain in balancing mass transport, maintaining catalytic efficiency, and ensuring long-term stability. Artificial cell coatings based on advanced composite materials, including polymeric layers, lipid bilayers, and MOF/HOF/COF-based shells, could offer a tunable strategy to optimize substrate diffusion, catalytic microenvironments, and continuous separation/purification of substrates/products while shielding cells from inhibitory conditions.

Porous shell design, scale-up, reproducibility, and manufacturing standards

Design of the porous shell and its stability. The first requirement of the MOF shell is that it should have minimal

interference with cell metabolic and apoptotic pathways to maintain cells viable. For example, different cations in different concentrations show different cytotoxicity effects;[214] thus, the selection of cations that can be better tolerated by living organisms should be prioritized. An additional strategy to reduce the cytotoxic effect of metal cations is to favor the rapid self-assembly of the MOF shell. An alternative route to circumvent the issue is the design of fully organic network materials (*e.g.*, COFs and HOFs). Furthermore, stable-yet-permeable shell formation under mild, aqueous/buffer conditions remains complex. For example, the presence of certain anions (*e.g.*, phosphate) or nucleophile groups (*e.g.*, COO^-) can lead to the decomposition of certain MOFs (*e.g.*, ZIFs).[139] An aspect often overlooked in the framework design is the effect of chemical functionalization on the ligands employed. Research into porous framework materials aimed at developing shells compatible with cell growth media will be critical for wide-scale adoption in biotechnological processes.

Responsiveness of the porous shell to cellular stimuli. Exciting opportunities can be found at the interface of synthetic biology and porous framework cell-encapsulation. For example, it was demonstrated that a functionalized MOF shell can be decomposed under external stimuli to release specific proteins that can modify the environment, enhancing biocompatibility.[16] However, a substantial conceptual improvement could involve pre-programmed cell biological pathways that, by sensing changes in the cellular microenvironment, would enable the cell to trigger modifications of the porous shell. For example, if cells detect elevated ROS, a feedback loop might induce degradation of the framework, releasing protective naturally produced (enzymes and vitamins) or artificial antioxidants.

Scaling-up barriers. A challenge in the field of artificial spore fabrication involves establishing robust manufacturing processes to ensure reproducibility and consistent material properties. The formation of the protective shell is a highly sensitive process: it critically depends on factors such as frameworks' precursor ratios and concentrations, cell type and density, reaction time and temperature, pH, the specific medium used, and the subsequent post-treatment (*e.g.*, washes). Small deviations in any of these parameters can alter shell thickness, homogeneity, crystal phase, and the viability of the cells. In current batch-synthesis methods, small deviations in any of these parameters can lead to significant batch-to-batch variability, hindering reliable data comparison and product validation.

Advanced manufacturing technologies. To address these inconsistencies, the field must move toward automated, continuous production methods. While control over particle size and crystalline phase has been successfully demonstrated for protein@ZIF systems using continuous-flow approaches,[57] this technology has yet to be developed for cell@MOF, COF, or HOF systems. Implementing microfluidic or continuous-flow reactors offers a promising pathway to achieve Gram-scale production. These systems allow for the meticulous regulation of precursor concentrations, temperature, pH, and mixing dynamics, which is expected to yield reliable, uniform coatings and high cell viability. Reproducible, large-scale coating of viable cells with finely tuned porous framework shells would advance industrial applications of cell@MOF/COF/HOF.

Standardization and benchmarking. Technological upscaling alone is insufficient without the establishment of rigorous community standards. Future efforts should focus on developing standardized protocols where every step, beginning with the preparation of framework precursor solutions and extending to post-encapsulation washing or storage, is meticulously detailed. Furthermore, the community should be encouraged to systematically publish details of both successful and suboptimal experiments (*e.g.*, those resulting in partial shells or lower viability). Establishing such transparency will create robust benchmarks, allowing researchers to validate new coating strategies and compare datasets across different laboratories. Ultimately, combining advanced continuous manufacturing with standardized reporting is essential to accelerate the transition of cell@framework materials from proof-of-concept studies to high-throughput industrial applications.

Conclusions and outlook

In summary, the functional properties of MOF-, COF-, and HOF-based coatings offer unprecedented opportunities for cell applications ranging from separation technology to medical treatments. By engineering framework materials with controlled pore size distribution, pore chemistry, stimulus-responsive behavior, and the ability to host and co-deliver functional agents, researchers can design novel microbial therapies and engineered tissues. Yet, significant scientific and regulatory hurdles remain, including reproducibility challenges, robust assessment of viability, finely tuned "on-demand" degradability, large-scale process optimization, and safety profiling. Through cross-disciplinary collaborations among chemists, materials scientists, bioengineers, and clinical researchers, these challenges could be addressed, enabling cells coated with porous shells to overcome current limitations of cell-based technologies in industrial biocatalysis and biomedicine.

Author contributions

FC and MVH: data curation, visualization, writing – original draft; AEM, DK, QW, RK, LYC, JG, FKS, CD: writing – original draft; PF: conceptualization, visualization, funding acquisition, project administration, writing – original draft; FC and PF: writing – review and editing.

Conflicts of interest

There are no conflicts to declare.

Data availability

No primary research results, software or code have been included and no new data were generated or analysed as part of this review.

Supplementary information: video S1 visualizes the role of artificial cell coatings as molecular sieves. See DOI: https://doi.org/10.1039/d4cs00071d.

Acknowledgements

We acknowledge the PMWS Lead Project (LP-03) and TU Graz for support.

Notes and references

1 J. Guo, Y. Yu, W. Zhu, R. E. Serda, S. Franco, L. Wang, Q. Lei, J. O. Agola, A. Noureddine, E. Ploetz, S. Wuttke and C. J. Brinker, *Adv. Funct. Mater.*, 2021, **31**, 2005935.
2 S. Yao, B. Jin, Z. Liu, C. Shao, R. Zhao, X. Wang and R. Tang, *Adv. Mater.*, 2017, **29**, 1605903.
3 I. Holzmeister, M. Schamel, J. Groll, U. Gbureck and E. Vorndran, *Acta Biomater.*, 2018, **74**, 17–35.
4 H. K. Baca, C. Ashley, E. Carnes, D. Lopez, J. Flemming, D. Dunphy, S. Singh, Z. Chen, N. Liu, H. Fan, G. P. López, S. M. Brozik, M. Werner-Washburne and C. J. Brinker, *Science*, 2006, **313**, 337–341.
5 W. A. M. Wolken, J. Tramper and M. J. van der Werf, *Trends Biotechnol.*, 2003, **21**, 338–345.
6 E. I. Tocheva, D. R. Ortega and G. J. Jensen, *Nat. Rev. Microbiol.*, 2016, **14**, 535–542.
7 M. Y. Galperin, S. L. Mekhedov, P. Puigbo, S. Smirnov, Y. I. Wolf and D. J. Rigden, *Environ. Microbiol.*, 2012, **14**, 2870–2890.
8 P. Setlow, *Cell*, 2008, **135**, 410–412.
9 M. Cuéllar-Cruz, *Prog. Cryst. Growth Charact. Mater.*, 2017, **63**, 94–103.
10 C. S. Kovacs, C. Chaussain, P. Osdoby, M. L. Brandi, B. Clarke and R. V. Thakker, *Nat. Rev. Endocrinol.*, 2021, **17**, 336–349.
11 D. Hong, M. Park, S. H. Yang, J. Lee, Y.-G. Kim and I. S. Choi, *Trends Biotechnol.*, 2013, **31**, 442–447.
12 K. Liang, J. J. Richardson, C. J. Doonan, X. Mulet, Y. Ju, J. Cui, F. Caruso and P. Falcaro, *Angew. Chem., Int. Ed.*, 2017, **56**, 8510–8515.
13 R. Kempaiah, S. Salgado, W. L. Chung and V. Maheshwari, *Chem. Commun.*, 2011, **47**, 11480.
14 G. Wang, L. Wang, P. Liu, Y. Yan, X. Xu and R. Tang, *ChemBioChem*, 2010, **11**, 2368–2373.
15 C. Sicard, M. Perullini, C. Spedalieri, T. Coradin, R. Brayner, J. Livage, M. Jobbágy and S. A. Bilmes, *Chem. Mater.*, 2011, **23**, 1374–1378.
16 L. Gan, M. de J. Velásquez-Hernández, A. Emmerstorfer-Augustin, P. Wied, H. Wolinski, S. D. Zilio, M. Solomon, W. Liang, C. Doonan and P. Falcaro, *Chem. Commun.*, 2022, **58**, 10004–10007.
17 S. H. Yang, D. Hong, J. Lee, E. H. Ko and I. S. Choi, *Small*, 2013, **9**, 178–186.
18 W. Youn, J. Y. Kim, J. Park, N. Kim, H. Choi, H. Cho and I. S. Choi, *Adv. Mater.*, 2020, **32**, 1907001.
19 J. H. Park, K. Kim, J. Lee, J. Y. Choi, D. Hong, S. H. Yang, F. Caruso, Y. Lee and I. S. Choi, *Angew. Chem., Int. Ed.*, 2014, **53**, 12420–12425.
20 Q. Lei, J. Guo, F. Kong, J. Cao, L. Wang, W. Zhu and C. J. Brinker, *J. Am. Chem. Soc.*, 2021, **143**, 6305–6322.
21 L. Yuan, H. Wei, X.-Y. Yang, W. Geng, B. W. Peterson, H. C. Van Der Mei and H. J. Busscher, *ACS Appl. Mater. Interfaces*, 2021, **13**, 15973–15982.
22 S. H. Yang, K.-B. Lee, B. Kong, J.-H. Kim, H.-S. Kim and I. Choi, *Angew. Chem., Int. Ed.*, 2009, **48**, 9160–9163.
23 S. H. Yang, E. H. Ko and I. S. Choi, *Langmuir*, 2012, **28**, 2151–2155.
24 Z. Cao and J. Liu, *Nat. Protoc.*, 2024, **19**, 3162–3190.
25 Z. Cao, S. Cheng, X. Wang, Y. Pang and J. Liu, *Nat. Commun.*, 2019, **10**, 3452.
26 Z. Cao and J. Liu, *Acc. Mater. Res.*, 2024, **5**, 872–883.
27 P. Feng, Z. Cao, X. Wang, J. Li and J. Liu, *Adv. Mater.*, 2020, **32**, 2002406.
28 H. Luo, F. Wu, X. Wang, S. Lin, M. Zhang, Z. Cao and J. Liu, *Mater. Today*, 2023, **62**, 98–110.
29 H. Luo, J. Xie, X. Su, P. Wang, H. Chen, X. Kuang and J. Liu, *Sci. China Mater.*, 2024, **67**, 3833–3848.
30 W. Yu, H. Luo, B. Han, S. Lin, Q. Li, R. Xue, H. Tang, X. Jia, L. Wang and J. Liu, *Nat. Commun.*, 2025, **16**, 7691.
31 M. de, J. Velásquez-Hernández, M. Linares-Moreau, E. Astria, F. Carraro, M. Z. Alyami, N. M. Khashab, C. J. Sumby, C. J. Doonan and P. Falcaro, *Coord. Chem. Rev.*, 2021, **429**, 213651.
32 O. M. Yaghi, *Nano Lett.*, 2020, **20**, 8432–8434.
33 D. Yu, H. Zhang, Z. Liu, C. Liu, X. Du, J. Ren and X. Qu, *Angew. Chem., Int. Ed.*, 2022, **61**, e202201485.
34 R. Riccò, W. Liang, S. Li, J. J. Gassensmith, F. Caruso, C. Doonan and P. Falcaro, *ACS Nano*, 2018, **12**, 13–23.
35 H. Furukawa, K. E. Cordova, M. O'Keeffe and O. M. Yaghi, *Science*, 2013, **341**, 1230444.
36 X. Song, Y. Wang, C. Wang, D. Wang, G. Zhuang, K. O. Kirlikovali, P. Li and O. K. Farha, *J. Am. Chem. Soc.*, 2022, **144**, 10663–10687.
37 P. Li, M. R. Ryder and J. F. Stoddart, *Acc. Mater. Res.*, 2020, **1**, 77–87.
38 S. Kandambeth, K. Dey and R. Banerjee, *J. Am. Chem. Soc.*, 2019, **141**, 1807–1822.
39 Z. Sun, R. Hübner, J. Li and C. Wu, *Nat. Commun.*, 2022, **13**, 3142.
40 M. H. O. Roshid, M. Moraskie, G. O'Connor, E. Dikici, J.-M. Zingg, S. Deo, L. G. Bachas and S. Daunert, *Microchem. J.*, 2023, **193**, 109088.
41 K. K. Sakimoto, A. B. Wong and P. Yang, *Science*, 2016, **351**, 74–77.
42 A. K. Singh, R. Awasthi and R. Malviya, *J. Controlled Release*, 2023, **354**, 439–452.
43 X. Lou, Z. Chen, Z. He, M. Sun and J. Sun, *Nano-Micro Lett.*, 2021, **13**, 37.
44 D. Zheng, Y. Zheng, J. Tan, Z. Zhang, H. Huang and Y. Chen, *Nat. Commun.*, 2024, **15**, 5510.
45 P. Falcaro, F. Normandin, M. Takahashi, P. Scopece, H. Amenitsch, S. Costacurta, C. M. Doherty, J. S. Laird,

M. D. H. Lay, F. Lisi, A. J. Hill and D. Buso, *Adv. Mater.*, 2011, **23**, 3901–3906.
46 C. M. Doherty, E. Knystautas, D. Buso, L. Villanova, K. Konstas, A. J. Hill, M. Takahashi and P. Falcaro, *J. Mater. Chem.*, 2012, **22**, 11470.
47 E. Zanchetta, L. Malfatti, R. Ricco, M. J. Styles, F. Lisi, C. J. Coghlan, C. J. Doonan, A. J. Hill, G. Brusatin and P. Falcaro, *Chem. Mater.*, 2015, **27**, 690–699.
48 M. J. Van Vleet, T. Weng, X. Li and J. R. Schmidt, *Chem. Rev.*, 2018, **118**, 3681–3721.
49 A. Veis and J. R. Dorvee, *Calcif. Tissue Int.*, 2013, **93**, 307–315.
50 in *The IUPAC Compendium of Chemical Terminology: The Gold Book*, ed. V. Gold, International Union of Pure and Applied Chemistry (IUPAC), Research Triangle Park, NC, 4th edn, 2019.
51 J. D. Clogston and A. K. Patri, in *Characterization of Nanoparticles Intended for Drug Delivery*, ed. S. E. McNeil, Humana Press, Totowa, NJ, 2011, vol. 697, pp. 63–70.
52 N. K. Maddigan, A. Tarzia, D. M. Huang, C. J. Sumby, S. G. Bell, P. Falcaro and C. J. Doonan, *Chem. Sci.*, 2018, **9**, 4217–4223.
53 W. Liang, P. Wied, F. Carraro, C. J. Sumby, B. Nidetzky, C.-K. Tsung, P. Falcaro and C. J. Doonan, *Chem. Rev.*, 2021, **121**, 1077–1129.
54 K. Alt, F. Carraro, E. Jap, M. Linares-Moreau, R. Riccò, M. Righetto, M. Bogar, H. Amenitsch, R. A. Hashad, C. Doonan, C. E. Hagemeyer and P. Falcaro, *Adv. Mater.*, 2022, **34**, 2106607.
55 E. Astria, M. Thonhofer, R. Ricco, W. Liang, A. Chemelli, A. Tarzia, K. Alt, C. E. Hagemeyer, J. Rattenberger, H. Schroettner, T. Wrodnigg, H. Amenitsch, D. M. Huang, C. J. Doonan and P. Falcaro, *Mater. Horiz.*, 2019, **6**, 969–977.
56 F. Carraro, M. de, J. Velásquez-Hernández, E. Astria, W. Liang, L. Twight, C. Parise, M. Ge, Z. Huang, R. Ricco, X. Zou, L. Villanova, C. O. Kappe, C. Doonan and P. Falcaro, *Chem. Sci.*, 2020, **11**, 3397–3404.
57 F. Carraro, J. D. Williams, M. Linares-Moreau, C. Parise, W. Liang, H. Amenitsch, C. Doonan, C. O. Kappe and P. Falcaro, *Angew. Chem.*, 2020, **132**, 8200–8204.
58 L. Heinke and C. Wöll, *Adv. Mater.*, 2019, **31**, 1806324.
59 P. Falcaro, D. Buso, A. J. Hill and C. M. Doherty, *Adv. Mater.*, 2012, **24**, 3153–3168.
60 K. Liang, C. Carbonell, M. J. Styles, R. Ricco, J. Cui, J. J. Richardson, D. Maspoch, F. Caruso and P. Falcaro, *Adv. Mater.*, 2015, **27**, 7293–7298.
61 M. R. Hafner, F. Carraro, L. A. Brandner, S. Maniam, G. Grenci, S. Ljubojevic-Holzer, H. Bischof, R. Malli, S. M. Borisov, C. Doonan and P. Falcaro, *Chem. Commun.*, 2020, **56**, 12733–12736.
62 R. M. Olabisi, *J. Biomed. Mater. Res.*, 2015, **103**, 846–859.
63 J. Lee, J. Choi, J. H. Park, M. Kim, D. Hong, H. Cho, S. H. Yang and I. S. Choi, *Angew. Chem., Int. Ed.*, 2014, **53**, 8056–8059.
64 W. Zhu, J. Guo, S. Amini, Y. Ju, J. O. Agola, A. Zimpel, J. Shang, A. Noureddine, F. Caruso, S. Wuttke, J. G. Croissant and C. J. Brinker, *Adv. Mater.*, 2019, **31**, 1900545.
65 T. J. Silhavy, D. Kahne and S. Walker, *Cold Spring Harbor Perspect. Biol.*, 2010, **2**, a000414.
66 S. I. Miller and N. R. Salama, *PLoS Biol.*, 2018, **16**, e2004935.
67 G. Zhang, T. C. Meredith and D. Kahne, *Curr. Opin. Microbiol.*, 2013, **16**, 779–785.
68 I. Bononi, V. Balatti, S. Gaeta and M. Tognon, *Appl. Environ. Microbiol.*, 2008, **74**, 6470–6472.
69 N. Ruiz and T. J. Silhavy, *J. Bacteriol.*, 2022, **204**, e00230.
70 S. Yan, X. Zeng, Y. Wang and B. Liu, *Adv. Healthcare Mater.*, 2020, **9**, 2000046.
71 G. Neumann, S. Cornelissen, F. Van Breukelen, S. Hunger, H. Lippold, N. Loffhagen, L. Y. Wick and H. J. Heipieper, *Appl. Environ. Microbiol.*, 2006, **72**, 4232–4238.
72 J. Li and L. A. McLandsborough, *Int. J. Food Microbiol.*, 1999, **53**, 185–193.
73 D. Montag, M. Frant, H. Horn and K. Liefeith, *Biofouling*, 2012, **28**, 315–327.
74 M. Rohde, *Microbiol. Spectrosc.*, 2019, **7**(3), 10.
75 K. Cremin, B. Jones, J. Teahan, G. N. Meloni, D. Perry, C. Zerfass, M. Asally, O. S. Soyer and P. R. Unwin, *Anal. Chem.*, 2020, **92**(24), 16024–16032.
76 M. L. F. Murga, G. Font De Valdez and A. E. Disalvo, *Cryobiology*, 2000, **41**, 10–16.
77 J. K. Oh, Y. Yegin, F. Yang, M. Zhang, J. Li, S. Huang, S. V. Verkhoturov, E. A. Schweikert, K. Perez-Lewis, E. A. Scholar, T. M. Taylor, A. Castillo, L. Cisneros-Zevallos, Y. Min and M. Akbulut, *Sci. Rep.*, 2018, **8**, 17247.
78 M. C. Van Loosdrecht, J. Lyklema, W. Norde, G. Schraa and A. J. Zehnder, *Appl. Environ. Microbiol.*, 1987, **53**, 1898–1901.
79 N. A. R. Gow, J.-P. Latge and C. A. Munro, *Microbiol. Spectrosc*, 2017, **5**(3), 01.
80 A. E. Smith, Z. Zhang, C. R. Thomas, K. E. Moxham and A. P. J. Middelberg, *Proc. Natl. Acad. Sci. U. S. A.*, 2000, **97**, 9871–9874.
81 D. Kregiel, J. Berlowska and B. Szubzda, *J. Ind. Microbiol. Biotechnol.*, 2012, **39**, 1881–1886.
82 L. M. Lavaisse, A. Hollmann, M. A. Nazareno and E. A. Disalvo, *Colloids Surf., B*, 2019, **174**, 63–69.
83 A. Rogowska, P. Pomastowski, M. Złoch, V. Railean-Plugaru, A. Król, K. Rafińska, M. Szultka-Młyńska and B. Buszewski, *Sci. Rep.*, 2018, **8**, 7261.
84 in *Molecular biology of the cell*, ed. B. Alberts, Garland Science, New York, 4th edn, 2002.
85 A. Melelli, O. Arnould, J. Beaugrand and A. Bourmaud, *Molecules*, 2020, **25**, 632.
86 G. Gilliard, E. Huby, S. Cordelier, M. Ongena, S. Dhondt-Cordelier and M. Deleu, *Front. Plant Sci.*, 2021, **12**, 749581.
87 T. B. Kinraide, U. Yermiyahu and G. Rytwo, *Plant Physiol.*, 1998, **118**, 505–512.
88 P. Durand-Smet, N. Chastrette, A. Guiroy, A. Richert, A. Berne-Dedieu, J. Szecsi, A. Boudaoud, J.-M. Frachisse, M. Bendahmane, O. Hamant and A. Asnacios, *Biophys. J.*, 2014, **107**, 2237–2244.

89 O. V. Bondar, D. V. Saifullina, I. I. Shakhmaeva, I. I. Mavlyutova and T. I. Abdullin, *Acta Naturae*, 2012, **4**, 78–81.
90 M. Nishino, I. Matsuzaki, F. Y. Musangile, Y. Takahashi, Y. Iwahashi, K. Warigaya, Y. Kinoshita, F. Kojima and S. Murata, *PLoS One*, 2020, **15**, e0236373.
91 F. Esposito, M. R. Fernandes, R. Lopes, M. Muñoz, C. P. Sabino, M. P. Cunha, K. C. Silva, R. Cayô, W. M. B. S. Martins, A. M. Moreno, T. Knöbl, A. C. Gales and N. Lincopan, *J. Clin. Microbiol.*, 2017, **55**, 3454–3465.
92 I. Obi, T. Kakutani, N. Imaizumi, Y. Ichikawa and M. Senda, *Plant Cell Physiol.*, 1990, **31**, 1031–1037.
93 M. J. Stoddart, in *Mammalian Cell Viability*, ed. M. J. Stoddart, Humana Press, Totowa, NJ, 2011, vol. 740, pp. 1–6.
94 M. R. Barer and C. R. Harwood, *Advances in Microbial Physiology*, Elsevier, 1999, vol. 41, pp. 93–137.
95 H. Wei, X.-Y. Yang, W. Geng, H. C. Van Der Mei and H. J. Busscher, *Nanoscale*, 2021, **13**, 7220–7233.
96 M. A. Luzuriaga, F. C. Herbert, O. R. Brohlin, J. Gadhvi, T. Howlett, A. Shahrivarkevishahi, Y. H. Wijesundara, S. Venkitapathi, K. Veera, R. Ehrman, C. E. Benjamin, S. Popal, M. D. Burton, M. A. Ingersoll, N. J. De Nisco and J. J. Gassensmith, *ACS Nano*, 2021, **15**, 17426–17438.
97 H. Li, A. Kang, B. An, L.-Y. Chou, F.-K. Shieh, C.-K. Tsung and C. Zhong, *Mater. Today Bio*, 2021, **10**, 100097.
98 Z. Ji, H. Zhang, H. Liu, O. M. Yaghi and P. Yang, *Proc. Natl. Acad. Sci. U. S. A.*, 2018, **115**, 10582–10587.
99 K. M. McKinnon, *CP Immunol.*, 2018, **120**, 5.1.1–5.1.11.
100 L. L.-Y. Chan, K. J. McCulley and S. L. Kessel, in *Cell Viability Assays*, ed. D. F. Gilbert and O. Friedrich, Springer New York, New York, NY, 2017, vol. 1601, pp. 27–41.
101 in *Cell Viability Assays: Methods and Protocols*, ed. D. F. Gilbert and O. Friedrich, Springer New York, New York, NY, 2017, vol. 1601.
102 P. Stiefel, S. Schmidt-Emrich, K. Maniura-Weber and Q. Ren, *BMC Microbiol.*, 2015, **15**, 36.
103 Lehninger Principles of Biochemistry – ISBN-13 978-1-4292-3414-6, https://www.books-by-isbn.com/1-4292/1429234148-Lehninger-Principles-of-Biochemistry-David-L-Nelson-Michael-M-Cox-1-4292-3414-8.html, (accessed March 3, 2026).
104 S. L. Fink and B. T. Cookson, *Infect. Immun.*, 2005, **73**, 1907–1916.
105 Z. Darzynkiewicz, S. Bruno, G. Del Bino, W. Gorczyca, M. A. Hotz, P. Lassota and F. Traganos, *Cytometry*, 1992, **13**, 795–808.
106 L. Shi, S. Günther, T. Hübschmann, L. Y. Wick, H. Harms and S. Müller, *Cytometry Part A*, 2007, **71A**, 592–598.
107 M. Rosenberg, N. F. Azevedo and A. Ivask, *Sci. Rep.*, 2019, **9**, 6483.
108 A. Permyakova, A. Kakar, J. Bachir, E. Gkaniatsou, B. Haye, N. Menguy, F. Nouar, C. Serre, N. Steunou, T. Coradin, F. M. Fernandes and C. Sicard, *ACS Mater. Lett.*, 2023, **5**, 79–84.
109 Y. Qin, L. Chen, Y. Cheng, S. Yang, Y. Liu, W. Fan, L. Wang, Q. Wang, L. Zheng and Q. Cao, *ACS Appl. Bio Mater.*, 2020, **3**, 3268–3275.
110 T. L. Riss, R. A. Moravec, A. L. Niles, S. Duellman, H. A. Benink, T. J. Worzella and L. Minor, in *Assay Guidance Manual*, ed. S. Markossian, A. Grossman, M. Arkin, D. Auld, C. Austin, J. Baell, K. Brimacombe, T. D. Y. Chung, N. P. Coussens, J. L. Dahlin, V. Devanarayan, T. L. Foley, M. Glicksman, K. Gorshkov, J. V. Haas, M. D. Hall, S. Hoare, J. Inglese, P. W. Iversen, M. Lal-Nag, Z. Li, J. R. Manro, J. McGee, O. McManus, M. Pearson, T. Riss, P. Saradjian, G. S. Sittampalam, M. Tarselli, O. J. Trask, J. R. Weidner, M. J. Wildey, K. Wilson, M. Xia and X. Xu, Eli Lilly & Company and the National Center for Advancing Translational Sciences, Bethesda (MD), 2004.
111 E. U. Karatop, C. E. Cimenci, A. M. Aksu, E. U. Karatop, C. E. Cimenci and A. M. Aksu, *Cytotoxicity – Understanding Cellular Damage and Response*, IntechOpen, 2022.
112 K. Präbst, H. Engelhardt, S. Ringgeler and H. Hübner, in *Cell Viability Assays*, ed. D. F. Gilbert and O. Friedrich, Springer New York, New York, NY, 2017, vol. 1601, pp. 1–17.
113 E. Grela, J. Kozłowska and A. Grabowiecka, *Acta Histochem.*, 2018, **120**, 303–311.
114 Q. Chen, S. Tang, Y. Li, Z. Cong, D. Lu, Q. Yang, X. Zhang and S. Wu, *ACS Appl. Mater. Interfaces*, 2021, **13**, 58382–58392.
115 R. Ohtani, K. Kawano, M. Kinoshita, S. Yanaka, H. Watanabe, K. Hirai, S. Futaki, N. Matsumori, H. Uji-i, M. Ohba, K. Kato and S. Hayami, *Angew. Chem., Int. Ed.*, 2020, **59**, 17931–17937.
116 L. Ha, K. M. Choi and D.-P. Kim, *ACS Appl. Mater. Interfaces*, 2021, **13**, 18545–18553.
117 S. Neri, E. Mariani, A. Meneghetti, L. Cattini and A. Facchini, *Clin. Diagn. Lab. Immunol.*, 2001, **8**, 1131–1135.
118 G. Adam and H. Duncan, *Soil Biol. Biochem.*, 2001, **33**, 943–951.
119 W. Chen, S. Kong, M. Lu, F. Chen, W. Cai, L. Du, J. Wang and C. Wu, *Soft Matter*, 2020, **16**, 270–275.
120 K. Liang, J. J. Richardson, J. Cui, F. Caruso, C. J. Doonan and P. Falcaro, *Adv. Mater.*, 2016, **28**, 7910–7914.
121 H. Arakawa, M. Shiokawa, O. Imamura and M. Maeda, *Anal. Biochem.*, 2003, **314**, 206–211.
122 S. Kamiloglu, G. Sari, T. Ozdal and E. Capanoglu, *Food Front.*, 2020, **1**, 332–349.
123 S. H. Yang, E. H. Ko, Y. H. Jung and I. S. Choi, *Angew. Chem., Int. Ed.*, 2011, **50**, 6115–6118.
124 N. Jeon, I. Jeong, E. Cho, I. Choi, J. Lee, E. H. Han, H. J. Lee, P. C. W. Lee and E. Lee, *JACS Au*, 2023, **3**, 154–164.
125 H. Yang, Y. Zhang, L. Zeng, W. Yin, Y. Xu, J. Chen, S. Liu, X. Zou, Z. He and Z. Dai, *Small Methods*, 2022, **6**, 2101391.
126 Y. Jiao, Y. Guo, Y. Fan, R. Wang, X. Li, H. Wu, Z. Meng, X. Yang, Y. Cui, H. Liu, L. Pan, T. Maimaitijuma, J. Zhang, Y. Wang, Y. Cao and T. Zhang, *BioMed Res. Int.*, 2020, **2020**, 2846297.
127 Y. Wang, C. Liu, X. Ma, A. Filppula, Y. Cui, J. Ye and H. Zhang, *Nanoscale*, 2024, **16**, 20925–20939.
128 F. Sivandzade, A. Bhalerao and L. Cucullo, *Bio-Protocol*, 2019, **9**, e3128.

129 K. S. Louis and A. C. Siegel, in *Mammalian Cell Viability*, ed. M. J. Stoddart, Humana Press, Totowa, NJ, 2011, vol. 740, pp. 7–12.
130 A. Kan, D. P. Birnbaum, P. Praveschotinunt and N. S. Joshi, *Appl. Environ. Microbiol.*, 2019, **85**, e00434–19.
131 M. Wu, Y. Liao, D. Guo, M. Zhai, D. Xia, Z. Zhang, X. Liu and Y. Huang, *RSC Adv.*, 2024, **14**, 14722–14741.
132 H. C. Moon, S. Han, J. Borges, T. Pesqueira, H. Choi, S. Y. Han, H. Cho, J. H. Park, J. F. Mano and I. S. Choi, *Soft Matter*, 2020, **16**, 6063–6071.
133 J. Guo, Y. Ping, H. Ejima, K. Alt, M. Meissner, J. J. Richardson, Y. Yan, K. Peter, D. von Elverfeldt, C. E. Hagemeyer and F. Caruso, *Angew. Chem., Int. Ed.*, 2014, **53**, 5546–5551.
134 H. Bunzen, *ChemNanoMat*, 2021, **7**, 998–1007.
135 M. R. Hafner, F. Carraro, B. Abbasgholi-NA, S. Dal Zilio, M. Schmallegger, H. Wiltsche, L. Ge, M. R. Reithofer, E. Astria, L. Villanova, H. Amenitsch, C. Doonan and P. Falcaro, *Adv. Funct. Mater.*, 2025, e18940.
136 W. Liang, R. Ricco, N. K. Maddigan, R. P. Dickinson, H. Xu, Q. Li, C. J. Sumby, S. G. Bell, P. Falcaro and C. J. Doonan, *Chem. Mater.*, 2018, **30**, 1069–1077.
137 M. Ge, Y. Wang, F. Carraro, W. Liang, M. Roostaeinia, S. Siahrostami, D. M. Proserpio, C. Doonan, P. Falcaro, H. Zheng, X. Zou and Z. Huang, *Angew. Chem., Int. Ed.*, 2021, **60**, 11391–11397.
138 A. D. Katsenis, A. Puškarić, V. Štrukil, C. Mottillo, P. A. Julien, K. Užarević, M.-H. Pham, T.-O. Do, S. A. J. Kimber, P. Lazić, O. Magdysyuk, R. E. Dinnebier, I. Halasz and T. Friščić, *Nat. Commun.*, 2015, **6**, 6662.
139 M. de, J. Velásquez-Hernández, R. Ricco, F. Carraro, F. T. Limpoco, M. Linares-Moreau, E. Leitner, H. Wiltsche, J. Rattenberger, H. Schröttner, P. Frühwirt, E. M. Stadler, G. Gescheidt, H. Amenitsch, C. J. Doonan and P. Falcaro, *CrystEngComm*, 2019, **21**, 4538–4544.
140 G. B. Whitfield, T. D. Brock, A. Ammann, D. Gottlieb and H. E. Carter, *J. Am. Chem. Soc.*, 1955, **77**, 4799–4801.
141 T. Sirec, A. Strazzulli, R. Isticato, M. De Felice, M. Moracci and E. Ricca, *Microb. Cell Fact.*, 2012, **11**, 100.
142 S. A. Polash, A. Poddar, S. Pyreddy, F. Carraro, A. M. D'Angelo, G. Bryant, P. Falcaro and R. Shukla, *ACS Appl. Mater. Interfaces*, 2025, **17**, 3002–3012.
143 Y. Lu, Y. Song, L. Peng, X. Rao, K. B. Tan, S. Zhou and G. Zhan, *ACS Appl. Mater. Interfaces*, 2023, **15**, 35552–35564.
144 L. Zheng, Z. Wang, H. Liu, N. Wang, J. Liu, M. Ma, X. Jia, M. Qian, Y. Liu, M. Li, Z. Wei and Y. Xiang, *ACS Nano*, 2025, **19**, 17900–17916.
145 M. R. Hafner, L. Villanova and F. Carraro, *CrystEngComm*, 2022, **24**, 7266–7271.
146 M. de, J. Velásquez-Hernández, E. Astria, S. Winkler, W. Liang, H. Wiltsche, A. Poddar, R. Shukla, G. Prestwich, J. Paderi, P. Salcedo-Abraira, H. Amenitsch, P. Horcajada, C. J. Doonan and P. Falcaro, *Chem. Sci.*, 2020, **11**, 10835–10843.
147 P. K. Lam, T. H. Vo, J.-H. Chen, S.-W. Lin, C.-L. Kuo, J.-J. Liao, K.-Y. Chen, S.-R. Huang, D. Li, Y.-H. Chang, H.-Y. Chen, H.-T. Hsieh, Y.-A. Hsu, H.-K. Tsao, H.-C. Yang and F.-K. Shieh, *J. Mater. Chem. A*, 2023, **11**, 24678–24685.
148 X. Luo, Y. Zhou, Y. Wang, X. Sun, J. Hu, X. Zi and Y. Fu, *Mol. Catal.*, 2024, **560**, 114131.
149 P. Horcajada, S. Surblé, C. Serre, D.-Y. Hong, Y.-K. Seo, J.-S. Chang, J.-M. Grenèche, I. Margiolaki and G. Férey, *Chem. Commun.*, 2007, 2820–2822.
150 J. Liang, Q. Chen, J. Yong, H. Suyama, J. Biazik, B. Njegic, A. Rawal and K. Liang, *Chem. Sci.*, 2024, **15**, 991–1002.
151 C. Li, M. Feng, B. Li, X. Feng, Y. Zhang and B. Wang, *ACS Nano*, 2025, **19**, 2890–2899.
152 L. Ha, U. Ryu, D.-C. Kang, J.-K. Kim, D. Sun, Y.-E. Kwon, K. M. Choi and D.-P. Kim, *ACS Biomater. Sci. Eng.*, 2021, **7**, 3075–3081.
153 L. R. Kummetha, J.-J. Oh, F. H. Van Der Linden and M.-E. Aubin-Tam, *Trends Biotechnol.*, 2025, **43**, 812–825.
154 Y. Liu, M. Wu, A. Kang, X. Zhang, R. Xie, Y. Huang, J. Huang, L. Chou and C. Zhong, *Adv. Funct. Mater.*, 2024, **34**, 2309288.
155 A. Date, P. Pasini and S. Daunert, *Anal. Chem.*, 2007, **79**, 9391–9397.
156 L. M. González, N. Mukhitov and C. A. Voigt, *Nat. Chem. Biol.*, 2020, **16**, 126–133.
157 J.-J. Oh, F. H. Van Der Linden, K. Malcı, R. A. Van Der Valk, T. Ellis and M.-E. Aubin-Tam, *Sci. Adv.*, 2025, **11**, eadw8278.
158 Y. Liu, L. Niu, N. Li, Y. Wang, M. Liu, X. Su, X. Bao, B. Yin and S. Shen, *Adv. Sci.*, 2023, **10**, 2205641.
159 X. Wu, J. Zhang, Z. Deng, X. Sun, Y. Zhang, C. Zhang, J. Wang, X. Yu and G. Yang, *Biomaterials*, 2025, **316**, 123000.
160 X. Kuang, Y. Liu, H. Luo, Q. Li, F. Wu, C. Fan and J. Liu, *J. Am. Chem. Soc.*, 2023, **145**, 26932–26946.
161 C. Zu and J. Wang, *Crit. Rev. Microbiol.*, 2014, **40**, 225–235.
162 N. S. Forbes, *Nat. Rev. Cancer*, 2010, **10**, 785–794.
163 W. Wang, H. Xu, Q. Ye, F. Tao, I. Wheeldon, A. Yuan, Y. Hu and J. Wu, *Nat. Biomed. Eng.*, 2022, **6**, 44–53.
164 B. Pang, X. Qiao, L. Janssen, A. Velds, T. Groothuis, R. Kerkhoven, M. Nieuwland, H. Ovaa, S. Rottenberg, O. Van Tellingen, J. Janssen, P. Huijgens, W. Zwart and J. Neefjes, *Nat. Commun.*, 2013, **4**, 1908.
165 A. Hak, M. S. Ali, S. A. Sankaranarayanan, V. R. Shinde and A. K. Rengan, *ACS Appl. Bio Mater.*, 2023, **6**, 349–364.
166 A. Barbora, O. Bohar, A. A. Sivan, E. Magory, A. Nause and R. Minnes, *PLoS One*, 2021, **16**, e0245350.
167 J. Zhou, C. Liu, Y. Wang, Y. Guo, X. Xu, E. Vuorimaa-Laukkanen, O. Koivisto, A. M. Filppula, J. Ye and H. Zhang, *Smart Med.*, 2025, **4**, e134.
168 M. Govender, Y. E. Choonara, P. Kumar, L. C. du Toit, S. van Vuuren and V. Pillay, *AAPS PharmSciTech*, 2014, **15**, 29–43.
169 C. Hill, F. Guarner, G. Reid, G. R. Gibson, D. J. Merenstein, B. Pot, L. Morelli, R. B. Canani, H. J. Flint, S. Salminen, P. C. Calder and M. E. Sanders, *Nat. Rev. Gastroenterol. Hepatol.*, 2014, **11**, 506–514.

170 O.-A. Praepanitchai, A. Noomhorm and A. K. Anal, *BioMed Res. Int.*, 2019, **2019**, 1–8.
171 M. Saarela, G. Mogensen, R. Fondén, J. Mättö and T. Mattila-Sandholm, *J. Biotechnol.*, 2000, **84**, 197–215.
172 C. C. Dodoo, J. Wang, A. W. Basit, P. Stapleton and S. Gaisford, *Int. J. of Pharm.*, 2017, **530**, 224–229.
173 J. Levy, *Am. J. Gastroenterol. Suppl.*, 2000, **95**, S8–S10.
174 F. J. Rodrigues, M. F. Cedran, J. L. Bicas and H. H. Sato, *Food Res. Int.*, 2020, **137**, 109682.
175 K. Vivek, S. Mishra, R. C. Pradhan, M. Nagarajan, P. K. Kumar, S. S. Singh, D. Manvi and N. N. Gowda, *Appl. Food Res.*, 2023, **3**, 100248.
176 X. Qi, F. Zhu, Z. Chang and Y. Deng, *Langmuir*, 2024, **40**, 16172–16179.
177 S. Ghasemi, J. B. Raoof, M. Ghani and R. Ojani, *Talanta*, 2024, **269**, 125403.
178 M. Liu, L. Zhang, R. Yang, H. Cui, Y. Li, X. Li and H. Huang, *J. Hazard. Mater.*, 2024, **461**, 132475.
179 N. Aziminia, M. Hadjipavlou, Y. Philippou, S. S. Pandian, S. Malde and M. Y. Hammadeh, *BJU Int.*, 2019, **123**, 753–768.
180 S. Li, X. Zhou, Z. Chen, F. C. Herbert, R. Jayawickramage, S. D. Panangala, M. A. Luzuriaga, S. B. Alahakoon, S. D. Diwakara, X. Meng, L. Fei, J. Ferraris, R. A. Smaldone and J. J. Gassensmith, *ACS Appl. Mater. Interfaces*, 2020, **12**, 11884–11889.
181 L. Ran, Y. Lin, G. Su, Z. Yang and H. Teng, *ChemBioChem*, 2024, **25**, e202400147.
182 Y. Xiang, H. Yan, B. Zheng, A. Faheem and Y. Hu, *Anal. Chem.*, 2020, **92**, 12338–12346.
183 A. Karnholz, K. Küsel, A. Gößner, A. Schramm and H. L. Drake, *Appl. Environ. Microbiol.*, 2002, **68**, 1005–1009.
184 M. Vázquez-González, C. Wang and I. Willner, *Nat Catal*, 2020, **3**, 256–273.
185 X. Liu, W. Qi, Y. Wang, R. Su and Z. He, *Nanoscale*, 2017, **9**, 17561–17570.
186 X. Lian, Y. Huang, Y. Zhu, Y. Fang, R. Zhao, E. Joseph, J. Li, J. Pellois and H. Zhou, *Angew. Chem., Int. Ed.*, 2018, **57**, 5725–5730.
187 Z. Xu, G. Xiao, H. Li, Y. Shen, J. Zhang, T. Pan, X. Chen, B. Zheng, J. Wu, S. Li, W. Zhang, W. Huang and F. Huo, *Adv. Funct. Mater.*, 2018, **28**, 1802479.
188 I. Koltover, T. Salditt, J. O. Rädler and C. R. Safinya, *Science*, 1998, **281**, 78–81.
189 C. LoPresti, H. Lomas, M. Massignani, T. Smart and G. Battaglia, *J. Mater. Chem.*, 2009, **19**, 3576.
190 S. Cao, L. C. Da Silva and K. Landfester, *Angew. Chem., Int. Ed.*, 2022, **61**, e202205266.
191 N. Martin, J.-P. Douliez, Y. Qiao, R. Booth, M. Li and S. Mann, *Nat. Commun.*, 2018, **9**, 3652.
192 H. Cai, Y.-L. Huang and D. Li, *Coord. Chem. Rev.*, 2019, **378**, 207–221.
193 S. Moon, Y. Liu, J. T. Hupp and O. K. Farha, *Angew. Chem., Int. Ed.*, 2015, **54**, 6795–6799.
194 J. Huo, M. Marcello, A. Garai and D. Bradshaw, *Adv. Mater.*, 2013, **25**, 2717–2722.
195 J. Zhang, N. Jin, N. Ji, X. Chen, Y. Shen, T. Pan, L. Li, S. Li, W. Zhang and F. Huo, *ACS Appl. Mater. Interfaces*, 2021, **13**, 52215–52233.
196 Z. Xu, J. Zhang, T. Pan, H. Li, F. Huo, B. Zheng and W. Zhang, *Chem. Mater.*, 2020, **32**, 3553–3560.
197 D. Tian, R. Hao, X. Zhang, H. Shi, Y. Wang, L. Liang, H. Liu and H. Yang, *Nat. Commun.*, 2023, **14**, 3226.
198 B. Zhang, J. Zhang, C. Liu, L. Peng, X. Sang, B. Han, X. Ma, T. Luo, X. Tan and G. Yang, *Sci. Rep.*, 2016, **6**, 21401.
199 D. Lee and D. A. Weitz, *Small*, 2009, **5**, 1932–1935.
200 K. S. Rabe, J. Müller, M. Skoupi and C. M. Niemeyer, *Angew. Chem., Int. Ed.*, 2017, **56**, 13574–13589.
201 A. C. Marr and S. Liu, *Trends Biotechnol.*, 2011, **29**, 199–204.
202 J. Zhang, Y. Shen, N. Jin, X. Zhao, H. Li, N. Ji, Y. Li, B. Zha, L. Li, X. Yao, S. Zhang, F. Huo and W. Zhang, *Research*, 2022, **2022**, 9847698.
203 H. Chang, X. Wen, Z. Li, Z. Ling, Y. Zheng and C. Xu, *Bioeng. Transla Med.*, 2023, **8**, e10457.
204 G. Kumar, Y. C. Wang, C. Co and C.-C. Ho, *Langmuir*, 2003, **19**, 10550–10556.
205 S. Z. Yow, C. H. Quek, E. K. F. Yim, C. T. Lim and K. W. Leong, *Biomaterials*, 2009, **30**, 1133–1142.
206 D. Dutta, A. Pulsipher, W. Luo and M. N. Yousaf, *J. Am. Chem. Soc.*, 2011, **133**, 8704–8713.
207 M. W. Eskew and A. S. Benight, *Thermochim. Acta*, 2022, **715**, 179274.
208 M. R. Banki, T. U. Gerngross and D. W. Wood, *Protein Sci.*, 2005, **14**, 1387–1395.
209 J. S. Decker, U. Yano, R. M. Melgar and M. D. Lynch, *Biotechnol. J.*, 2024, **19**, 2400005.
210 M. Cárdenas-Fernández, W. Neto, C. López, G. Álvaro, P. Tufvesson and J. M. Woodley, *Biotechnol. Prog.*, 2012, **28**, 693–698.
211 R. R. Chen, *Appl. Microbiol. Biotechnol.*, 2007, **74**, 730–738.
212 Y. Ni and R. R. Chen, *Biotech. Bioeng.*, 2004, **87**, 804–811.
213 R. A. Sheldon and J. M. Woodley, *Chem. Rev.*, 2018, **118**, 801–838.
214 C. Ning, X. Wang, L. Li, Y. Zhu, M. Li, P. Yu, L. Zhou, Z. Zhou, J. Chen, G. Tan, Y. Zhang, Y. Wang and C. Mao, *Chem. Res. Toxicol.*, 2015, **28**, 1815–1822.
215 A. G. Renehan, *BMJ*, 2001, **322**, 1536–1538.
216 S. L. Fink and B. T. Cookson, *Infect. Immun.*, 2005, **73**, 1907–1916.
217 K. Simu, K. Holmfeldt, U. L. Zweifel and Å. Hagström, *Appl. Environ. Microbiol.*, 2005, **71**, 4793–4800.
218 V. Kilin, O. Glushonkov, L. Herdly, A. Klymchenko, L. Richert and Y. Mely, *Biophys. J.*, 2015, **108**, 2521–2531.

